Copyright Warning & Restrictions

The copyright law of the United States (Title 17, United States Code) governs the making of photocopies or other reproductions of copyrighted material.

Under certain conditions specified in the law, libraries and archives are authorized to furnish a photocopy or other reproduction. One of these specified conditions is that the photocopy or reproduction is not to be "used for any purpose other than private study, scholarship, or research." If a, user makes a request for, or later uses, a photocopy or reproduction for purposes in excess of "fair use" that user may be liable for copyright infringement,

This institution reserves the right to refuse to accept a copying order if, in its judgment, fulfillment of the order would involve violation of copyright law.

Please Note: The author retains the copyright while the New Jersey Institute of Technology reserves the right to distribute this thesis or dissertation

Printing note: If you do not wish to print this page, then select "Pages from: first page # to: last page #" on the print dialog screen

ABSTRACT

ADAPTIVE BOOTSTRAP SIGNAL SEPARATORS FOR BPSK/QAM-MODULATED WIRELESS CDMA SYSTEMS IN A MULTIPATH ENVIRONMENT

by
Nico J.M. van Waes

CDMA is an attractive multiple-access scheme, because of its potential capacity increase and its anti-multipath fading capability. For satisfactory performance, however, the effect of the "near-far" problem has to be resolved. This problem can be combated by using power-control, which, however, results in an overall reduction in communication ranges, and thus in a loss of capacity. Among other methods for mitigating the near-far problem is the use of decorrelating receivers, both of fixed type, which directly utilizes the cross-correlation of the users codes, and of adaptive type, which uses recursive algorithms that leads to signal decorrelation. Not to lessen the importance of other adaptive algorithms, the current research concentrates on what was termed in the literature "bootstrap algorithm" . Although the emphasis will be on applying the adaptive bootstrap decorrelator, the fixed type will be used primarily to provide comparison. Also used for comparison are both blind adaptive and training sequence based MMSE.

Most of the literature on multiuser detection has been assuming BPSK. However, a need for transferring wideband data demands using modulation schemes with high bits/cycle, such as QAM. Therefore, modification of the receiver is considered, so that QAM-modulation can be applied efficiently, using the complex signal approach of this modulation.

For the asynchronous channel, vast amounts of research have been devoted to using one-shot matched filter banks followed by conventional decorrelators which implement the inverse of some (partial) correlation matrix. In this work, an adaptive

bootstrap version is presented, which is suitable for the one-shot structure shown previously to be more robust to errors in delay estimation. It has also been noted that such a correlation matrix can, depending on the channel characteristics, become ill-conditioned or even singular. Therefore, another matched filtering structure, followed by what is called a multishot conventional (fixed type) decorrelator, has been previously suggested to mitigate this singularity problem. However, the fixed type of the multishot decorrelator is expected to have similar non-robustness to errors in delay estimation as was previously shown for the one-shot. Therefore, the adaptive multishot bootstrap decorrelator is presented and evaluated. Also, by adding an adaptive canceler, an extension to the above matched filter-decorrelator combination, will be proposed and evaluated. A multipath time-variant fading environment will be used in some of these performance evaluations.

Finally, when handling multipath channels, the question is raised whether path combining should be done before or after the signals are decorrelated. For the asynchronous case, a one-shot extension of the bootstrap algorithm is presented, which is capable of decorrelating the signals from resolved paths of different users, to facilitate the decorrelate before combining case.

ADAPTIVE BOOTSTRAP SIGNAL SEPARATORS FOR BPSK/QAM-MODULATED WIRELESS CDMA SYSTEMS IN A MULTIPATH ENVIRONMENT

by
Nico J.M. van Waes

A Dissertation
Submitted to the Faculty of
New Jersey Institute of Technology
in Partial Fulfillment of the Requirements for the Degree of
Doctor of Philosophy

Department of Electrial and Computer Engineering

August 1998

APPROVAL PAGE

ADAPTIVE BOOTSTRAP SIGNAL SEPARATORS FOR BPSK/QAM-MODULATED WIRELESS CDMA SYSTEMS IN A MULTIPATH ENVIRONMENT

Nico J.M. van Waes

Dr. Y. Bar-Ness, Dissertation Advisor — Date
Distinguished Professor, Department of Electrial and Computer Engineering, NJIT

Dr. H. Ge, Committee Member — Date
Assistant Professor, Department of Electrial and Computer Engineering, NJIT

Dr. A. Haimovich, Committee Member — Date
Associate Professor, Department of Electrial and Computer Engineering, NJIT

Dr. Z.-H. Michalopoulou, Committee Member — Date
Assistant Professor, Department of Mathematics, NJIT

Dr. H.V. Poor, Committee Member — Date
Professor, Department of Electrical Engineering, Princeton University

BIOGRAPHICAL SKETCH

Author: Nico J.M. van Waes

Degree: Doctor of Philosophy

Date: August 1998

Graduate Education:

- Doctor of Philosophy in Electrical Engineering,
  New Jersey Institute of Technology, Newark, NJ, U.S.A., 1998
- Master of Science in Electrical Engineering,
  Delft University of Technology, Delft, the Netherlands, 1994

Publications and Presentations:

- Bar-Ness Y., and van Waes, N.J.M., "Implementing the Bootstrap Algorithm to Multishot Matched Filtering, Multiuser Detection," *Melecon'98*, Tel Aviv, Israel.
- N.J.M. van Waes and Y. Bar-Ness, "Adaptive Algorithm for the Multishot Matched Detector in a Multipath Rayleigh Fading Environment.," *Vehicular Technology Conference (VTC'98)*, pp. 179-183, Ottawa, Canada.
- N.J.M. van Waes and Y. Bar-Ness, "The Bootstrap Algorithm for One-Shot Matched Filtering Multiuser Detector in a Multipath Environment," *Vehicular Technology Conference (VTC'98)*, pp. 184-188, Ottawa, Canada.
- Y. Bar-Ness and N.J.M. van Waes, "Adaptive blind signal separation and interference cancellation of co-channel QAM signals over dispersive fading environment," *Interference Rejection and Signal Separation symposium (IRSS'97)*, Washington
- Y. Bar-Ness, and N.J.M. van Waes, "Multistage Detector for Adaptive Separation of QAM-modulated Multiuser CDMA Signals," accepted for presentation at *the International Symposium on Spread Spectrum Techniques and Applications (ISSSTA'98)*, Sun City, South Africa
- N.J.M. van Waes and Y. Bar-Ness, "The Complex Bootstrap Algorithm for Blind Separation of Co-channel QAM Signals," *Wireless personal Communications, An International Journal.*, accepted pending review.

Aan mijn ouders, omdat het hun harde werk en conditieloze zorg en liefde is, die dit werk mogelijk hebben gemaakt.

(To my parents, as it is their hard work and conditionless care and love that made this work possible.)

ACKNOWLEDGMENT

I would like to express my sincere gratitude to my advisor and mentor, Professor Bar-Ness, whose relentless enthusiasm for research in the field of telecommunications and signal processing, as well as his belief in my abilities, instilled in me the perseverance to successfully finish my Ph.D.

I would also like to thank him and the other staff-members of the Center for Communications and Signal Processing Research (CCSPR) for their ongoing efforts in providing the Center's students with high-quality courses, research-topics, and computational resources.

TABLE OF CONTENTS

LIST OF FIGURES

CHAPTER 1

INTRODUCTION

1.1 Wireless Communications

The demand for wireless services has grown exponentially over the last few decades. Items like cellular phones, advanced cordless phones, and pagers have become commonplace gadgets. Since bandwidth is scarce, the need arises to serve more and more users simultaneously within a given limited bandwidth. And this without reducing the quality of transmission, but rather with better transmission quality as new systems are designed to handle data, which requires higher transmission quality, as well as voice-transmission.

1.2 Multiple Access Transmission Schemes

To allow the simultaneous transmission of data streams, methods need to be devised, which allow the receiving end to extract the desired data stream from the received composite signal. For this purpose, there exist a number of basic concepts, termed multiple access (MA), which (including some hybrid forms) are used in present operational systems. Below, a brief description of the most commonly used multiple access schemes.

- **Frequency Division Multiple Access**

  Frequency Division Multiple Access (FDMA) is the oldest and most basic technique. Using this scheme, the available bandwidth for a physical area, termed a cell, is divided into a number of sub-bands, each of which is allocated to a single transmitter receiver pair. Provided the guard-bands between the sub-bands are sufficiently large, no multiple access interference (MAI) will occur. Disadvantages of FDMA are, among others, the fact that if the traffic in a sub-band is sporadic, thus bandwidth is essentially wasted, the fact that the

same bandwidth can only be reused in another cell if the intermittent distance is large enough to cause sufficiently low intercell interference (large frequency-reuse factor) and the fact that a separate transceiver has to be dedicated to each sub-band. Usage of FDMA leads to very slow handoffs between cells, thus causing a high probability of loss of connection [1].

- **Time Division Multiple Access**

  Time Division Multiple Access (TDMA) is a technique used for example in the European GSM systems, allocates the whole available bandwidth in the cell to each user sequentially for a short duration of time, termed a timeslot. Thus, to avoid MAI, strict synchronization is required. At the cost of some additional signaling, it is possible to avoid allocating the bandwidth to users which have no data to send, thereby avoiding waste of bandwidth. Using TDMA, the same transmitter can be used to communicate with many mobiles, and, due to the fact that the mobile can acquire information on the signal strength of surrounding base-stations while it is not in its active timeslot, much faster handoffs can be achieved than with FDMA, causing reduction of the probability of connection-loss [1]. TDMA requires similar frequency-reuse factors as FDMA to avoid inter-cell interference.

- **Direct Sequence Code Division Multiple Access**

  In Direct Sequence Code Division Multiple Access (DS-CDMA), each data-symbol is convolved with a user-specific code (each element of which is called a chip), after which the result is transmitted in serial using one carrier and the whole bandwidth of the cell. The data-symbol is acquired at the receiver by again multiplying the received data with the user-specific code and summing the results. Synchronization of the received signals code with the receivers code can be performed by maximizing the correlation between the two. Since

it is difficult or impossible (due to channel behavior and requirements on the code-design) to keep the signals of the different users orthogonal, MAI will be introduced, the effect of which is aggravated by what is termed the "near-far problem". The near-far problem results in MAI reaches unacceptable levels, due to the interfering user(s) being significantly closer to the base-station, and hence being received with significantly higher power-levels. Advantages of DS-CDMA are increased capacity among others due to the possibility for a frequency-reuse factor of 1, (meaning all cells use the same bandwidth, but different code-sets), the more reliable soft-handoff possibility [1], and the voice-activity factor, which increases the capacity by approximately a factor of two.

- **Multi Carrier Code Division Multiple Access**

  Multi Carrier Code Division Multiple Access (MC-CDMA), also known as OFDM-CDMA, is a technique in which a user, like in DS-CDMA, convolves each data-symbol with a code, after which each element of the result is modulated on a different carrier (generally using a DFT). All users use the same carrier frequencies. The data-symbol is retrieved at the receiver by again multiplying the received data of all carriers with the user-specific code and adding the results up. Just as with DS-CDMA, using MC-CDMA will almost unavoidably lead to MAI. Also the system capacity, and soft-handoff feature are similar.

1.3 Motivation

Multiple Access Receivers

Multiple access schemes like FDMA and TDMA allow for simple single user detectors, as the schemes themselves ensure MAI-free reception. Unfortunately, the achievable capacity these schemes provide is comparatively low, which is a serious disadvantage given the explosive growth of the demand for wireless services. Therefore, a lot of

research has and is being devoted to MC-CDMA and DS-CDMA using multiuser detectors, which promise to provide higher capacity at the cost of higher complexity. In this study, only DS-CDMA is being considered, although the discussed receiver structures could easily be adapted to fit MC-CDMA systems.

The main disadvantage of both MC-CDMA and DS-CDMA is the presence of MAI, which is in most cases the main limiting factor on the performance. Hence, to improve the performance, the system has to either limit the MAI by applying power control (as for example implemented in IS95), which limits the usable power to that of the worst-case user and hence severely reduces capacity, or employ a near-far tolerant (or resistant), MAI-reducing scheme in the receiver.

Beside the optimal receiver proposed by Verdú[2], which is rather complex to implement, many suboptimal, less complicated, schemes were proposed. These schemes can roughly be divided into three categories; fixed (like Lupas and Verdú's decorrelator based on correlation matrix inversion [3]), adaptive learning by means of training-sequences (like adaptive LMS or type-based [4], and blind adaptive schemes (like BAMD [5] and bootstrap [6, 7]).

Signal Decorrelation

Since it can be safely assumed that data-streams of different users are independent, and thus uncorrelated, the MAI cancelling can effectively be done by decorrelating the different user signals. In this study, two basic types of decorrelators, inversion based decorrelator [3] (fixed type, assumes accurate knowledge of codes and relative delays) and bootstrap decorrelator [6] (blind adaptive type decorrelator, assumes knowledge of codes and relative delays with allowed errors) are being used and compared. Their performance is investigated for both synchronous (an approximation to the forward link in mobile systems, or fixed wireless systems) and

asynchronous (backward link in mobile systems) systems and to forward links in mobile systems with multipath.

Bootstrap Decorrelator

The idea of the bootstrap algorithm as a way to cancel interference was first proposed in 1981 [8] and later used for cancelling cross-polarization in satellite communications [9] and in microwave terrestrial radio links [10]. Two of the bootstrap structures were then proposed. They are, respectively, the backward-backward structure controlled by power minimization, and the forward-forward structure controlled by decorrelating the outputs. It was shown that for the algorithms to converge to a state of signal separation, a signal distinguisher, termed discriminator, is needed. Such a discriminator uses a known, simple difference between the signals to be separated, rather than needing high-quality estimates of the signals themselves as in the case of the regular LMS noise canceler. In general the adaptive weights are controlled with recursive equations as follows:

For the case of power criterion,

$$w_{ij}^{n+1} = w_{ij}^{(n)} + \mu f\left[|D(z_i)|^2\right] \qquad j \neq i \quad i,k = 1 \cdots K,$$

and for the decorrelation control,

$$w_{ij}^{n+1} = w_{ij}^{(n)} + \mu f\left[|D(z_i)z_j|^2\right] \qquad j \neq i \quad i,k = 1 \cdots K,$$

where $z_i \quad i = 1, \cdots, K$ are the outputs, corresponding to the different user signals (K is the number of co-users), $D(\cdot)$ is the discriminator operator. In this study, only the forward-forward structure is being considered, with the signum function used as discriminator, as this structure was found to be more suitable to digital signals.

One-shot versus Multi-shot

In an asynchronous environment, the matched filter output of the data-symbol of a desired user generally contains interference from not one (like in the synchronous

case), but more data-symbols of each other user. To handle such situations, two schemes for matched filter banks are considered, one using the so called "one-shot" approach, in which one filter is matched to one of the user codes, called the desired user, while other filters are matched to the left $(0, \tau_k \quad k = 2, \cdots, K)$ and right $(\tau_k, \cdots, T \quad k = 2, \cdots, K)$ parts of the other user codes respectively. Following such a bank of filters, a decorrelator is used followed by a combiner which adds the results that correspond to the left and right part, to estimate the symbols. The other, termed multi-shot approach, in which each filter is matched to the code of the respective filter user and sampled corresponding to the bit timing $(\tau_k, T + \tau_k)$ of this user. Following such a bank of filters, a decorrelator is used, either fixed or adaptive, to obtain the current symbol using information from the samples of the current, previous and following symbols of all users.

Multipath Combining and Decorrelation Processing Order in Dispersive Environments

Due to channel dispersion, signals will be received via multipath separated by time delays. Rake receivers have been used to combine these multipath signals, to achieve diversity gain and improve performance. The effect of the order of these processes (combiner followed by decorrelator, or decorrelator followed by combiner) on the system performance and complexity will be studied. For the one-shot asynchronous case, a version of the bootstrap decorrelator, which allows for decorrelating before combining, is presented and evaluated.

Two-stage Receivers

When using very loose or no power-control, the power of the interfering users may be significantly larger than the power of the desired user. It has been shown that the performance, of some of the aforementioned decorrelators and for certain channel types, is significantly worse than the single-user (i.e., no MAI) performance. In those

cases, a second (canceler) stage can be added to improve the performance. Such a matched filter, decorrelator and canceler is called parallel interference canceler (PIC). In this study, the efficiency of several of these cascaded receivers is considered.

Modulation Considerations

Most of the work done with multi-user receivers assumed binary phase shift keying (BPSK) modulation. However, a need for transferring wideband data demands using modulation schemes with high bits/cycle rates. Quadrature amplitude modulation (QAM) is one of these schemes. Therefore, in this study, part of the focus will be on applying QAM as modulation, rather than BPSK. Also, for this case, attention will be paid to reducing hardware by directly using complex signal presentation.

General Channel Model

For the (asynchronous) uplink flat fading channel with dispersion, the following widely accepted (see for example [11, 12, 13]) equivalent low-pass model will be used

$$r(t) = \sum_{i} \sum_{k=1}^{K} \sqrt{a_k}(i) \sum_{m=1}^{M} b_k(i)\gamma_{km}(i)s_k(t - iT - \tau_k - \delta_{km}) + n(t) \qquad (1.1)$$

where K is the number of users, M the number of paths (assumed equal for all users), $\sqrt{a_{km}} = \sqrt{a_k}\gamma_{km}$, and $\tau_{km} = \tau_k + \delta_{km}$ are the amplitude and relative delay of the m^{th} path of the k^{th} user and b_k and s_k are the data symbol and signature waveform of the k^{th} user respectively (in the presented results, all signature wave-forms were taken to be length 15 binary Gold-codes, unless specified otherwise). γ_{km} is the fading coefficient of path m of user k such that $\sum_m E[\gamma_{km}^2] = 1$. δ_{km} is the delay of path m of user k relative to τ_k, the delay of the first path of this user. This means $\delta_{k1} = 0$ and $\delta_{km} > \delta_{kn}, m > n \geq 0$. $n(t)$ is the zero mean AWGN, with a two-sided power spectral density of $N_0/2$. (1.1) also describes the synchronous (downlink) channel model by taking $\tau_k = 0 \ \ \forall k = 1, \cdots, K$ and $\delta_{km} = \delta_m \ \ \forall k = 1, \cdots K$, meaning that

the relative delays of the paths are the same for each user. A channel model without dispersion is easily created by choosing $M = 1$.

1.4 Outline

The bootstrap algorithm has been proposed and used as an adaptive decorrelator for multiuser BPSK signals. In chapter 2, the application of QAM data, rather than BPSK is investigated. The synchronous (downlink) channel is considered. The performance of a receiver using the bootstrap algorithm with QAM modulated signals is evaluated analytically, as well as through simulations. Further, a new model of the algorithm, termed 'Complex Bootstrap', is developed, which deals directly with the complex signals in the complex domain, as a result of which hardware can be saved.

In chapter 3, the asynchronous one-shot bootstrap algorithm, which enables the receiver to decorrelate the signals received over the resolved paths of a multipath channel. The performance is evaluated through simulations, and the total separation of the user's signals from strong interference is shown both analytically as well as through the simulation results.

In [3], Lupas and Verdú suggest a decorrelator based on the inverse of the correlation matrix for synchronous systems. In [14], they suggested an extension for asynchronous systems, i.e. they use the inverse of a larger "partial correlation matrix". However, in the latter case, the correlation matrix may be ill-conditioned or even singular, something which is ignored in most publications. Hence, in chapter 4, by use of examples, the condition number of the correlation matrix is examined and it is shown that the matrix may very well be singular, which makes inversion impossible.

Chapter 5 deals with the multi-shot receiver; an asynchronous receiver which does not exhibit the singular-matrix problem examined in chapter 4. The fixed (non-adaptive) type of multishot decorrelator has been proposed earlier and shown

to perform satisfactory when only three successive bits of each user are stacked and processed together [15]. In this work, an adaptive bootstrap structure of this decorrelator is proposed and examined. Also, a canceler stage to follow this decorrelator is presented, hence exhibiting PIC based on the multishot structure, the error performance of which is obtained.

In a dispersive environment, signals arrive through different paths at the receiver. These signals can be combined to achieve a diversity gain which improves the performance. In chapter 6, the effects of performing this combining before or after decorrelating is investigated for the synchronous receiver case.

Lastly, in chapter 6, simulation results are presented, which compare the conventional single-user receiver (with MAI), the one- and multi-shot decorrelator based on matrix inversion, one- and multi-shot bootstrap, and both the blind adaptive and training sequence initialized MMSE structures. A comparison is based on their near-far resistance (function of interfere to desired user's power), as well as their robustness to errors in estimations of the user's relative delays.

CHAPTER 2
SYNCHRONOUS QAM-MODULATED CDMA RECEIVER

In this chapter the adaptive synchronous QAM-modulated CDMA receiver, based on the bootstrap approach, is studied. This receiver is practically most suited for the base station of fixed point wireless networks, as synchronization is easily achieved there. Synchronization is also present in mobile stations, but the complexity of the receiver, and the requirement of the knowledge of all user codes, might be an obstacle for practical implementations. The synchronous assumption might also be made to simplify the channel model and can be used for obtaining performance bounds.

This receiver will be studied in three steps. First we will assume that there is no correlation between the real and imaginary parts of all signals, meaning the real rail of one user suffers only interference from the real rail of the other users and likewise for the imaginary rail. This reduced the problem to that of two separate receivers using PAM modulation. The steady state performance analysis, which follows the analysis for BPSK in [7], will be shown. Assuming a perfect estimate of the power level of each user after the decorrelator, symbol level decision is performed. An adaptive method for power level estimation is also proposed and used for simulation purposes.

Next, it is assumed, more realistically, that there exists cross-correlation between the real and imaginary rail of signals of different users, but at first it is assumed that there is no interference between the two rails of the same user. However, it will be shown that whether the rails of the same user are correlated before processing is irrelevant, since decorrelating with other users' signals will cause correlation between these two rails, even when they are a priori uncorrelated. Hence intra-rail decorrelation becomes necessary.

The second step of study presents the receiver in real domain representation, from which the complex domain description is derived in the third step.

2.1 Decorrelator Model

The equivalent low-pass signal of a synchronous system (in channels without dispersion) at the input of the matched filter bank is taken from (1.1) to be

$$r(t) = \sum_{i} \sum_{k=1}^{K} b_k(i)\sqrt{a_k}s_k(t - iT) + n(t), \tag{2.1}$$

Using QAM, the symbols b_k are complex, with their real and imaginary part belonging to the set $\left[-(\sqrt{M}-1)c, -(\sqrt{M}-3)c, \cdots, (\sqrt{M}-3)c, (\sqrt{M}-1)c\right]$. M, a power of 2, is the size of the square constellation. The constant c is chosen such that the principle constellation power is normalized to one. Thus,

$$c = \frac{1}{\sqrt{(\frac{2}{3}(M-1)T_b)}} \tag{2.2}$$

Following the matched filter, the composite signal can be written in matrix form as

$$\boldsymbol{x} = \boldsymbol{P}^H \boldsymbol{A}\boldsymbol{b} + \boldsymbol{n} = \boldsymbol{P}^H \boldsymbol{\theta} + \boldsymbol{n}, \tag{2.3}$$

where $\boldsymbol{x}$,$\boldsymbol{\theta}$, and $\boldsymbol{b}$ are complex vectors of dimension K. $\boldsymbol{P}$ is a $K \times K$ complex matrix containing the correlation coefficients,

$$\boldsymbol{P} = \begin{bmatrix} 1 & \rho_{12} & \cdots & \rho_{1K} \\ \rho_{21} & \ddots & & \rho_{2K} \\ \vdots & & \ddots & \vdots \\ \rho_{K1} & \rho_{K2} & \cdots & 1 \end{bmatrix}, \tag{2.4}$$

where ρ_{ij} is the complex correlation between between the signature of user i and user j. The ones on the diagonal stem from the assumption that the rails of the same user remain orthonormal in the channel. Omitting this assumption is examined in section 2.4.4.

$\boldsymbol{A} = \text{diag}\left[\sqrt{a_1} \cdots \sqrt{a_K}\right]$, is real and $\theta_k = \sqrt{a_k}b_k$. To keep the model general, it is assumed that $\boldsymbol{P}$ is not Hermitian. The noise covariance matrix is Hermitian, $\boldsymbol{P}_N = (\boldsymbol{P} + \boldsymbol{P}^H)/2$.

For two inputs only, as in dually polarized QAM signals,

$$\begin{bmatrix} x_1 \\ x_2 \end{bmatrix} = \begin{bmatrix} 1 & \rho_{12} \\ \rho_{21} & 1 \end{bmatrix}^H \begin{bmatrix} \theta_1 \\ \theta_2 \end{bmatrix} + \begin{bmatrix} n_1 \\ n_2 \end{bmatrix}. \tag{2.5}$$

Rewriting (2.5) in its real representation by expanding

$$\rho = \rho_{\Re} + j\rho_{\Im} \equiv \begin{bmatrix} \rho_{\Re} & \rho_{\Im} \\ -\rho_{\Im} & \rho_{\Re} \end{bmatrix},$$

we obtain

$$\begin{bmatrix} x_{1\Re} \\ x_{1\Im} \\ x_{2\Re} \\ x_{2\Im} \end{bmatrix} = \begin{bmatrix} 1 & 0 & \rho_{12\Re} & -\rho_{12\Im} \\ 0 & 1 & \rho_{12\Im} & \rho_{12\Re} \\ \rho_{21\Re} & -\rho_{21\Im} & 1 & 0 \\ \rho_{21\Im} & \rho_{21\Re} & 0 & 1 \end{bmatrix}^T \begin{bmatrix} \theta_{1\Re} \\ \theta_{1\Im} \\ \theta_{2\Re} \\ \theta_{2\Im} \end{bmatrix} + \begin{bmatrix} n_{1\Re} \\ n_{1\Im} \\ n_{2\Re} \\ n_{2\Im} \end{bmatrix}. \tag{2.6}$$

The decorrelator we are seeking is a linear transformation of the matched filter output $\boldsymbol{x}$ with a matrix $\boldsymbol{V}$, which equals $\boldsymbol{P}^{-1}$ if Lupas' and Verdú's approach is used (although this approach was previously only applied to BPSK modulation), and $\boldsymbol{I} - \boldsymbol{W}^H$ if the adaptive bootstrap decorrelator is used. $\boldsymbol{I}$ is the $K \times K$ identity matrix and $\boldsymbol{W}$ is a weight matrix with zeroes on the diagonal. Thus:

$$\boldsymbol{z} = \boldsymbol{V}\boldsymbol{x} \tag{2.7}$$

Concentrating on the bootstrap decorrelator,

$$\begin{aligned} \boldsymbol{z} = (\boldsymbol{I} - \boldsymbol{W}^H)\boldsymbol{x} &= (\boldsymbol{I} - \boldsymbol{W}^H)\boldsymbol{P}^H\boldsymbol{A}\boldsymbol{b} + (\boldsymbol{I} - \boldsymbol{W}^H)\boldsymbol{n} \\ &= (\boldsymbol{I} - \boldsymbol{W}^H)\boldsymbol{P}^H\boldsymbol{A}\boldsymbol{b} + \boldsymbol{\zeta} \end{aligned} \tag{2.8}$$

We try choosing the weight matrix $\boldsymbol{W}$ such that all outputs of the decorrelator are uncorrelated with each other,

$$E\left[z_k \mathrm{sgn}\left(\boldsymbol{z}_k^*\right)\right] = 0 \quad \text{for } k = 1, 2, \ldots, K \tag{2.9}$$

where $\boldsymbol{z}_k$ is $\boldsymbol{z}$ without the k^{th} element. This means that, except for the conjugation, the discriminator function is used; the signum function, is exactly the same as the one used for BPSK modulation (the introduced conjugate will have no effect on real signals). This makes the decorrelator totally transparent to the constellation used.

2.2 The Bootstrap Separator for Orthogonal QAM Signals

First, we will examine the performance of orthogonal QAM. Orthogonal in this context means that there is no cross-rail interference between any of the users' signals. This, in fact, reduces the QAM-constellation to two PAM constellations. We can thus examine the performance for each rail separately.

We will examine the performance of the real rail, whereby from all complex vectors, matrices and symbols only the real part is used without using the real subscript, $\Re$, to avoid unnecessary notational complexity.

From 2.8

$$\begin{aligned} z_1 &= \sqrt{a_1}b_1 + \boldsymbol{\rho}_1^T \boldsymbol{A}_1 \boldsymbol{b}_1 + n_1 - \boldsymbol{w}_1^T \left(\boldsymbol{P}_1 A_1 \boldsymbol{b}_1 + \boldsymbol{\rho}_1 \sqrt{a_1} b_1 + \boldsymbol{n}_1\right) \\ &= \sqrt{a_1}\left(1 - \boldsymbol{w}_1^T \boldsymbol{\rho}_1\right) b_1 + \left(\boldsymbol{\rho}_1^T - \boldsymbol{w}_1^T \boldsymbol{P}_1\right) \boldsymbol{A}_1 \boldsymbol{b}_1 + \left(n_1 - \boldsymbol{w}_1^T \boldsymbol{n}_1\right) \\ z_i &= \sqrt{a_i}\left(1 - \boldsymbol{w}_i^T \boldsymbol{\rho}_i\right) b_i + \left(\boldsymbol{\rho}_i^T - \boldsymbol{w}_i^T \boldsymbol{P}_i\right) \boldsymbol{A}_i \boldsymbol{b}_i + \left(n_i - \boldsymbol{w}_i^T \boldsymbol{n}_i\right), \end{aligned} \tag{2.10}$$

where $i = 2, 3, \cdots, K$, and $\boldsymbol{b}_i$, $\boldsymbol{\rho}_i$ and $\boldsymbol{w}_i$ are respectively the data vector $\boldsymbol{b}$, the i^{th} column of $\boldsymbol{P}$, and the i^{th} column of $\boldsymbol{W}$ without the i^{th} element. $\boldsymbol{P}_i$ is the matrix $\boldsymbol{P}$ without the i^{th} column and row. $\boldsymbol{\rho}_i$ is the i^{th} column of $\boldsymbol{P}$ without the element $\boldsymbol{P}_{ii}$ and $\boldsymbol{n}_i$ is the vector $\boldsymbol{n}$ without the i^{th} element. If z_1 corresponds to a high SNR signal, and all other signals are equally strong, having high SNIR, then the constraint 2.9 can be approximated by $E\left[z_i \text{sgn}(\boldsymbol{b}_i)\right]$ and results in $\boldsymbol{w}_i = \boldsymbol{P}_i^{-1}\boldsymbol{\rho}_i, \quad i = 2 \cdots K$. This will be proven section 2.4.2 for fully complex signals.

When these conditions are met, let

$$\boldsymbol{w}_1 = \boldsymbol{P}_1^{-1}\left(\boldsymbol{\rho}_1 + \boldsymbol{\delta}_1\right) \tag{2.11}$$

where $\boldsymbol{\delta}_1 = \left[\delta_{12}, \delta_{13}, \cdots, \delta_{1K}\right]^T$.

[1]For convenience to the reader, some of the notational descriptions will be repeated in different places.

With these values of $\boldsymbol{w}_1$ and $\boldsymbol{w}_i$ we get

$$\begin{aligned} z_1 &= \sqrt{a_1}\left(1-\boldsymbol{\rho}_1^T\boldsymbol{P}_1^{-1}\boldsymbol{\rho}_1-\boldsymbol{\delta}_1^T\boldsymbol{P}_1^{-1}\boldsymbol{\rho}_1\right)b_1-\boldsymbol{\delta}_1^T\boldsymbol{A}_1\boldsymbol{b}_1+\zeta_1' \\ z_i &= \sqrt{a_1}\left(1-\boldsymbol{\rho}_i^T\boldsymbol{P}_i^{-1}\boldsymbol{\rho}_i\right)b_i+\zeta_i \end{aligned} \tag{2.12}$$

where

$$\begin{aligned} \zeta_1' &= n_1-\left(\boldsymbol{\rho}_1^T+\boldsymbol{\delta}_1^T\right)\boldsymbol{P}_1^{-1}\boldsymbol{n}_1 \\ \zeta_i &= n_1-\boldsymbol{\rho}_i^T\boldsymbol{P}_i^{-1}\boldsymbol{n}_i \end{aligned} \tag{2.13}$$

To find the components of $\boldsymbol{\delta}_1$, the following must be equated to zero:

$$\begin{aligned} E\left[z_1\mathrm{sgn}(z_i)\right] = E\Big[&\left(\sqrt{a_1}\left(1-\boldsymbol{\rho}_1^T\boldsymbol{P}_1^{-1}\boldsymbol{\rho}_1-\boldsymbol{\delta}_1^T\boldsymbol{P}_1^{-1}\boldsymbol{\rho}_1\right)b_1-\boldsymbol{\delta}_1^T\boldsymbol{A}_1\boldsymbol{b}_1+\zeta_1'\right)\cdot \\ &\mathrm{sgn}\left(\sqrt{a_i}\left(1-\boldsymbol{\rho}_i^T\boldsymbol{P}_i^{-1}\boldsymbol{\rho}_i\right)b_i+\zeta_i\right)\Big] \quad i=2,\cdots,K \end{aligned} \tag{2.14}$$

In Appendix A, it is shown that in the steady state, when $E\left[z_1\mathrm{sgn}z_i\right]=0$, $\boldsymbol{\delta}_1$ is given by

$$\boldsymbol{\delta}_1=\boldsymbol{P}_1\left[\boldsymbol{I}+\left(\boldsymbol{\psi}_1\boldsymbol{\rho}_1^T+\boldsymbol{\Gamma}\boldsymbol{P}_1\right)^{-1}\boldsymbol{D}_1^{-1}\left(\frac{c}{2}\boldsymbol{I}-\boldsymbol{Q}_1\right)\boldsymbol{P}_1\right]^{-1}\left(\boldsymbol{\psi}_1\boldsymbol{\rho}_1^T+\boldsymbol{\Gamma}\boldsymbol{P}_1\right)^{-1}\left(1-\boldsymbol{\rho}_1^T\boldsymbol{P}_1^{-1}\boldsymbol{\rho}_1\right)\boldsymbol{\psi}_1, \tag{2.15}$$

where $\boldsymbol{\psi}_1$ is defined as

$$\boldsymbol{\psi}_1=\left[\begin{array}{ccc}\left(-\boldsymbol{P}_2^{-1}\boldsymbol{\rho}_2\right)_1 & \cdots & \left(-\boldsymbol{P}_K^{-1}\boldsymbol{\rho}_K\right)_1\end{array}\right]^T, \tag{2.16}$$

and $\boldsymbol{\Gamma}$ s defined as the $K-1\times K-1$ matrix of which the rows are given by $T_i\left\{-\boldsymbol{\rho}_i^T\boldsymbol{P}_i^{-1}\right\}$. The transformation $T_i\left\{\boldsymbol{x}^T\right\}$ removes the first element of the row-vector $\boldsymbol{x}^T$, shifts elements 2 through $i-1$ one place to the left and inserts a 1 on the now open place $i-1$. $\mathrm{LSNR}_i\triangleq\frac{a_i}{\sigma^2}\left(1-\boldsymbol{\rho}_i^T\boldsymbol{P}_i^{-1}\boldsymbol{\rho}_i\right)$,

$$\boldsymbol{Q}_1=\frac{2}{\sqrt{M}}\sum_{m=1}^{\frac{\sqrt{M}}{2}}(2m-1)c\cdot\mathrm{diag}\left(Q(\sqrt{\mathrm{LSNR}_2}(2m-1)c),\cdots,Q(\sqrt{\mathrm{LSNR}_K}(2m-1)c)\right), \tag{2.17}$$

where $Q(\cdot)$ is the error function, and

$$\boldsymbol{D}_1 = \sqrt{\frac{2}{M\pi}} \sum_{m=1}^{\frac{\sqrt{M}}{2}} \text{diag}\left(\frac{\exp\left(-\frac{1}{2}\text{LSNR}_2(2m-1)^2c^2\right)}{\sqrt{\text{LSNR}_2}}, \cdots, \frac{\exp\left(-\frac{1}{2}\text{LSNR}_K(2m-1)^2c^2\right)}{\sqrt{\text{LSNR}_K}} \right), \tag{2.18}$$

which should be recognized as an upperbound on $\boldsymbol{Q}_1$, which is tight when all LSNR_k are large. When $M = 4$ and $c = 1$ so as to achieve the same E_b/N_0 (contrary to its original definition, which achieves the same E_s/N_0) , then (2.15) reduces to the special case of BPSK, the result for which was derived in [7].

For user 1, an error occurs when the absolute value of the noise ζ_1' plus interference $\boldsymbol{\delta}_1^T \boldsymbol{A}_1 \boldsymbol{b}_1$ exceeds the threshold c (the constellation scaling factor), modified due to the channel, amplification and decorrelation by the factor $\sqrt{a_1}\left(1 - \boldsymbol{\rho}_1^T \boldsymbol{P}_1^{-1} \boldsymbol{\rho}_1 - \boldsymbol{\delta}_1^T \boldsymbol{P}_1^{-1} \boldsymbol{\rho}_1\right)$ (see (2.12)).

$$\begin{aligned} Pe_1 &= \frac{\sqrt{M}-1}{\sqrt{M} M^{\frac{K}{2}}} \sum_{\boldsymbol{b}_1} \Big(Pr\left\{ \zeta_1' > \sqrt{a_1}\left(1 - \boldsymbol{\rho}_1^T \boldsymbol{P}_1^{-1} \boldsymbol{\rho}_1 - \boldsymbol{\delta}_1^T \boldsymbol{P}_1^{-1} \boldsymbol{\rho}_1\right) c + \boldsymbol{\delta}_1^T \boldsymbol{A}_1 \boldsymbol{b}_1 \right\} + \\ &\qquad Pr\left\{ \zeta_1' < -\sqrt{a_1}\left(1 - \boldsymbol{\rho}_1^T \boldsymbol{P}_1^{-1} \boldsymbol{\rho}_1 - \boldsymbol{\delta}_1^T \boldsymbol{P}_1^{-1} \boldsymbol{\rho}_1\right) c + \boldsymbol{\delta}_1^T \boldsymbol{A}_1 \boldsymbol{b}_1 \right\} \Big) \\ &= \frac{2(\sqrt{M}-1)}{M^{\frac{K+1}{2}}} \sum_{\boldsymbol{b}_1} Q\left(\frac{\sqrt{a_1}\left(1 - \boldsymbol{\rho}_1^T \boldsymbol{P}_1^{-1} \boldsymbol{\rho}_1 - \boldsymbol{\delta}_1^T \boldsymbol{P}_1^{-1} \boldsymbol{\rho}_1\right) c + \boldsymbol{\delta}_1^T \boldsymbol{A}_1 \boldsymbol{b}_1}{\sigma\left(1 - \boldsymbol{\rho}_1^T \boldsymbol{P}_1^{-1} \boldsymbol{\rho}_1 + \boldsymbol{\delta}_1^T \boldsymbol{P}_1^{-1} \boldsymbol{\delta}_1\right)^{1/2}} \right) \end{aligned} \tag{2.19}$$

where the summation on $\boldsymbol{b}_1$ is on all possible vectors $\boldsymbol{b}_1$, whose entries are taken from the constellation set. Thus, the symbol error probability of the QAM constellation (assuming no cross-rail correlation) is given by

$$\begin{aligned} \boldsymbol{P}_{M_1} &= 1 - (1 - Pe_1)^2 \qquad (2.20) \\ &= 1 - \left(1 - \frac{2(\sqrt{M}-1)}{M^{\frac{K+1}{2}}} \sum_{\boldsymbol{b}_1} \left[Q\left(\frac{\sqrt{a_1}\left(1 - \boldsymbol{\rho}_1^T \boldsymbol{P}_1^{-1} \boldsymbol{\rho}_1 - \boldsymbol{\delta}_1^T \boldsymbol{P}_1^{-1} \boldsymbol{\rho}_1\right) c + \boldsymbol{\delta}_1^T \boldsymbol{A}_1 \boldsymbol{b}_1}{\sigma\left(1 - \boldsymbol{\rho}_1^T \boldsymbol{P}_1^{-1} \boldsymbol{\rho}_1 + \boldsymbol{\delta}_1^T \boldsymbol{P}_1^{-1} \boldsymbol{\delta}_1\right)^{1/2}} \right) \right] \right)^2 \end{aligned}$$

In figure 2.1, the case of 16-QAM is compared with BPSK for the same average energy per bit ($E_{b_1} = 8dB$). Also, for comparison, the limiting single-user performance (no MAI), and the performance as would be achieved by using the inversion decorrelator $\boldsymbol{P}^{-1}$ are shown. The figure shows the performance of user 1 in a 3 user scenario, with correlations $\rho_{12} = 3/7$, $\rho_{13} = \rho_{23} = -5/7$.

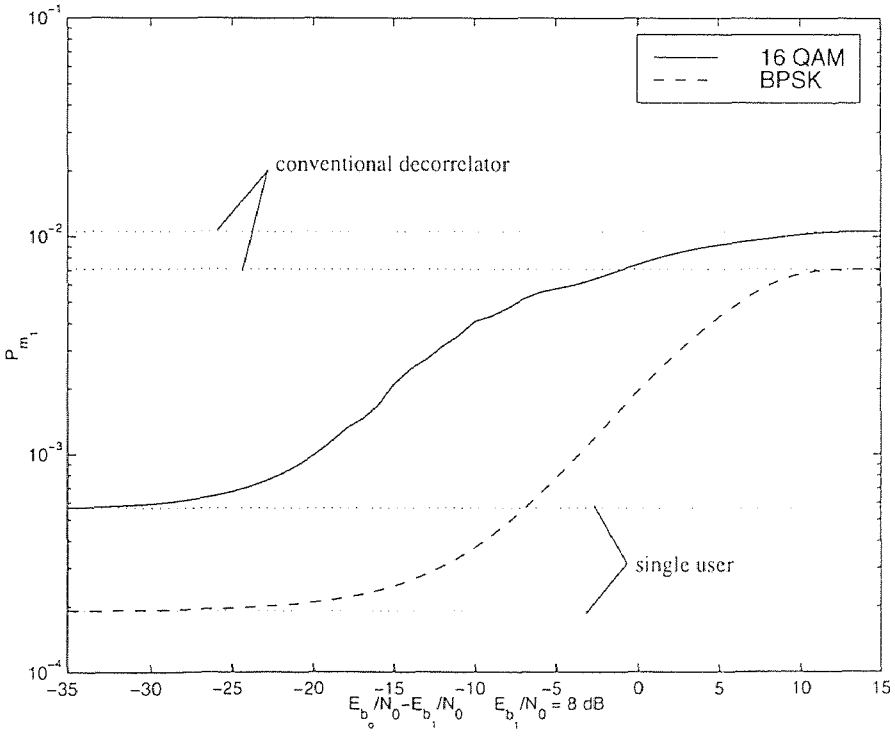

Figure 2.1 Theoretical performance comparison of 16-QAM and BPSK, three users.

In figure 2.2, the simulated performance of the bootstrap for different numbers of users in a 16-QAM modulated CDMA system, using Gold codes with a spreading gain of 15, is given.

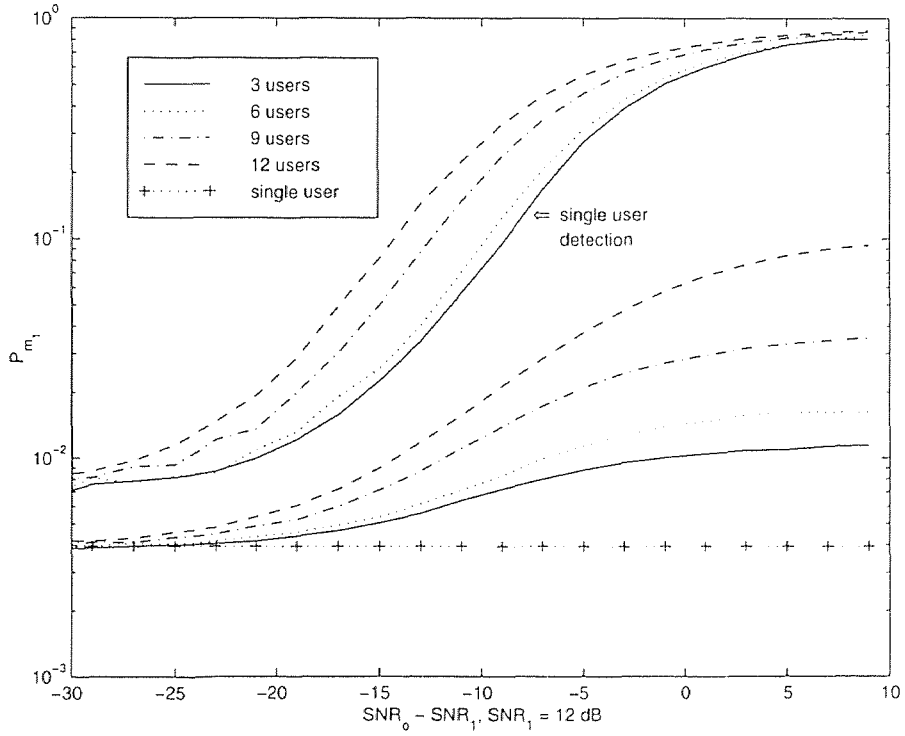

Figure 2.2 Performance of bootstrap compared to conventional detection for 16-QAM.

Extending the above to the case of non-orthogonal QAM (i.e. the case in which there is interaction between the rails of different users), can be done by expressing the system in its real representation as shown in the next section. Computing the performance of the equivalent $2K \times 2K$ system using (2.19) and combining the 2 performances of the rails of a user (under the assumption of independent errors), will result in the desired symbol error probability of this user.

2.3 The Real Bootstrap Separator for QAM Signals

For two users, the bootstrap algorithm in the real representation may be expressed as

$$\begin{bmatrix} z_{1\Re} \\ z_{1\Im} \\ z_{2\Re} \\ z_{2\Im} \end{bmatrix} = \left(\boldsymbol{I}_4 - \begin{bmatrix} 0 & w'_{11\Im} & w_{12\Re} & w'_{12\Im} \\ w_{11\Im} & 0 & w_{12\Im} & w'_{12\Re} \\ w_{21\Re} & w'_{21\Im} & 0 & w'_{22\Im} \\ w_{21\Im} & w'_{21\Re} & w_{22\Im} & 0 \end{bmatrix} \right)^T \begin{bmatrix} x_{1\Re} \\ x_{1\Im} \\ x_{2\Re} \\ x_{2\Im} \end{bmatrix}. \tag{2.21}$$

It should be noticed, that although the channel is assumed to generate no cross-correlation between the I and Q rail of the same user, we nevertheless need to include the weights $w_{ii\Im}$ and $w'_{ii\Im}$, as the bootstrap algorithm, and any other vector rotation, introduces such a correlation. Without these weights , these cross-correlations would otherwise not be taken care off. This fact can be seen for example by expanding $z_{1\Re}$ from (2.6) without the weight $w'_{ii\Im}$ (and omitting the noise terms)

$$\begin{aligned} z_{1\Re} \;=\; & \left(1 - w_{21\Re}\rho_{12\Re} + w_{21\Im}\rho_{12\Im}\right)\theta_{1\Re} + \left(\rho_{21\Re} - w_{21\Re}\right)\theta_{2\Re} - \left(\rho_{21\Im} - w_{21\Im}\right)\theta_{2\Im} \\ & - \left(w_{21\Re}\rho_{12\Im} + w_{21\Im}\rho_{21\Re}\right)\theta_{1\Im}. \end{aligned}$$

Clearly, to clean $z_{1\Re}$ from interference of the second user, the values of $w_{21\Re}$ and $w_{21\Im}$ are dictated by the second and third term, leaving the last term non-zero. This means that $z_{1\Re}$ remains a function of $\theta_{1\Im}$ and hence that there exists interference across the I and Q rails of the same user after the decorrelator. Removal of this interference will be further discussed in section 2.4.3.

The recursive weight updates for the bootstrap algorithm, which will lead to the steady state when the outputs are uncorrelated, are defined in the same way as for the BPSK bootstrap structure (see [7]):

$$\begin{aligned} w_{ij\Re} &\leftarrow w_{ij\Re} - \mu z_{j\Re}\mathrm{sgn}\left(z_{i\Re}\right) \\ w_{ij\Im} &\leftarrow w_{ij\Im} - \mu z_{j\Re}\mathrm{sgn}\left(z_{i\Im}\right) \\ w'_{ij\Re} &\leftarrow w'_{ij\Re} - \mu z_{j\Im}\mathrm{sgn}\left(z_{i\Im}\right) \\ w'_{ij\Im} &\leftarrow w'_{ij\Im} - \mu z_{j\Im}\mathrm{sgn}\left(z_{i\Re}\right) \end{aligned} \tag{2.22}$$

The factor μ is a small number, which needs to be set such that the weights are able to track changes in the channel. Weight $w_{ij\Re}$ is according to (2.21) the weight from the $i\Re^{\text{th}}$ input to the $j\Re^{\text{th}}$ output, intended to remove the interfering component $\theta_{i\Re}$ from $z_{j\Re}$. Assuming $\text{sgn}(z_{i\Re})$ is $\text{sgn}(\theta_{i\Re})$, this means that if $E\left[z_{j\Re}\text{sgn}\left(z_{i\Re}\right)\right]$ is zero, the steady state requirement for the weight $w_{ij\Re}$, then $z_{j\Re}$ must be independent from $z_{i\Re}$ and thus the decision on $z_{j\Re}$ will be (approximately) independent of $\theta_{i\Re}$. A similar reasoning can be made for the other three equations of (2.22).

It's important to emphasize that only samples of the composite signal vector are needed in the operation of the algorithm in (2.22). Neither explicit values of the amplitude of the signals nor the cross-interference matrix are required (although the signature codes are needed for the matched filters). It is also easy to conclude that if the cross-interference matrix is symbol independent (as is usually the case) then the aforementioned real bootstrap algorithm will perform the same for any M-QAM.

2.4 The "Complex Bootstrap Algorithm"

2.4.1 Decorrelator model

Instead of (2.21) we write directly in the complex domain

$$z = (I - W)^H x, \tag{2.23}$$

where $\boldsymbol{z}$ and $\boldsymbol{x}$ are K-dimensional complex vectors, $z = (z_1, \cdots, z_K)^T$ and $\boldsymbol{x} = (x_1, \cdots, x_K)^T$

$$\boldsymbol{W} = \begin{bmatrix} 0 & w_{12} & \cdots & w_{1K} \\ w_{21} & 0 & \cdots & w_{2K} \\ \vdots & & \ddots & \\ w_{K1} & & & 0 \end{bmatrix}, \tag{2.24}$$

where $\boldsymbol{W}$ is a complex matrix. Therefore,

$$z_k = x_k - \boldsymbol{w}_k^H \boldsymbol{x}_k, \tag{2.25}$$

For convenience, the same letters are used to describe complex vectors and matrices.

For the two-user case, we have from (2.25) for user 1

$$z_1 = x_1 - w_{21}^* x_2, \tag{2.26}$$

or

$$\begin{aligned} z_{1\Re} &= x_{1\Re} - w_{21\Re}x_{2\Re} - w_{21\Im}x_{2\Im} \\ z_{1\Im} &= x_{1\Im} + w_{21\Im}x_{2\Im} - w_{21\Re}x_{2\Re}. \end{aligned} \tag{2.27}$$

Comparing (2.27) and (2.21), we notice that for considering the problem in the complex domain we must take

$$\begin{aligned} w'_{21\Re} &= w_{21\Re} \\ w'_{21\Im} &= -w_{21\Im} \end{aligned} . \tag{2.28}$$

That is, $w'_{21\Re}$ and $w'_{21\Im}$ must be copies of $w_{21\Re}$ and $-w_{21\Im}$ respectively.

Substituting (2.28) in (2.22) we get

$$\begin{aligned} w_{21\Re} &\leftarrow w_{21\Re} - \mu z_{1\Re}\mathrm{sgn}\left(z_{2\Re}\right) \\ w_{21\Im} &\leftarrow w_{21\Im} - \mu z_{1\Re}\mathrm{sgn}\left(z_{2\Im}\right) \\ w_{21\Re} &\leftarrow w_{21\Re} - \mu z_{1\Im}\mathrm{sgn}\left(z_{2\Im}\right) \\ w_{21\Im} &\leftarrow w_{21\Im} + \mu z_{1\Im}\mathrm{sgn}\left(z_{2\Re}\right). \end{aligned} \tag{2.29}$$

This means that in steady state, since both $z_{1\Re}$ and $z_{1\Im}$ have the same term $w_{21\Re}x_{2\Re}$ and $x_{1\Re}$ and $x_{1\Im}$ contain the same term of $\theta_{2\Re}$, $E\left[z_{1\Re}\mathrm{sgn}\left(z_{2\Re}\right)\right]$ and $E\left[z_{1\Im}\mathrm{sgn}\left(z_{2\Re}\right)\right]$ go to zero simultaneously in order to produce $z_{1\Re}$ and $z_{1\Im}$ free from $x_{2\Re}$. Similarly $E\left[z_{1\Re}\mathrm{sgn}\left(z_{2\Im}\right)\right]$ and $E\left[z_{1\Im}\mathrm{sgn}\left(z_{2\Im}\right)\right]$ go to zero simultaneously to free $z_{1\Re}$ and $z_{1\Im}$ from the residue of $x_{2\Im}$.

We can now combine the updates of (2.29) to create fast convergence or use only half to save hardware.

Combining (2.29) we get

$$\begin{aligned} w_{21\Re} &\leftarrow w_{21\Re} - \mu\left(z_{1\Re}\mathrm{sgn}\left(z_{2\Re}\right) + z_{1\Im}\mathrm{sgn}\left(z_{2\Im}\right)\right) \\ w_{21\Im} &\leftarrow w_{21\Im} - \mu\left(z_{1\Re}\mathrm{sgn}\left(z_{2\Im}\right) - z_{1\Im}\mathrm{sgn}\left(z_{2\Re}\right)\right), \end{aligned} \tag{2.30}$$

which can be written in complex notation as

$$w_{21} \leftarrow w_{21} - \mu \left(z_1^* \mathrm{sgn}\left(z_2 \right) \right), \tag{2.31}$$

where $\mathrm{sgn}(\cdot) = \mathrm{sgn}(\Re(\cdot)) + j\mathrm{sgn}(\Im(\cdot))$.

Fig. 2.3 depicts the complex bootstrap algorithm. It should be noticed that the weights w_{ij}^* are directly calculated instead of w_{ij}, hence the seeming discrepancy between the figure and (2.31)

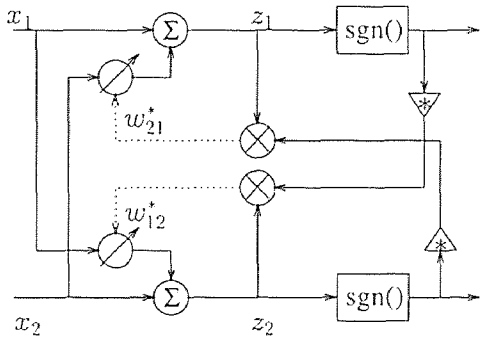

Figure 2.3 The complex bootstrap algorithm.

The real time implementation of the complex bootstrap algorithm is given in Fig. 2.4 for user 1. The same scheme must be repeated for user 2.

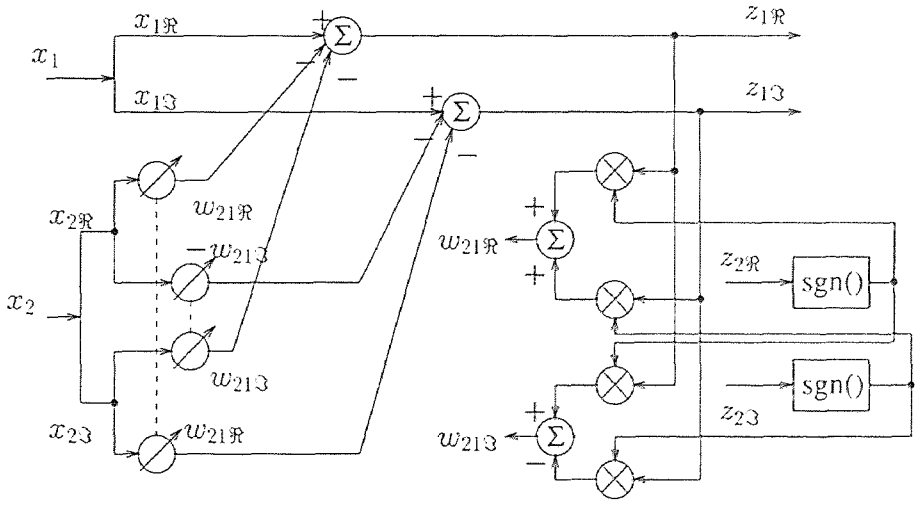

Figure 2.4 Real time implementation of the complex algorithm.

Clearly (2.30) has (in the mean) other singular points, where $\mathrm{E}\left[z_{1\Re}\mathrm{sgn}\left(z_{2\Re}\right)\right] = -\mathrm{E}\left[z_{1\Im}\mathrm{sgn}\left(z_{2\Im}\right)\right]$ or $\mathrm{E}\left[z_{1\Re}\mathrm{sgn}\left(z_{2\Im}\right)\right] = \mathrm{E}\left[z_{1\Im}\mathrm{sgn}\left(z_{2\Re}\right)\right]$ instead of having all these terms equal to zero. However, as we will show next, the algorithm of (2.31) will have a unique steady state point at which total cancellation of interference occurs, particularly, when the SNIR at $z_{2\Re}$ and $z_{2\Im}$ is sufficiently high.

From (2.31), it is quite simple to conclude the following recursion for the complex algorithm in the multi-user case.

$$\boldsymbol{w}_k(n+1) = \boldsymbol{w}_k(n) - \mu z_k^*(n)\mathrm{sgn}\left(\boldsymbol{z}_k(n)\right). \tag{2.32}$$

2.4.2 The Steady State Complex Weights

Substituting (2.3) in (2.23) we get

$$\begin{aligned} \boldsymbol{z} &= (\boldsymbol{I}-\boldsymbol{W})^H\left(\boldsymbol{P}^H\boldsymbol{\theta}+\boldsymbol{n}\right) \\ &= (\boldsymbol{I}-\boldsymbol{W})^H\boldsymbol{P}^H\boldsymbol{\theta}+\boldsymbol{\zeta}. \end{aligned} \tag{2.33}$$

Two-User Case

We first consider the two-user case:

$$\begin{bmatrix} z_1 \\ z_2 \end{bmatrix} = \begin{bmatrix} 1 & -w_{21}^* \\ -w_{12}^* & 1 \end{bmatrix}\left(\begin{bmatrix} 1 & \rho_{21}^* \\ \rho_{12}^* & 1 \end{bmatrix}\begin{bmatrix} \theta_1 \\ \theta_2 \end{bmatrix} + \begin{bmatrix} n_1 \\ n_2 \end{bmatrix}\right). \tag{2.34}$$

Therefore, for user 1

$$z_1 = \left(1 - w_{21}^*\rho_{21}^*\right)\theta_1 + \left(\rho_{21}^* - w_{12}^*\right)\theta_2 + n_1 - w_{12}^* n2, \tag{2.35}$$

Now to rid z_1 of the interference by b_2, it is required that (from (2.31))

$$\mathrm{E}\left[z_1^*\mathrm{sgn}\left(b_2\right)\right] = \mathrm{E}\left[z_1\mathrm{sgn}\left(b_2^*\right)\right] = 0, \tag{2.36}$$

If the SNIR for user two is high and the inphase-quadrature interference is sufficiently low, then $\mathrm{sgn}\left(z_2\right) \approx \mathrm{sgn}\left(b_2\right)$ Under this condition (2.36) is an approximation of

$$\mathrm{E}\left[z_1\mathrm{sgn}\left(z_2^*\right)\right] = 0, \tag{2.37}$$

By using (2.35), we get for (2.37)

$$\begin{aligned} \mathrm{E}\left[z_1 \mathrm{sgn}\left(z_2^*\right)\right] &= \mathrm{E}\left[\sqrt{a_2}\left(\rho_{21}^* - w_{21}^*\right) b_2 \mathrm{sgn}\left(b_2^*\right)\right] \\ &= \sqrt{a_2}\left(\rho_{21}^* - w_{21}^*\right)\sqrt{M}c. \end{aligned} \tag{2.38}$$

From this a unique solution follows: $\rho_{21} = w_{21}$

Multi-User Case

For the multiuser case, we note from (2.33) that the output of the detector for user k is:

$$z_k = x_k - \boldsymbol{w}_k^H \boldsymbol{x}_k + \zeta_k. \tag{2.39}$$

Now if the SNIR at any $z_j, j \neq k$ is large and the I-Q separation for all $z_j, j \neq k$ is sufficiently accurate, we have $\mathrm{sgn}\left(\boldsymbol{z}_k^*\right) \approx \mathrm{sgn}\left(\boldsymbol{b}_k^*\right)$. Thus to rid z_k of interference we use as an approximation

$$E\left[z_k \mathrm{sgn}\left(\boldsymbol{z}_k^*\right)\right] \approx E\left[z_k \mathrm{sgn}\left(\boldsymbol{b}_k^*\right)\right] = 0 \quad \text{for } k = 1, 2, \ldots, K. \tag{2.40}$$

By using (2.39) we get for (2.40):

$$E\left[\left(x_k - \boldsymbol{w}_k^H \boldsymbol{x}_k\right) \mathrm{sgn}\left(\boldsymbol{b}_k^*\right)\right] = 0 \quad \text{for } k = 1, 2, \ldots, K. \tag{2.41}$$

Also from (2.33)

$$\boldsymbol{x}_k = P_k^H A_k \boldsymbol{b}_k + \sqrt{a_k} b_k \boldsymbol{\rho}_k^* + \boldsymbol{n}_k, \tag{2.42}$$

where $\boldsymbol{\rho}_k$ is the k_{th} column of $\boldsymbol{P}$ without $\boldsymbol{P}_{kk}$, $\boldsymbol{P}_k$ and $\boldsymbol{A}_k$ are the matrices $\boldsymbol{P}$ and $\boldsymbol{A}$ respectively without the k^{th} row and columns and $\boldsymbol{n}_k$ is $\boldsymbol{n}$ without its k^{th} element.

$$\begin{aligned} E\left[x_k \mathrm{sgn}\left(\boldsymbol{z}_k^*\right)\right] &= E\left[\left(\sqrt{a_k} b_k + \boldsymbol{\rho}_k^H A_k \boldsymbol{b}_k + n_k\right) \mathrm{sgn}\left(\boldsymbol{z}_k^*\right)\right] \\ &\approx E\left[\boldsymbol{\rho}_k^H A_k \boldsymbol{b}_k \mathrm{sgn}\left(\boldsymbol{b}_k^*\right)\right] \\ &= E\left[\mathrm{sgn}\left(\boldsymbol{b}_k^*\right) \boldsymbol{b}_k^T\right] A_k \boldsymbol{\rho}_k^* \end{aligned}$$

We note that

$$E\left[\mathrm{sgn}\left(\boldsymbol{b}_k^*\right)\boldsymbol{b}_k^T\right] = E\begin{bmatrix} |b_{1\Re}|+|b_{1\Im}| & & 0 \\ & \ddots & \\ 0 & & |b_{K\Re}|+|b_{K\Im}| \end{bmatrix}_k$$
$$= \begin{bmatrix} \sqrt{M}c & & 0 \\ & \ddots & \\ 0 & & \sqrt{M}c \end{bmatrix}_k = \sqrt{M}c\boldsymbol{I}_k \tag{2.43}$$

Hence

$$E\left[x_k \mathrm{sgn}\left(\boldsymbol{z}_k^*\right)\right] \approx \sqrt{M}cA_k\boldsymbol{\rho}_k^*. \tag{2.44}$$

In the derivation above, the assumption is used that the data of the different users are uncorrelated and independent of the noise Further it was assumed that the real and imaginary part of a data symbol are uncorrelated. Also, using (2.42) we have

$$E\left[\mathrm{sgn}\left(\boldsymbol{z}_k^*\right)\boldsymbol{x}_k^T\right] = E\left[\mathrm{sgn}\left(\boldsymbol{z}_k^*\right)\left(\boldsymbol{b}_k^T A_k P_k^* + \sqrt{a_k}b_k\boldsymbol{\rho}_k^{*T} + \boldsymbol{n}_k^T\right)\right]$$
$$\approx E\left[\mathrm{sgn}\left(\boldsymbol{b}_k^*\right)\boldsymbol{b}_k^T\right]A_k P_k^*., \tag{2.45}$$

and substituting (2.43) gives

$$E\left[\mathrm{sgn}\left(\boldsymbol{z}_k^*\right)\boldsymbol{x}_k^T\right] = \sqrt{M}cA_k P_k^*. \tag{2.46}$$

Therefore, substituting (2.44) and (2.46) in (2.41) we get

$$\boldsymbol{w}_k = P_k^{-1}\boldsymbol{\rho}_k. \tag{2.47}$$

These are the steady state complex columns of the matrix $\boldsymbol{W}$, under the assumption of high interference levels, and a sufficient SNR.

2.4.3 Steady State Separator's Output and Elimination of the Resultant I-Q Interaction

For the two users case (2.47) reduces to $w_{ij} = \rho_{ij}$. Hence from (2.35), by substituting $w_{21} = \rho_{21}$, we have a total cancellation of the θ_2 term leaving

$$z_1 = (1 - \rho_{21}^* \rho_{12}^*)\,\theta_1 + n_1 - \rho_{21}^* n_2.$$

Again transforming into a real representation as in section 2 gives

$$\begin{bmatrix} z_{1\Re} \\ z_{1\Im} \end{bmatrix} = \left(\boldsymbol{I}_2 - \begin{bmatrix} \rho_{21\Re}\rho_{12\Re} - \rho_{21\Im}\rho_{12\Im} & \rho_{21\Re}\rho_{12\Im} + \rho_{21\Im}\rho_{12\Re} \\ -(\rho_{21\Re}\rho_{12\Im} + \rho_{21\Im}\rho_{12\Re}) & \rho_{21\Re}\rho_{12\Re} - \rho_{21\Im}\rho_{12\Im} \end{bmatrix} \right) \begin{bmatrix} \theta_{1\Re} \\ \theta_{1\Im} \end{bmatrix} + \begin{bmatrix} n_{1\Re} \\ n_{1\Im} \end{bmatrix} - \begin{bmatrix} \rho_{21\Re} & \rho_{21\Im} \\ -\rho_{21\Im} & \rho_{21\Re} \end{bmatrix} \begin{bmatrix} n_{2\Re} \\ n_{2\Im} \end{bmatrix}. \tag{2.48}$$

Equation (2.48) shows the generation of interaction between I and Q of channel 1. As mentioned earlier, the weights $w_{kk\Im}$ and $w'_{kk\Im}$ are introduced to eliminate this interaction.

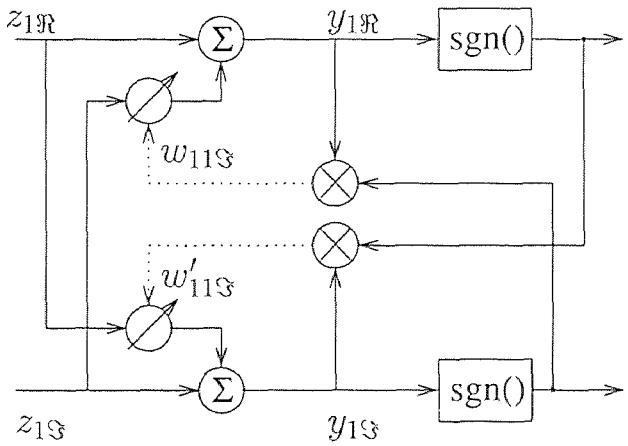

Figure 2.5 Real two signal bootstrap algorithm.

From Fig. 2.5

$$\begin{aligned} y_{1\Re} &= z_{1\Re} - w_{11\Im} z_{1\Im} \\ &= ((1-\lambda)\theta_{1\Re} - \delta\theta_{1\Im}) - w_{11\Im}\,(\delta\theta_{1\Re} + (1-\lambda)\theta_{1\Im}) + n_{1\Re} - \rho_{21\Re} n_{2\Re} - \rho_{21\Im} n_{2\Im} \end{aligned} \tag{2.49}$$

where

$$\begin{aligned}\lambda &= \rho_{21\Re}\rho_{12\Im} - \rho_{21\Im}\rho_{12\Re} \\ \delta &= \rho_{21\Re}\rho_{12\Im} + \rho_{21\Im}\rho_{12\Re}.\end{aligned} \tag{2.50}$$

The real bootstrap algorithm for controlling $w_{11\Im}$ (see (2.22)):

$$w_{11\Im} \leftarrow w_{11\Im} - \mu y_{1\Re}\mathrm{sgn}\left(y_{1\Im}\right).$$

Again, if the SNIR at $y_{1\Im}$ is high, then $\mathrm{sgn}\left(y_{1\Im}\right) \approx \mathrm{sgn}\left(b_{\Im}\right)$. At the steady state of $w_{11\Im}$ we must have

$$\mathrm{E}\left[y_{1\Re}\mathrm{sgn}\left(b_{1\Im}\right)\right] = 0,$$

But $\theta_{1\Re} = \sqrt{a_1}b_{\Re}$ is independent of $\theta_{1\Im} = \sqrt{a_1}b_{\Im}$ and of the noise, leads to

$$w_{11\Im} = -\frac{\delta}{1-\lambda} = -\frac{\rho_{21\Re}\rho_{12\Im} + \rho_{21\Im}\rho_{12\Re}}{1-\left(\rho_{21\Re}\rho_{12\Re} - \rho_{21\Im}\rho_{12\Im}\right)}. \tag{2.51}$$

Similarly

$$\begin{aligned}y_{1\Im} &= z_{1\Im} - w'_{11\Im}z_{1\Re} \\ &= \left(\delta\theta_{1\Re} + (1-\lambda)\theta_{1\Im}\right) - w'_{11\Im}\left((1-\lambda)\theta_{1\Re} - \delta\theta_{1\Im}\right) \\ &\quad + n_{1\Re} - \rho_{21\Re}n_{2\Re} - \rho_{21\Im}n_{2\Im}.\end{aligned} \tag{2.52}$$

The control $\mathrm{E}\left(y_{1\Im}\mathrm{sgn}\left(b_{1\Re}\right)\right) = 0$ will lead to

$$w'_{11\Im} = \frac{\delta}{1-\lambda} = \frac{\rho_{21\Re}\rho_{12\Im} + \rho_{21\Im}\rho_{12\Re}}{1-\left(\rho_{21\Re}\rho_{12\Re} - \rho_{21\Im}\rho_{12\Im}\right)} = -w_{11\Im}. \tag{2.53}$$

Since $\begin{bmatrix} 0 & w_{ii\Im} \\ -w_{ii\Im} & 0 \end{bmatrix}$ is equivalent to a purely imaginary weight w_{ii}, we can be apply this either in $\boldsymbol{W}$ or in a separate 2×2 real bootstrap (Fig. 2.5) after the inter-user interference canceler of Fig. 2.3.

2.4.4 Effect of Non-zero Interaction Between I and Q Channels of Each User

For this case, the incoming signal of each user can be presented as

$$s(t) = \sqrt{a}\left(b_{\Re}\cos\left(w_0 t\right) + b_{\Im}\sin\left(w_0 t\right)\right).$$

If for example the local oscillator has a phase-offset ϕ then we have

$$\begin{aligned}\begin{bmatrix}\theta_{\Re}\\ \theta_{\Im}\end{bmatrix} &= \sqrt{a}\begin{bmatrix}\cos\left(\phi\right) & \sin\left(\phi\right)\\ -\sin\left(\phi\right) & \cos\left(\phi\right)\end{bmatrix}\begin{bmatrix}b_{\Re}\\ b_{\Im}\end{bmatrix}\\ \theta &= \sqrt{a}\left(\cos\left(\phi\right) + j\sin\left(\phi\right)\right)b = \sqrt{a}e^{j\phi}b. \end{aligned} \tag{2.54}$$

Using (2.35) and the same steps as before, we end up with

$$\mathrm{E}\left[z_1^{*}\mathrm{sgn}\left(z_2\right)\right] = \sqrt{a_2}\left(\rho_{21}^{*} - w_{21}^{*}\right)\mathrm{E}\left[e^{-j\phi}b_2^{*}\mathrm{sgn}\left(e^{j\phi}b_2\right)\right] \tag{2.55}$$

which has, the same unique solution as (2.38). This means that the complex bootstrap algorithm is invariant to phase-offsets in the local oscillators. This phase-offset is subsequently eliminated by the real two signal bootstrap algorithm described in 2.4.3 (or directly in the complex bootstrap algorithm if the pure complex weights w_{ii} are added), which purpose is to rotate z_i such that no interaction between I and Q remains.

2.4.5 Complexity Comparison of Real and Complex Bootstrap Algorithm

Applying a real algorithm (i.e. splitting all K inputs into I and Q and proceed as if there were $2K$ real users), we need $2K(2K-1)$ controlled weights and $2K$ signum operators. The complex algorithm requires $4K(K-1)$ (see Fig. 2.4) plus 2K for removing the I-Q interaction. That is the same number of weights and signum operators. However, half of the weights are copies of others, allowing for a saving in hardware of $K(2K-1)$ correlators, weights and controls.

2.4.6 Adaptive Symbol Sorter

At this point, it should be noted that at the calculations in the previous section, it was assumed that the symbol decision levels are known. However, due to the decorrelator and the channel, these values are not known and have to be estimated. A practical way to do this, is to normalize the input signal to decision stage. For this, we use the adaptive scheme as shown in figure 2.6,

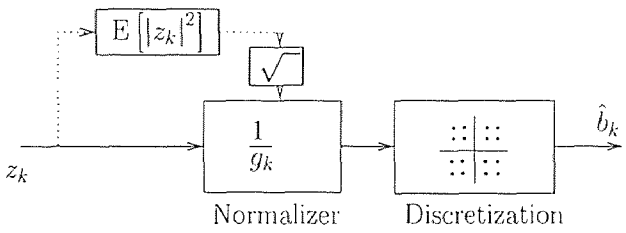

Figure 2.6 Adaptive symbol sorter.

in which

$$g_k = \sqrt{2\mathrm{E}\left[z_k^2\right]}, \tag{2.56}$$

where g_k is the estimate of the channel gain of the k^{th} user. The factor 2 stems from the fact that we normalized the constellation power to be 1, and thus each rail to have power 1/2. Notice that the input z_k here is again one rail only. If z_k is the full complex signal, then $g_k = \sqrt{\mathrm{E}\left[z_k z_k^*\right]}$, assuming the gain g_k is the same for both rails of the same user. Normalization is performed by dividing z_k by g_k corresponding to each user separately. Thus the estimate of the sorter's principle energy is made unity.

The adaptation for the i-th bit-interval is performed by

$$\widehat{\mathrm{E}\left[|z_k|\right]}(i) = (1-\mu)\cdot\widehat{\mathrm{E}\left[|z_k|\right]}(i-1) + \mu|z_k|(i)$$

which is a discrete implementation of a low-pass filter. μ is a small constant number, which should be set according to the fading properties of the channel.

2.5.6 Simulation Results

Fig. 2.7 depicts the performance of the complex bootstrap algorithm with two users 16-QAM. Note that without the separator the probability of error may go very high when interference is high, particularly for high M-QAM. For comparison, the single user (no MAI) as a lower bound, the the performance without any separation, and the complex version of the conventional decorrelator [3] are shown. The cross-coupling matrix was chosen to be

$$\begin{bmatrix} 1 & .7+.3j \\ .7+.3j & 1 \end{bmatrix}.$$

Fig. 2.8 gives results for a three user case. The cross-coupling matrix was chosen to be

$$\begin{bmatrix} 1 & .7+.3j & .5+.2j \\ .7+.3j & 1 & .2+.5j \\ .5+.2j & .2+.5j & 1 \end{bmatrix}.$$

In order to show the effect of the separator on the signal constellation, we show in Fig. 2.9 this constellation before and after the separator.

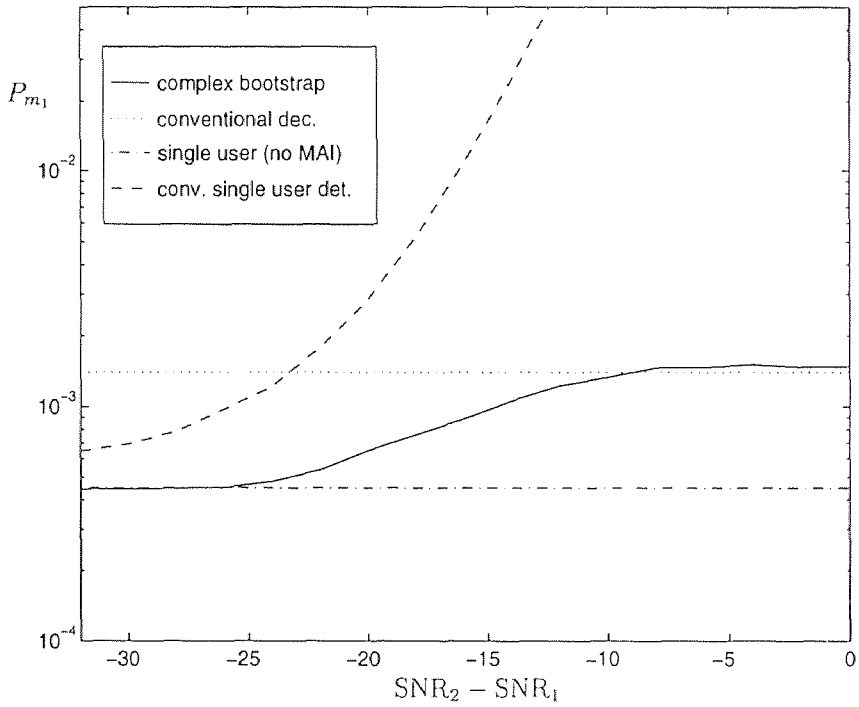

Figure 2.7 Performance of the complex bootstrap algorithm, two users 16-QAM, $\mathrm{SNR}_1 = 12\mathrm{dB/bit}$, coupling $\rho = .7 + .3j$.

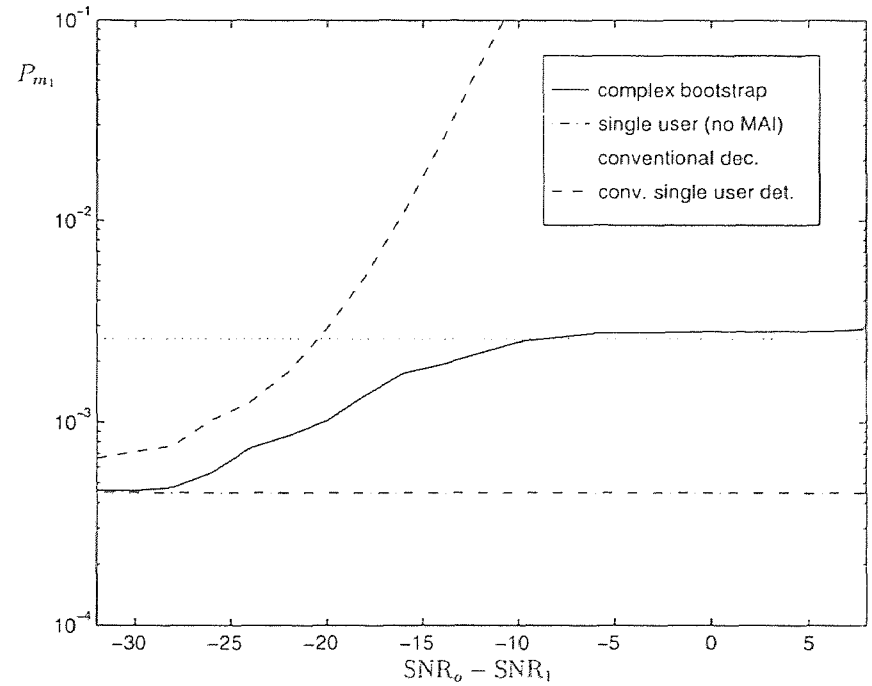

Figure 2.8 Performance of the complex bootstrap algorithm, three users $\mathrm{SNR}_1 = 12$ dB/bit.

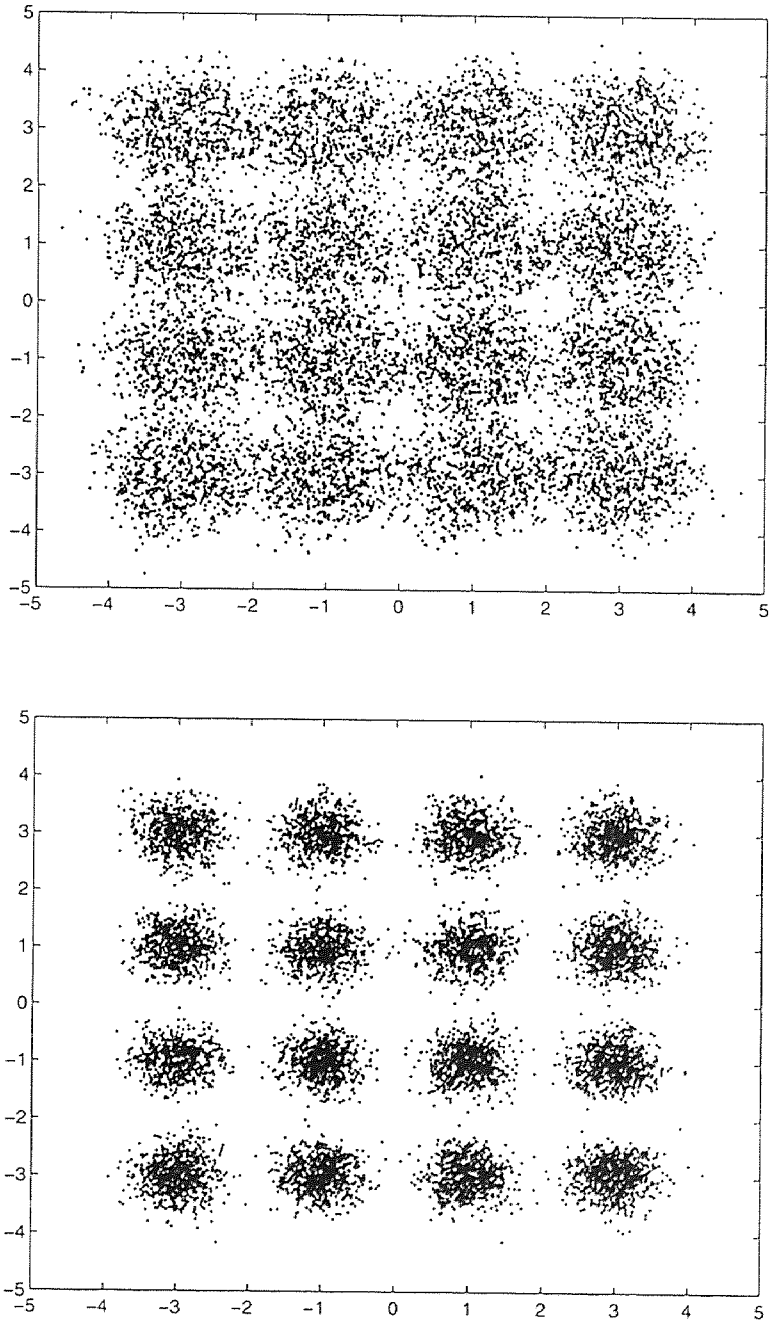

Figure 2.9 16-QAM Constellation before and after the complex bootstrap 2 users, SNR = 12dB/bit.

2.5 The Canceler Stage

As in the case of BPSK, we can use an adaptive canceler following the symbol estimator (the sorter) in order to further improve performance, particularly in the region where interference-to-desired user's SNR is high. This leads to multistage (PIC) receiver for QAM signals.

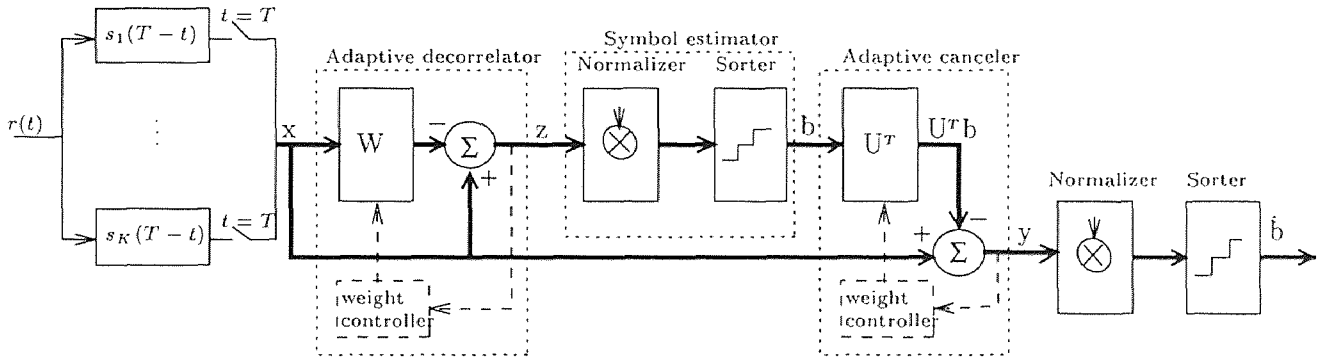

Figure 2.10 Multistage synchronous receiver.

The output of the canceler (Fig. 2.10)

$$y_k = x_k - \boldsymbol{u}_k^H \hat{\boldsymbol{b}}_k. \tag{2.57}$$

Using steepest descent algorithm in minimizing $\mathrm{E}\left[|y_k|^2\right]$ leads to

$$\begin{aligned} \boldsymbol{u}_k &= \left\{\mathrm{E}\left[\hat{\boldsymbol{b}}_k \hat{\boldsymbol{b}}_k^H\right]\right\}^{-1} \mathrm{E}\left[x_k^* \hat{\boldsymbol{b}}_k\right] \\ &= \left\{\mathrm{E}\left[\hat{\boldsymbol{b}}_k \hat{\boldsymbol{b}}_k^H\right]\right\}^{-1} \mathrm{E}\left[(\sqrt{a_k} b_k^* + \boldsymbol{\rho}_k^T \boldsymbol{A}_k \boldsymbol{b}_k^H + n_k)\hat{\boldsymbol{b}}_k\right]. \end{aligned} \tag{2.58}$$

If the linear decorrelator of [3] is used, a total separation of signals occurs at the output, so that $\mathrm{E}\left[\hat{b}_k^* \hat{\boldsymbol{b}}_k\right] = 0$ and $\mathrm{E}\left[\boldsymbol{b}_k \hat{\boldsymbol{b}}_k^H\right]$ is a diagonal matrix. This is not the case with the bootstrap decorrelator. However, simulation results showed that with either decorrelator, the probability of error of any user at the canceler outputs is almost the same. Hence, for the sake of simplicity, we will use these assumptions and we get from (2.58)

$$\boldsymbol{u}_k = \left\{\mathrm{E}\left[\hat{\boldsymbol{b}}_k \hat{\boldsymbol{b}}_k^H\right]\right\}^{-1} \boldsymbol{A}_k \mathrm{E}\left[\boldsymbol{b}_k \hat{\boldsymbol{b}}_k^H\right] \boldsymbol{\rho}_k \tag{2.59}$$

Assuming total elimination of inter-rail coupling after the decorrelator (effectively creating two PAM systems) , the terms of $\mathrm{E}\left[\hat{\boldsymbol{b}}_k\hat{\boldsymbol{b}}_k^H\right]$, $\mathrm{E}\left[\hat{b}_i\hat{b}_j^*\right]$ are given by

$$\begin{aligned}
\mathrm{E}\left[\hat{b}_i\hat{b}_j^*\right] &= \frac{2}{(\sqrt{M}-1)^2}\sum_{m=-\frac{\sqrt{M}}{2}+1}^{\frac{\sqrt{M}}{2}-2}\sum_{l=-\frac{\sqrt{M}}{2}+1}^{\frac{\sqrt{M}}{2}-2}(2m+1)(2l+1)c^2\cdot \\
&\qquad \mathrm{P_r}\left[2m<2m+1+\frac{\zeta_i}{g_ic}<2m+2,\ 2l<2l+1+\frac{\zeta_j}{g_jc}<2l+2)\right] \\
&\quad +\frac{4}{\sqrt{M}-1}\sum_{m=-\frac{\sqrt{M}}{2}+1}^{\frac{\sqrt{M}}{2}-2}(2m+1)(\sqrt{M}-1)c^2\cdot \\
&\qquad \mathrm{P_r}\left[2m<2m+1+\frac{\zeta_i}{g_ic}<2m+2,\ (\sqrt{M}-2)<(\sqrt{M}-1)+\frac{\zeta_j}{g_jc}\right] \\
&\quad +2c^2\left\{\mathrm{P_r}\left[(\sqrt{M}-2)>(\sqrt{M}-1)+\frac{\zeta_i}{g_ic},\ (\sqrt{M}-2)>(\sqrt{M}-1)+\frac{\zeta_j}{g_jc}\right]\right. \\
&\qquad \left.-\mathrm{P_r}\left[(\sqrt{M}-2)>(\sqrt{M}-1)+\frac{\zeta_i}{g_ic},\ -(\sqrt{M}-2)<-(\sqrt{M}-1)+\frac{\zeta_j}{g_jc}\right]\right\}
\end{aligned}$$

where each of the terms in the summation is an integral over a bivariate Gaussian density function. $\boldsymbol{\zeta}$ is a zero mean Gaussian random vector who's covariance matrix is $\mathrm{N}_0(\boldsymbol{P}+\boldsymbol{P}^H)^{-1}$. Also, for $\sqrt{M}$-PAM

$$\begin{aligned}
\mathrm{E}\left[b_i\hat{b}_i\right] &= \frac{1}{\sqrt{M}}\sum_{i,j}b_ib_j\mathrm{P_r}\left[b_j|bi,b_j=\hat{b}_i\right] \\
&= \frac{2}{\sqrt{M}}\sum_{m=0}^{\frac{\sqrt{M}}{2}-1}\sum_{l=-\frac{\sqrt{M}}{2}+1}^{\frac{\sqrt{M}}{2}-2} \\
&\qquad (2m+1)(2l+1)c^2\mathrm{P_r}\left[2l<2m+1+\frac{\zeta_i}{g_ic}<2l+2\right] \\
&\qquad +(2m+1)(\sqrt{M}-1)c^2\cdot\left\{\mathrm{P_r}\left[(2m+1)+\frac{\zeta_i}{g_ic}>(\sqrt{M}-2)\right]\right. \\
&\qquad\qquad \left.-\mathrm{P_r}\left[2m+1+\frac{\zeta_i}{g_ic}<-(\sqrt{M}-2)\right]\right\}
\end{aligned}$$

and hence under the assumption of a total lack of inter-rail coupling, for M-QAM, $\mathrm{E}\left[b_i^*\hat{b}_i\right]$ is twice the above due to the two rails.

One can show that the probability of error at $\hat{\hat{b}}_k$ is given by

$$
\begin{aligned}
P_{\mathrm{m}_k} = & \; 1 - \left\{ 1 - \mathrm{E}_{b_k, \boldsymbol{b}_k, \hat{b}_k} \mathrm{P_r} \left[\hat{\hat{b}}_{k\Re} \text{ in error} / b_k, \boldsymbol{b}_k, \hat{b}_k \right] \right\}^2 \\
= & 1 - \left\{ 1 - \frac{1}{M^{(K-1)}} \sum_{\boldsymbol{b}_k \hat{\boldsymbol{b}}_k} \mathrm{P_r} \left[\hat{\boldsymbol{b}}_k | \boldsymbol{b}_k \right] \cdot \right. \\
& \left(\mathrm{P_r} \left[\sum_{l=0}^{\sqrt{M}-2} 2l\sqrt{a_k} - v_{k\Re} < n_{k\Re} < 2(l+1)\sqrt{a_k} - v_{k\Re} \right] \right. \\
& \left. \left. + \mathrm{P_r} \left[(\sqrt{M-1})\sqrt{a_k} - v_{k\Re} < n_{k\Re} \right] \right) \right\}^2
\end{aligned}
$$

where $v_k = \boldsymbol{\rho}_k^H \boldsymbol{A}_k \boldsymbol{b}_k - \boldsymbol{u}_k^H \hat{\boldsymbol{b}}_k$. The conditional probability $\mathrm{P_r}\left[\hat{\boldsymbol{b}}_k | \boldsymbol{b}_k\right]$ is the integral of the $2(K-1)$-variate Gaussian density, specified in detail in [16]

In figure 2.5, the performance of the multistage receiver with 4,6, and 8 users, 16 QAM modulated, is shown, assuming no inter-rail interference and implemented with the real bootstrap decorrelator. As comparison, the performance of the conventional decorrelator only is provided, as well as the single-user (no MAI) lower bound.

In figure 2.12 the multistage receiver that uses the complex bootstrap described in section 2.5 is presented. For the three users, cross-correlations of $0.7 + 03j$ and $0.5 + 0.2j$ were assumed with 16-QAM modulation as in the previous section. For comparison, we again add the probability of error at the output of the matched filter (conventional single user detection) and with single user (no MAI). We also add a curve obtained by using $\boldsymbol{P}^{-H}$ (conventional decorrelator).

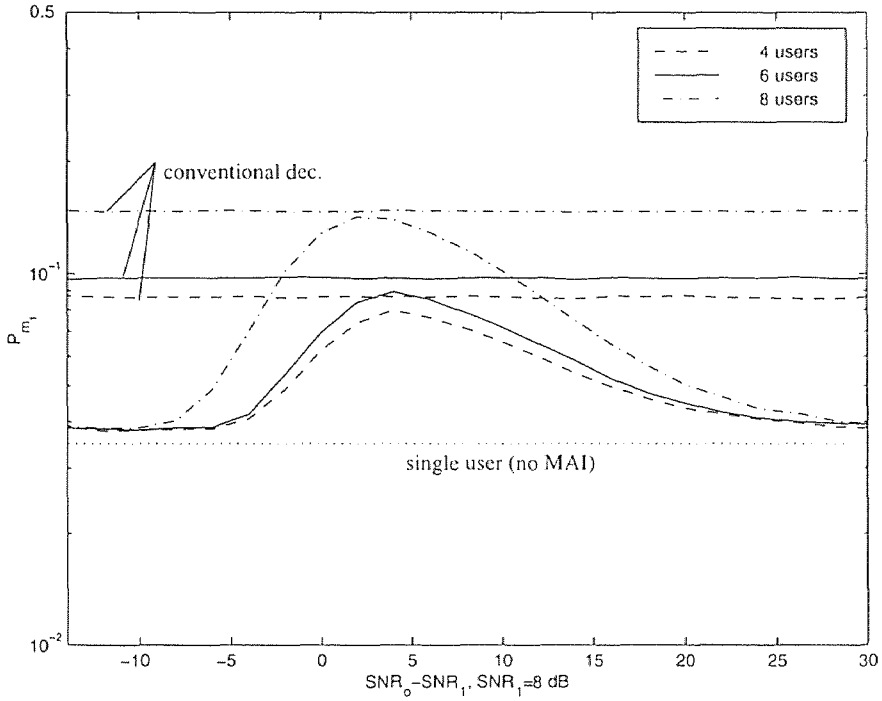

Figure 2.11 Performance of (multistage) receiver using 'real' bootstrap, compared to conventional decorrelator.

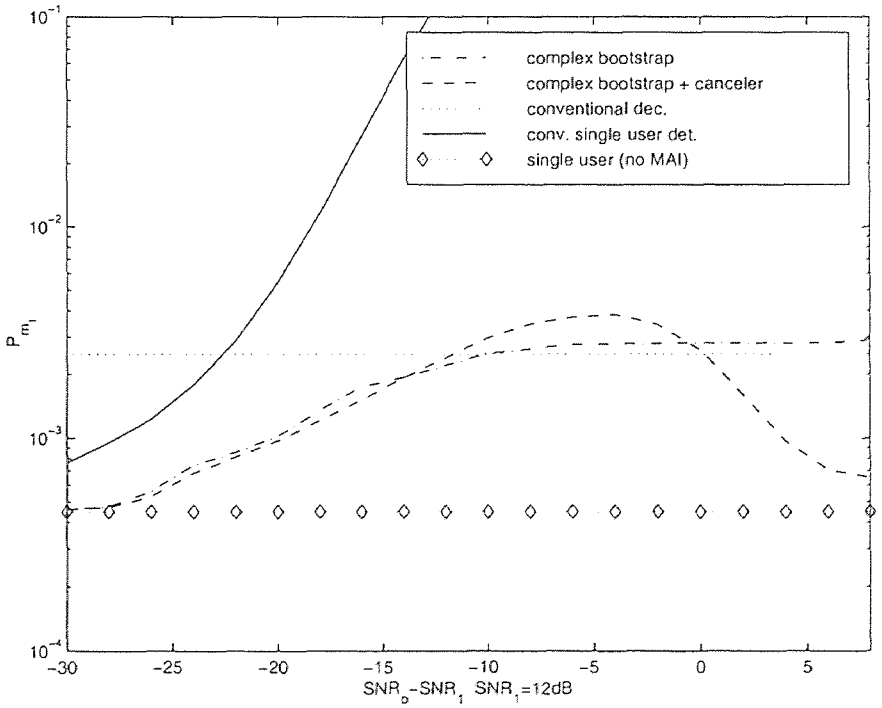

Figure 2.12 Performance comparison of (multistage) receiver using complex bootstrap, three user case.

CHAPTER 3
ONE-SHOT CDMA RECEIVER FOR DISPERSIVE CHANNELS

In a wireless system, both indoors and outdoors, a signal sent from a transmitter generally arrives at the receiver though a large number of paths. Apart from the direct line of sight path (if existent), signals can arrive at the receiver due to reflection from obstacles. Because the length of the paths traversed by the signal are different, the time of incident at the receiver will be different for each path. When the relative delay between signals from different paths is large enough, particularly if it is larger than the coherence time, these paths can be resolved. In combining the additional energy contained in these paths, and thus obtaining additional information, the performance of the receiver increases. The effects of a multi-path channel are however the creation of a number of extra interference sources. For the (synchronous) downlink channel without dispersion, interference solely consists of terms related to the simultaneously transmitted symbols of other users (Multi-Access Interference (MAI)). If the channel is dispersive however, this MAI will contain extra terms from the previous and following symbols of these other users, equivalent to an asynchronous channel (with or without dispersion).

Also, a dispersive channel causes interference by each user to itself. This does not only consist of Inter Symbol Interference (ISI), but also of interference between the signals of the same symbol on different paths, which we will term Self-Interference (SI) for convenience. This SI can be both constructive and destructive. This effect will be explained in more detail in the next section.

Typically, if the dispersion is only a few chips, and the code-length significantly long, the ISI and adjacent symbol MAI can be neglected in the downlink. This case is further examined in chapter 6.

In this chapter, an extension of the one-shot asynchronous bootstrap algorithm [2] is presented, which is suited for dispersive channels. The idea is to separate

the user's paths, treating each path principally as if it is a separate user with its corresponding partial code. However, it should be noted that decorrelating signals from one user carrying the same data-symbol is not possible as the data on each path is the same. This is true for any decorrelator which doesn't assume the correlations to be known, including the bootstrap.

3.1 One-shot Matched Filtering

Representing the received signal from (1.1) in one-shot of (i.e. synchronous to) the first path of the i^{th} bit of user one, and without loss of generality, letting $i = 0$:

$$\begin{aligned} r(t) &= \sqrt{a_{11}}s_1(t)b_1(0) + n(t) + \\ &\sum_{k=1}^{K}\sum_{m=1}^{M}\sqrt{a_{km}\epsilon_{km}}\frac{1}{\sqrt{\epsilon_{km}}}s_k^{m\mathrm{L}}(t)b_k(-1) + \\ &\sum_{k=1}^{K}\sum_{m=1}^{M}\sqrt{a_{km}(1-\epsilon_{km})}\frac{1}{\sqrt{1-\epsilon_{km}}}s_k^{m\mathrm{R}}(t)b_k(0) \end{aligned} \tag{3.1}$$

where it is assumed that $0 \leq \tau_{km} \leq T \quad \forall\ k, m$ [1], which means that all delays are assumed to be shorter than one symbol interval, and

$$\begin{aligned} s_k^{m\mathrm{L}}(t) &= \begin{cases} s_k(t+T-\tau_{km}) & 0 \leq t \leq \tau_{km} \\ 0 & \tau_{km} < t \leq T \end{cases} \\ s_{km}^{\mathrm{R}}(t) &= \begin{cases} 0 & 0 \leq t \leq \tau_{km} \\ s_k(t-\tau_{km}) & \tau_{km} < t \leq T \end{cases} \\ \epsilon_{km} &= \int_0^{\tau_{km}} s_k^2(t-\tau_{km})dt \end{aligned}$$

for all k, m except $s_1^{1\mathrm{L}}(t) = s_1^{1\mathrm{R}}(t) = 0$.

An example of one-shot timing (synchronized to the first path of the first user) is given in Fig. 3.1. In this figure, the total received signal of 2 users, each with 3 paths, is split up per path.

The received signal is fed into a matched filter bank, in which one filter is matched to the left and right part of each path, [2] except for that matched to the

[1] This assumption can be released without much effort

[2] We will use left path (signal), or left part of the path (signal), losely to indicate the time interval $[T-\tau_{km}, T]$ of the bit carried by this path and spreaded by the corresponding

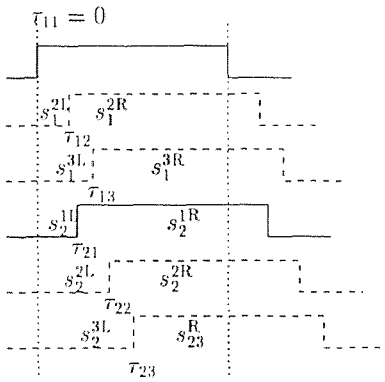

Figure 3.1 One-shot timing.

first path of the first user. Since we match synchronously to the first path of an arbitrary first user, a total of $2KM-1$ matched filters is needed. The structure of this matched filter bank is shown in Fig. 3.2.

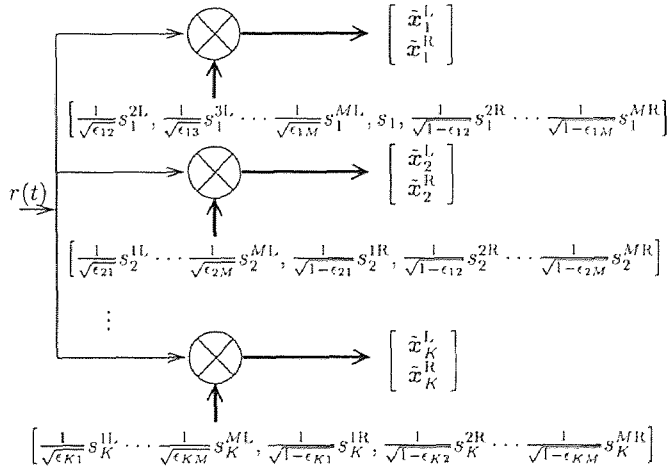

Figure 3.2 Matched filter scheme.

The outputs of the matched filters are ordered:

$$x=\left[\tilde{x}_1^{L\,T},\tilde{x}_1^{R\,T},\cdots,\tilde{x}_K^{L\,T},\tilde{x}_K^{R\,T}\right]^T, \tag{3.2}$$

partial signature codes. Similarly for the right path etc., which indicate the time interval $[0,T-\tau_{km}]$.

where each vector $\tilde{\boldsymbol{x}}_k^{\mathrm{L}} = \left[x_k^{1\mathrm{L}}, x_k^{2\mathrm{L}} \cdots x_k^{M\mathrm{L}}\right]^T$ contains all matched filter outputs for the left parts of user k's signal. $\tilde{\boldsymbol{x}}_k^{\mathrm{R}}$ is similarly defined for the right parts. Since we synchronized to the first path of user 1, this path has no left side and hence $\tilde{\boldsymbol{x}}_1^{\mathrm{L}}$ is $M-1$ dimensional.

Defining the correlation coefficients

$$\begin{aligned}
\rho_{1k}^{m\mathrm{L}} &= \frac{1}{\sqrt{\epsilon_{km}}} \int_0^T s_1(t) s_k^{m\mathrm{L}}(t) dt, \\
\rho_{1k}^{m\mathrm{R}} &= \frac{1}{\sqrt{1-\epsilon_{km}}} \int_0^T s_1(t) s_k^{m\mathrm{R}}(t) dt, \\
\rho_{lk}^{mLnL} &= \frac{1}{\sqrt{\epsilon_{lm}\epsilon_{kn}}} \int_0^T s_l^{m\mathrm{L}}(t) s_k^{n\mathrm{L}}(t) dt \\
\rho_{lk}^{mRnR} &= \frac{1}{\sqrt{(1-\epsilon_{lm})(1-\epsilon_{kn})}} \int_0^T s_l^{m\mathrm{R}}(t) s_k^{n\mathrm{R}}(t) dt \qquad (3.3) \\
\rho_{lk}^{m\mathrm{L}n\mathrm{R}} &= \frac{1}{\sqrt{\epsilon_{lm}(1-\epsilon_{kn})}} \int_0^T s_l^{m\mathrm{L}}(t) s_k^{n\mathrm{R}}(t) dt \\
\rho_{lk}^{m\mathrm{R}n\mathrm{L}} &= \frac{1}{\sqrt{(1-\epsilon_{lm})\epsilon_{kn}}} \int_0^T s_l^{m\mathrm{R}}(t) s_k^{n\mathrm{L}}(t) dt,
\end{aligned}$$

where $k, l = 1, 2, \ldots, K$, and $m, n = 1, 2, \ldots, M$, $\rho_{kl}^{m\mathrm{R}n\mathrm{L}}$ is the correlation of the right part of path m of user k with the left part of path n of user l etc. Also $\rho_{kl}^{m\mathrm{R}}$ and $\rho_{1k}^{m\mathrm{L}}$ are the correlations of the first path of the first user and the m^{th} path of the k^{th} user.

In matrix notation, the output of the matched filter bank can be written as

$$\boldsymbol{x}(0) = \boldsymbol{P}\boldsymbol{A}\boldsymbol{b}(0) + \boldsymbol{n}(0), \qquad (3.4)$$

where

$$\boldsymbol{P}=\begin{bmatrix}
1 & \cdots & \rho_{11}^{2\mathrm{L}ML} & \rho_{11}^{2\mathrm{L}} & \cdots & \rho_{11}^{2\mathrm{L}MR} & \rho_{12}^{2\mathrm{L}1\mathrm{L}} & \cdots & \rho_{12}^{2\mathrm{L}ML} & \rho_{12}^{2\mathrm{L}1\mathrm{R}} & \cdots & \rho_{12}^{2\mathrm{L}MR} & & \rho_{1K}^{2\mathrm{L}MR} \\
\vdots & \ddots & \vdots & \vdots & & \vdots & \vdots & & \vdots & \vdots & & \vdots & \cdots & \vdots \\
\rho_{11}^{ML2\mathrm{L}} & \cdots & 1 & \rho_{11}^{ML} & \cdots & \rho_{11}^{MLMR} & \rho_{12}^{ML1\mathrm{L}} & \cdots & \rho_{12}^{MLML} & \rho_{12}^{ML1\mathrm{R}} & \cdots & \rho_{12}^{MLMR} & & \rho_{1K}^{MLMR} \\
\rho_{11}^{2\mathrm{L}} & \cdots & \rho_{11}^{ML} & 1 & \cdots & \rho_{11}^{MR} & \rho_{12}^{1\mathrm{L}} & \cdots & \rho_{12}^{ML} & \rho_{12}^{1\mathrm{R}} & \cdots & \rho_{12}^{MR} & & \rho_{1K}^{MR} \\
\vdots & & \vdots & \vdots & \ddots & \vdots & \vdots & & \vdots & \vdots & & \vdots & \cdots & \vdots \\
\rho_{11}^{MR2\mathrm{L}} & \cdots & \rho_{11}^{MRML} & \rho_{11}^{MR} & \cdots & 1 & \rho_{12}^{MR1\mathrm{L}} & \cdots & \rho_{12}^{MRML} & \rho_{12}^{MR1\mathrm{R}} & \cdots & \rho_{12}^{MRMR} & & \rho_{1K}^{MRMR} \\
\rho_{21}^{1\mathrm{L}2\mathrm{L}} & \cdots & \rho_{21}^{1\mathrm{L}ML} & \rho_{21}^{1\mathrm{L}} & \cdots & \rho_{21}^{1\mathrm{L}MR} & 1 & \cdots & \rho_{22}^{1\mathrm{L}ML} & \rho_{22}^{1\mathrm{L}1\mathrm{R}} & \cdots & \rho_{22}^{1\mathrm{L}MR} & & \rho_{1K}^{MLMR} \\
\vdots & & \vdots & \vdots & & \vdots & \vdots & \ddots & \vdots & \vdots & & \vdots & \cdots & \vdots \\
\rho_{21}^{ML2\mathrm{L}} & \cdots & \rho_{21}^{MLML} & \rho_{21}^{ML} & \cdots & \rho_{21}^{MLMR} & \rho_{22}^{MLML} & \cdots & 1 & \rho_{22}^{ML1\mathrm{R}} & \cdots & \rho_{22}^{MLMR} & & \rho_{1K}^{MLMR} \\
\rho_{21}^{1\mathrm{R}2\mathrm{L}} & \cdots & \rho_{21}^{1\mathrm{L}ML} & \rho_{21}^{1\mathrm{R}} & \cdots & \rho_{21}^{1\mathrm{R}1\mathrm{R}} & \rho_{22}^{1\mathrm{R}1\mathrm{L}} & \cdots & \rho_{22}^{1\mathrm{R}ML} & 1 & \cdots & \rho_{22}^{1\mathrm{R}MR} & & \rho_{1K}^{MRMR} \\
\vdots & & \vdots & \vdots & & \vdots & \vdots & & \vdots & \vdots & \ddots & \vdots & \cdots & \vdots \\
\rho_{21}^{MR2\mathrm{L}} & \cdots & \rho_{21}^{MLML} & \rho_{21}^{MR} & \cdots & \rho_{21}^{MRMR} & \rho_{22}^{MR1\mathrm{L}} & \cdots & \rho_{22}^{MRML} & \rho_{22}^{MR1\mathrm{R}} & \cdots & 1 & & \rho_{1K}^{MRMR} \\
& \vdots & & & \vdots & & & \vdots & & & \vdots & & \ddots & \vdots \\
\rho_{K1}^{MR2\mathrm{L}} & \cdots & \rho_{K1}^{MRML} & \rho_{K1}^{MR} & \cdots & \rho_{K1}^{MRMR} & \rho_{K2}^{ML1\mathrm{L}} & \cdots & \rho_{K2}^{MLML} & \rho_{K2}^{ML1\mathrm{R}} & \cdots & \rho_{K2}^{MLMR} & & 1
\end{bmatrix}$$

The input data vector is defined as

$$\boldsymbol{b}^T(0)=\left[\boldsymbol{b}_1^T(-1),\boldsymbol{b}_1^T(0),\boldsymbol{b}_2^T(-1),\cdots,\boldsymbol{b}_K^T(0)\right],$$

where each vector $\boldsymbol{b}_k(-1)$ and $\boldsymbol{b}(0)$ contains M copies of $b_k(-1)$, and $b_k(0)$ respectively, with the exception of $\boldsymbol{b}_1(-1)$, which contains only $M-1$ copies. Also defined is a diagonal matrix

$$\boldsymbol{A}=\mathrm{diag}[\boldsymbol{\alpha}_1^{\mathrm{L}},\boldsymbol{\alpha}_1^{\mathrm{R}},\boldsymbol{\alpha}_2^{\mathrm{L}},\boldsymbol{\alpha}_2^{\mathrm{R}}\cdots,\boldsymbol{\alpha}_K^{\mathrm{L}},\boldsymbol{\alpha}_K^{\mathrm{R}}]$$

with $\boldsymbol{\alpha}_k^{\mathrm{R}};\ k=1,\cdots K$, a $M\times M$ diagonal matrix containing respectively $\sqrt{a_{km}(1-\epsilon_{km})},\ m=1\cdots M$, while $\boldsymbol{\alpha}_k^{\mathrm{L}}$ contains the elements respectively equal $\sqrt{a_{km}(\epsilon_{km})}$, except that $\boldsymbol{\alpha}_1^{\mathrm{L}}$ is $M-1\times M-1$ containing the elements $\sqrt{a_{1m}(\epsilon_{1m})}$, $m=2\cdots M$. Finally $\boldsymbol{n}(0)$ is a zero-mean Gaussian vector with covariance $\boldsymbol{P}N_0/2$. Corresponding to the block vector (3.2), $\boldsymbol{P}$ is divided into block matrices as follows

$$\boldsymbol{P}=\begin{bmatrix}
\tilde{P}_{1\mathrm{L},1\mathrm{L}} & \tilde{P}_{1\mathrm{L},1\mathrm{R}} & \cdots & \tilde{P}_{1\mathrm{L},K\mathrm{L}} & \tilde{P}_{1\mathrm{L},K\mathrm{R}} \\
\tilde{P}_{1\mathrm{R},1\mathrm{L}} & \tilde{P}_{1\mathrm{R},1\mathrm{R}} & \cdots & \tilde{P}_{1\mathrm{R},K\mathrm{L}} & \tilde{P}_{K\mathrm{R},1\mathrm{R}} \\
\vdots & & \ddots & & \vdots \\
\tilde{P}_{K\mathrm{L},1\mathrm{L}} & \tilde{P}_{K\mathrm{L},1\mathrm{R}} & \cdots & \tilde{P}_{K\mathrm{L},K\mathrm{L}} & \tilde{P}_{K\mathrm{L},K\mathrm{R}} \\
\tilde{P}_{K\mathrm{R},1\mathrm{L}} & \tilde{P}_{K\mathrm{R},1\mathrm{R}} & \cdots & \tilde{P}_{K\mathrm{R},K\mathrm{L}} & \tilde{P}_{K\mathrm{R},K\mathrm{R}}
\end{bmatrix} \tag{3.5}$$

where the block matrices are defined as follows:

$$\tilde{P}_{1\mathrm{L},l\mathrm{R}} = \begin{bmatrix} \rho_{11}^{2\mathrm{L}} & 0 & \rho_{11}^{2\mathrm{L}3\mathrm{R}} & \cdots & \rho_{11}^{2\mathrm{L}M\mathrm{R}} \\ \rho_{11}^{3\mathrm{L}} & \rho_{11}^{3\mathrm{L}2\mathrm{R}} & 0 & & \rho_{11}^{3\mathrm{L}M\mathrm{R}} \\ \vdots & & \ddots & & \\ \rho_{11}^{M\mathrm{L}} & \rho_{11}^{M\mathrm{L}2\mathrm{R}} & & \cdots & \rho_{11}^{M\mathrm{L}M\mathrm{R}} \end{bmatrix}_{(M-1)\times M} \quad \tilde{P}_{1\mathrm{L},1\mathrm{L}} = \begin{bmatrix} 1 & \rho_{11}^{2\mathrm{L}3\mathrm{L}} & \cdots & \rho_{11}^{2\mathrm{L}M\mathrm{L}} \\ \rho_{11}^{3\mathrm{L}2\mathrm{L}} & 1 & & \\ \vdots & & \ddots & \\ \rho_{11}^{M\mathrm{L}2\mathrm{L}} & \cdots & & 1 \end{bmatrix}_{(M-1)\times(M-1)}$$

$$\underset{\substack{\mathrm{G}=\mathrm{L}\text{ or }\mathrm{R}\\ k=2\cdots K}}{\tilde{P}_{1\mathrm{L},k\mathrm{G}}} = \begin{bmatrix} \rho_{1k}^{2\mathrm{L}1\mathrm{G}} & \rho_{1k}^{2\mathrm{L}2\mathrm{G}} & \cdots & \rho_{1k}^{2\mathrm{L}M\mathrm{G}} \\ \rho_{1k}^{3\mathrm{L}1\mathrm{G}} & \rho_{1k}^{3\mathrm{L}2\mathrm{G}} & & \rho_{1k}^{3\mathrm{L}M\mathrm{G}} \\ \vdots & & & \\ \rho_{1k}^{M\mathrm{L}1\mathrm{G}} & \rho_{1k}^{M\mathrm{L}2\mathrm{G}} & \cdots & \rho_{1k}^{M\mathrm{L}M\mathrm{G}} \end{bmatrix}_{(M-1)\times M} \quad \underset{\substack{\mathrm{G}=\mathrm{L}\text{ or }\mathrm{R}\\ k=2\cdots K}}{\tilde{P}_{1\mathrm{R},k\mathrm{G}}} = \begin{bmatrix} \rho_{1k}^{1\mathrm{G}} & \rho_{1k}^{2\mathrm{G}} & \cdots & \rho_{1k}^{M\mathrm{G}} \\ \rho_{1k}^{2\mathrm{R}1\mathrm{G}} & \rho_{1k}^{2\mathrm{R}2\mathrm{G}} & & \rho_{1k}^{2\mathrm{R}M\mathrm{G}} \\ \vdots & & & \\ \rho_{1k}^{M\mathrm{R}1\mathrm{G}} & \rho_{1k}^{M\mathrm{R}2\mathrm{G}} & \cdots & \rho_{1k}^{M\mathrm{R}M\mathrm{G}} \end{bmatrix}_{M\times M}$$

$$\tilde{P}_{1\mathrm{R},1\mathrm{R}} = \begin{bmatrix} 1 & \rho_{11}^{2\mathrm{R}} & \cdots & \rho_{11}^{M\mathrm{R}} \\ \rho_{11}^{2\mathrm{R}} & 1 & & \rho_{11}^{2\mathrm{R}2\mathrm{R}} \\ \vdots & & \ddots & \\ \rho_{11}^{M\mathrm{R}} & \rho_{11}^{M\mathrm{R}2\mathrm{R}} & & 1 \end{bmatrix}_{M\times M} \quad \underset{\substack{\mathrm{G},\mathrm{H}=\mathrm{L}\text{ or }\mathrm{R}\\ \mathrm{k},\mathrm{l}=2\cdots\mathrm{K}}}{\tilde{P}_{1\mathrm{G},k\mathrm{H}}} = \begin{bmatrix} \rho_{kl}^{1\mathrm{G}1\mathrm{H}} & \cdots & \rho_{kl}^{1\mathrm{G}M\mathrm{H}} \\ \vdots & & \\ \rho_{kl}^{M\mathrm{G}1\mathrm{H}} & \cdots & \rho_{kl}^{M\mathrm{G}M\mathrm{H}} \end{bmatrix}_{M\times M}$$

It should be noticed that these matrices are not all sized $M \times M$ due to the fact that the rows and columns pertaining to the left part of the first user should be omitted. This is due to the synchronous matching to this path, hence the left part does not exist, and the synchronously matched result is considered the right part.

In Appendix B.1, the above definitions are applied to a two user case with two paths per channel to provide some additional clarity.

The off-diagonal elements in the blocks $\tilde{P}_{k\mathrm{L},k\mathrm{L}}\boldsymbol{\alpha}_k^{\mathrm{L}}$ and $\tilde{P}_{k\mathrm{R},k\mathrm{R}}\boldsymbol{\alpha}_k^{\mathrm{R}}$ represent the aforementioned SI, which essentially is the interference between the same parts of the paths of the same user. This interference can not be canceled as the data on these path-parts, $\boldsymbol{b}_k^T(-1)$ and $\boldsymbol{b}_k^T(0)$ respectively, is exactly the same. The total self-interference on a path-part after the matched filters is thus given by the sum of the off-diagonal elements of a row of these blocks.

As a simple example, consider a single user with a two-path channel, while for simplicity omitting a left or right subscript, with correlations ρ_1 and ρ_2 (i.e.

$\tilde{P} = \begin{bmatrix} 1 & \rho_1 \\ \rho_2 & 1 \end{bmatrix}$) and amplitudes α_1 and α_2 ($\boldsymbol{\alpha} = \begin{bmatrix} \alpha_1 & 0 \\ 0 & \alpha_2 \end{bmatrix}$). Now at the output of the filter matched to the first partial code, we get $(\alpha_1 + \rho\alpha_2)b$. The SI here is thus $\rho\alpha_2$, which is constructive if ρ is positive, yet destructive when ρ is negative. As will be shown later, the self-interference is modified by the application of the bootstrap decorrelator. For example if the ISR is very high, (3.15) shows the self-interference term to become

$$\left(\tilde{P}_k^{\mathrm{R}} - \boldsymbol{\rho}_k^{\mathrm{R}^T} \boldsymbol{P}_k^{\mathrm{R}^{-T}} \boldsymbol{\rho}_k^{\mathrm{R}}\right) \boldsymbol{\alpha}_k^{\mathrm{R}}.$$

In a dispersive downlink, in which the delays for the m^{th} path of each user are the same (see (1.1)), the rows and columns in $\boldsymbol{W}$ pertaining to the left part of the paths with relative delay 0 should be removed. This should also been done in creating the matrix P, necessary for the conventional detector, as it would otherwise contain rows with all zeroes, which obviously makes the matrix singular, and hence not invertable. Other than this, the correlation coefficients $\rho_{kl}^{m\mathrm{L}m\mathrm{R}}$ and $\rho_{kl}^{m\mathrm{R}m\mathrm{L}}$, $\forall k, l \in 1 \cdots K$ will become zero, which has however no effect on the structure of the decorrelator. The same is true in the uplink case where the relative delay of a path of another user but the one matched to synchronously, is zero.

3.2 The Decorrelator

To the output of the matched filter bank we apply a linear transformation to separate the signals.

$$z = Vx$$

For the transformation, a modified version of the Bootstrap decorrelator [2], and for comparison the conventional decorrelator, which implements the inverse of the $(2KM - 1 \times 2KM - 1)$ partial cross-correlation matrix ($V = P^{-1}$) is used. This "modified bootstrap decorrelator", which will take into consideration the correlation

data in different paths, has the form

$$\boldsymbol{V} = \boldsymbol{I} - \boldsymbol{W}^T \tag{3.6}$$

where $\boldsymbol{I}$ is the identity matrix and

$$\boldsymbol{W} = \begin{bmatrix} & & & w_{11}^{2\mathrm{L}} \cdots w_{11}^{2\mathrm{L}MR} & w_{12}^{2\mathrm{L}1\mathrm{L}} \cdots w_{1K}^{2\mathrm{L}MR} \\ & \mathbf{0} & & \vdots \quad\quad \vdots & \vdots \quad\quad \vdots \\ & & & w_{11}^{ML} \cdots w_{1K}^{MLMR} & w_{12}^{ML1\mathrm{L}} \cdots w_{1K}^{MLMR} \\ w_{11}^{2\mathrm{L}} & \cdots & w_{11}^{ML} & & w_{12}^{1\mathrm{L}} \cdots w_{1K}^{MR} \\ \vdots & & \vdots & \mathbf{0} & \vdots \quad\quad \vdots \\ w_{11}^{MR2\mathrm{L}} \cdots & & w_{11}^{MRML} & & w_{12}^{MR1\mathrm{R}} \cdots w_{1K}^{MRMR} \\ w_{21}^{1\mathrm{L}2\mathrm{L}} & \cdots & w_{21}^{1\mathrm{L}ML} & w_{21}^{1\mathrm{R}} \cdots w_{21}^{1\mathrm{R}MR} & 0 \quad \cdots w_{2K}^{MRMR} \\ \vdots & & \vdots & \vdots \quad\quad \vdots & \vdots \quad \ddots \quad \vdots \\ w_{K1}^{MR2\mathrm{L}} \cdots & & w_{K1}^{MRML} & w_{K1}^{MR} \cdots w_{K1}^{MRMR} & w_{K2}^{MR1\mathrm{L}} \cdots \quad 0 \end{bmatrix} \tag{3.7}$$

$$= \begin{bmatrix} \tilde{W}_{1\mathrm{L},1\mathrm{L}} & \tilde{W}_{1\mathrm{L},1\mathrm{R}} & \cdots & \tilde{W}_{1\mathrm{L},K\mathrm{L}} & \tilde{W}_{1\mathrm{L},K\mathrm{R}} \\ \tilde{W}_{1\mathrm{R},1\mathrm{L}} & \tilde{W}_{1\mathrm{R},1\mathrm{R}} & \cdots & \tilde{W}_{1\mathrm{R},K\mathrm{L}} & \tilde{W}_{K\mathrm{R},1\mathrm{R}} \\ \vdots & & \ddots & & \vdots \\ \tilde{W}_{K\mathrm{L},1\mathrm{L}} & \tilde{W}_{K\mathrm{L},1\mathrm{R}} & \cdots & \tilde{W}_{K\mathrm{L},K\mathrm{L}} & \tilde{W}_{K\mathrm{L},K\mathrm{R}} \\ \tilde{W}_{K\mathrm{R},1\mathrm{L}} & \tilde{W}_{K\mathrm{R},1\mathrm{R}} & \cdots & \tilde{W}_{K\mathrm{R},K\mathrm{L}} & \tilde{W}_{K\mathrm{R},K\mathrm{R}} \end{bmatrix}$$

in which the block matrices are defined correspondingly, similar to (3.1)

Following the same argument in earlier sections, that all weights $w_{kk}^{m\mathrm{L}n\mathrm{L}}$ and $w_{kk}^{m\mathrm{R}n\mathrm{R}}$, which would separate matched filter outputs reflecting the same $b_k(i)$ through different paths, are forced to zero. Clearly, these data are not independent and hence can not be separated. Therefore all block-matrices $\tilde{W}_{k\mathrm{L},k\mathrm{L}} = 0$ and $\tilde{W}_{k\mathrm{R},k\mathrm{R}} = 0$. This is different from the one-shot bootstrap implementation for asynchronous non-dispersive channels [17], in which only the diagonal contains zeroes, which is, in fact, a special case of the above for $M = 1$.

Also, even though the original left and right path parts carry uncorrelated data, i.e., $\rho_{kk}^{mLmR} = \rho_{kk}^{mRmL} = 0$, correlation at the corresponding matched filter outputs is created through transformation (by $\boldsymbol{W}$), which requires additional weights, to eliminate this correlation. Hence the weights w_{kk}^{mLmR} and w_{kk}^{mRmL} are added to assure separation of z_k^{mL} and z_k^{mR}.

3.3 Steady State Bootstrap Weights

For controlling the weights, we use a recursive scheme which simultaneously reduces the absolute value of the correlation between the outputs of the decorrelator and the decision on all other outputs. That is, the weight, $w_{kl}^{m\mathrm{G},n\mathrm{H}}$ is controlled by the recursion,

$$w_{kl}^{m\mathrm{G},n\mathrm{H}} \leftarrow w_{kl}^{m\mathrm{G},n\mathrm{H}} + \mu z_k^{m\mathrm{G}} \mathrm{sgn}(z_l^{n\mathrm{H}}) \qquad \begin{matrix} k,l = 1 \cdots K \\ m,n = 1 \cdots M, \quad m \neq n \end{matrix} \tag{3.8}$$

where G, H are either R or L. We define the vector $\boldsymbol{x}_k^{\mathrm{G}}$ as the vector $\boldsymbol{x}$ of dimension $(2KM-1)$ without the vector $\tilde{\boldsymbol{x}}_k^{\mathrm{G}}$ (as defined in Fig 3.2), and we define $\boldsymbol{z}_k^{\mathrm{G}}$, $\tilde{\boldsymbol{z}}_k^{\mathrm{G}}$ and $z_k^{m\mathrm{G}}$ in the same fashion as parts of $\boldsymbol{z}$. Similarly, we define the matrix $\boldsymbol{P}_k^{\mathrm{G}}$ as the matrix $\boldsymbol{P}$ without the block rows $\tilde{P}_{k\mathrm{G}l\mathrm{H}}$ and columns $\tilde{P}_{l\mathrm{H}k\mathrm{G}}$, $l = 1 \cdots K$.

Also, we call $\boldsymbol{\rho}_k^{\mathrm{G}}$ the block columns of $\boldsymbol{P}$, $\tilde{P}_{l\mathrm{H}k\mathrm{G}}, l = 1 \cdots K$, without the block $\tilde{P}_{k\mathrm{G}k\mathrm{G}}$. For example, $\boldsymbol{\rho}_1^{\mathrm{L}} = \left[\tilde{P}_{1\mathrm{R},1\mathrm{L}}, \cdots, \tilde{P}_{K\mathrm{L},1\mathrm{L}}, \tilde{P}_{K\mathrm{R},1\mathrm{L}}\right]^T$, which is the first column in (3.5) without $P_{1\mathrm{L},1\mathrm{L}}$. $\boldsymbol{\rho}_k^{m\mathrm{G}}$ is the column-vector pertaining to the right, respectively left part of the m^{th} path of user k from $\boldsymbol{\rho}_k^{\mathrm{G}}$.

In exactly the same way, we define $\boldsymbol{W}_k^{\mathrm{G}}$, $\boldsymbol{w}_k^{\mathrm{G}}$ as parts of $\boldsymbol{W}$, Similarly, we also define $\boldsymbol{b}_k^{\mathrm{G}}$, $\tilde{A}_k^{\mathrm{G}}$ and $\boldsymbol{A}_k^{\mathrm{G}}$.

For the readers convenience, in Appendix B.2, the above definitions are clarified using a two user, two channels per path example.

We may now rewrite from (3.4),

$$\begin{bmatrix} \tilde{\boldsymbol{x}}_k^{\mathrm{G}} \\ \boldsymbol{x}_k^{\mathrm{G}} \end{bmatrix} = \begin{bmatrix} \tilde{P}_k^{\mathrm{G}} \boldsymbol{\rho}_k^{\mathrm{G}T} \\ \boldsymbol{\rho}_k^{\mathrm{G}} \boldsymbol{P}_k^{\mathrm{G}} \end{bmatrix} \begin{bmatrix} \tilde{A}_k^{\mathrm{G}} & 0 \\ 0 & \boldsymbol{A}_k^{\mathrm{G}} \end{bmatrix} \begin{bmatrix} \tilde{\boldsymbol{b}}_k^{\mathrm{G}} \\ \boldsymbol{b}_k^{\mathrm{G}} \end{bmatrix} + \begin{bmatrix} \tilde{\boldsymbol{n}}_k^{\mathrm{G}} \\ \boldsymbol{n}_k^{\mathrm{G}} \end{bmatrix} \tag{3.9}$$

The update of the weights from (3.8) can now be written as

$$\boldsymbol{w}_k^{m\mathrm{G}} \leftarrow \boldsymbol{w}_k^{m\mathrm{G}} + \mu z_k^{m\mathrm{G}} \mathrm{sgn}\left(\boldsymbol{z}_k^{\mathrm{G}}\right). \tag{3.10}$$

where we define $\boldsymbol{w}_k^{\mathrm{R}}$ and $\boldsymbol{w}_k^{m\mathrm{R}}$ similar to $\boldsymbol{\rho}_k^{\mathrm{R}}$ and $\boldsymbol{\rho}_k^{m\mathrm{R}}$ respectively.

In the mean, the steady state is reached when

$$\mathrm{E}\left[z_k^{m\mathrm{G}} \mathrm{sgn}\left(\boldsymbol{z}_k^{\mathrm{G}}\right)\right] = 0. \tag{3.11}$$

The decorrelator output, pertaining to the G$^{\text{th}}$ part of the m^{th} path of user k can be written as

$$z_k^{m\mathrm{G}} = x_k^{m\mathrm{G}} - \left(\boldsymbol{w}_k^{m\mathrm{G}}\right)^T \boldsymbol{x}_k^{\mathrm{G}}$$

in which the matched filter output $x_k^{m\mathrm{G}}$ is found from (3.9) to be

$$x_k^{m\mathrm{G}} = \left(\tilde{P}_k^{m\mathrm{G}}\right)^T \tilde{A}_k^{\mathrm{G}} \tilde{\boldsymbol{b}}_k^{\mathrm{G}} + \left(\boldsymbol{\rho}_k^{m\mathrm{G}}\right)^T \boldsymbol{A}_k^{\mathrm{G}} \boldsymbol{b}_k^{\mathrm{G}} + n_k^{m\mathrm{G}} \tag{3.12}$$

Generalizing over m gives

$$\tilde{z}_k^{\mathrm{G}} = \tilde{x}_k^{\mathrm{G}} - \left(\boldsymbol{w}_k^{\mathrm{G}}\right)^T \boldsymbol{x}_k^{\mathrm{G}} \tag{3.13}$$

If the condition occurs that the SNR's of all users are sufficiently high to approximate $\operatorname{sgn}\left(\boldsymbol{z}_k^{\mathrm{G}}\right) \approx \boldsymbol{b}_k^{\mathrm{G}}$, than in order to find the steady state of $\boldsymbol{w}_k^{\mathrm{G}}$, we may write instead of (3.11)

$$\begin{aligned}
\mathrm{E}\left[z_k^{m\mathrm{G}} \boldsymbol{b}_k^{\mathrm{G}}\right] &= \mathrm{E}\left[\left(x_k^{m\mathrm{G}} - \boldsymbol{w}_k^{m\mathrm{G}^T} \boldsymbol{x}_k^{\mathrm{G}}\right) \boldsymbol{b}_k^{\mathrm{G}}\right] = 0 \\
\mathrm{E}\left[x_k^{m\mathrm{G}} \boldsymbol{b}_k^{\mathrm{G}}\right] &= \mathrm{E}\left[\left(\tilde{P}_k^{m\mathrm{G}^T} \tilde{A}_k^{\mathrm{G}} \tilde{\boldsymbol{b}}_k^{\mathrm{G}} + \boldsymbol{\rho}_k^{m\mathrm{G}^T} \boldsymbol{A}_k^{\mathrm{G}} \boldsymbol{b}_k^{\mathrm{G}}\right) \boldsymbol{b}_k^{\mathrm{G}}\right] \\
&= \mathrm{E}\left[\boldsymbol{b}_k^{\mathrm{G}} \boldsymbol{b}_k^{\mathrm{G}^T}\right] \boldsymbol{A}_k^{\mathrm{G}} \boldsymbol{\rho}_k^{m\mathrm{G}}
\end{aligned}$$

where we used the fact that $\boldsymbol{b}_k^{\mathrm{G}}$ and $\tilde{\boldsymbol{b}}_k^{\mathrm{G}}$ are uncorrelated.

$$\begin{aligned}
\mathrm{E}\left[\boldsymbol{b}_k^{\mathrm{G}} \boldsymbol{x}_k^{\mathrm{G}^T}\right] &= \mathrm{E}\left[\boldsymbol{b}_k^{\mathrm{G}} \left(\boldsymbol{P}_k^{\mathrm{G}} \boldsymbol{A}_k^{\mathrm{G}} \boldsymbol{b}_k^{\mathrm{G}} + \boldsymbol{\rho}_k^{\mathrm{G}} \tilde{A}_k^{\mathrm{G}} \tilde{\boldsymbol{b}}_k^{\mathrm{G}}\right)^T\right] \\
&= \mathrm{E}\left[\boldsymbol{b}_k^{\mathrm{G}} \boldsymbol{b}_k^{\mathrm{G}^T}\right] \boldsymbol{A}_k^{\mathrm{G}} \left(\boldsymbol{P}_k^{\mathrm{G}}\right)^T
\end{aligned}$$

$$\begin{aligned}
\mathrm{E}\left[z_k^{m\mathrm{G}} \boldsymbol{b}_k^{\mathrm{G}}\right] &= \mathrm{E}\left[\left(x_k^{m\mathrm{G}} - \boldsymbol{w}_k^{m\mathrm{G}^T} \boldsymbol{x}_k^{\mathrm{G}}\right) \boldsymbol{b}_k^{\mathrm{G}}\right] = 0 \\
&\Rightarrow \mathrm{E}\left[\boldsymbol{b}_k^{\mathrm{G}} \boldsymbol{b}_k^{\mathrm{G}^T}\right] \boldsymbol{A}_k^{\mathrm{G}} \boldsymbol{\rho}_k^{m\mathrm{G}} = \mathrm{E}\left[\boldsymbol{w}_k^{m\mathrm{G}^T} \boldsymbol{x}_k^{\mathrm{G}} \boldsymbol{b}_k^{\mathrm{G}}\right] \\
&= \mathrm{E}\left[\boldsymbol{b}_k^{\mathrm{G}} \boldsymbol{b}_k^{\mathrm{G}^T}\right] \boldsymbol{A}_k^{\mathrm{G}} \left(\boldsymbol{P}_k^{\mathrm{G}}\right)^T \boldsymbol{w}_k^{m\mathrm{G}} \\
&\Rightarrow \boldsymbol{w}_k^{m\mathrm{G}} = \left(\boldsymbol{P}_k^{\mathrm{G}}\right)^{-T} \boldsymbol{\rho}_k^{m\mathrm{G}} \\
&\Rightarrow \boldsymbol{w}_k^{\mathrm{G}} = \left(\boldsymbol{P}_k^{\mathrm{G}}\right)^{-T} \boldsymbol{\rho}_k^{\mathrm{G}}
\end{aligned} \tag{3.14}$$

Substituting the steady state weights from (3.14) in (3.13) and using (3.9) to expand $\tilde{x}_k^{\mathrm{G}}$ and $\boldsymbol{x}_k^{\mathrm{G}}$ we have

$$\begin{aligned}
\tilde{z}_k^{\mathrm{G}} &= \tilde{x}_k^{\mathrm{G}} - \boldsymbol{w}_k^{\mathrm{G}^T}\boldsymbol{x}_k^{\mathrm{G}} \\
&= \tilde{x}_k^{\mathrm{G}} - \boldsymbol{\rho}_k^{\mathrm{G}^T}\boldsymbol{P}_k^{\mathrm{G}^{-1}}\boldsymbol{x}_k^{\mathrm{G}} \\
&= \tilde{P}_k^{\mathrm{G}}\tilde{A}_k^{\mathrm{G}}\tilde{\boldsymbol{b}}_k^{\mathrm{G}} + \boldsymbol{\rho}_k^{\mathrm{G}^T}\boldsymbol{A}_k^{\mathrm{G}}\boldsymbol{b}_k^{\mathrm{G}} + \tilde{\boldsymbol{n}}_k^{\mathrm{G}} \\
&\quad -\boldsymbol{\rho}_k^{\mathrm{G}^T}\boldsymbol{P}_k^{\mathrm{G}^{-1}}\left(\boldsymbol{\rho}_k^{\mathrm{G}}\tilde{A}_k^{\mathrm{G}}\tilde{\boldsymbol{b}}_k^{\mathrm{G}} + \boldsymbol{P}_k^{\mathrm{G}}\boldsymbol{A}_k^{\mathrm{G}}\boldsymbol{b}_k^{\mathrm{G}} + \boldsymbol{n}_k^{\mathrm{G}}\right) \\
&= \tilde{P}_k^{\mathrm{G}}\tilde{A}_k^{\mathrm{G}}\tilde{\boldsymbol{b}}_k^{\mathrm{G}} - \boldsymbol{\rho}_k^{\mathrm{G}^T}\boldsymbol{P}_k^{\mathrm{G}^{-T}}\boldsymbol{\rho}_k^{\mathrm{G}}\tilde{A}_k^{\mathrm{G}}\tilde{\boldsymbol{b}}_k^{\mathrm{G}} \\
&\quad +\boldsymbol{\rho}_k^{\mathrm{G}^T}\boldsymbol{A}_k^{\mathrm{G}}\boldsymbol{b}_k^{\mathrm{G}} - \boldsymbol{\rho}_k^{\mathrm{G}^T}\boldsymbol{P}_k^{\mathrm{G}^{-T}}\boldsymbol{P}_k^{\mathrm{G}}\boldsymbol{A}_k^{\mathrm{G}}\boldsymbol{b}_k^{\mathrm{G}} \\
&\quad +\tilde{\boldsymbol{n}}_k^{\mathrm{G}} - \boldsymbol{\rho}_k^{\mathrm{G}^T}\boldsymbol{P}_k^{\mathrm{G}^{-T}}\boldsymbol{n}_k^{\mathrm{G}} \\
\tilde{z}_k^{\mathrm{G}} &= \left(\tilde{P}_k^{\mathrm{G}} - \boldsymbol{\rho}_k^{\mathrm{G}^T}\boldsymbol{P}_k^{\mathrm{G}^{-T}}\boldsymbol{\rho}_k^{\mathrm{G}}\right)\tilde{\boldsymbol{A}}\tilde{\boldsymbol{b}}_k^{\mathrm{G}} \\
&\quad +\tilde{\boldsymbol{n}}_k^{\mathrm{G}} - \boldsymbol{\rho}_k^{\mathrm{G}^T}\boldsymbol{P}_k^{\mathrm{G}^{-T}}\boldsymbol{n}_k^{\mathrm{G}}.
\end{aligned} \tag{3.15}$$

This shows the perfect cancellation of the other users' interfering signal energy "in the limit of interference SNR". This result is not exactly equal to that of using $\boldsymbol{V} = \boldsymbol{P}^{-1}$ as we do not (and, using adaptive schemes, can not) decorrelate the signals originating from the same symbol of a user. For the case of $\boldsymbol{V} = \boldsymbol{P}^{-1}$,

$$z_{\mathrm{D}k}^{m\mathrm{G}} = \left(1 - \boldsymbol{\rho}_{\mathrm{D}k}^{m\mathrm{G}^T}\boldsymbol{P}_{\mathrm{D}k}^{m\mathrm{G}^{-T}}\boldsymbol{\rho}_{\mathrm{D}k}^{m\mathrm{G}}\right)\alpha_k^{m\mathrm{G}}\tilde{b}_k^{m\mathrm{G}} + \zeta_k^{m\mathrm{G}} \tag{3.16}$$

in which $\boldsymbol{\rho}_{\mathrm{D}k}^{m\mathrm{G}}$ is the column vector of $\boldsymbol{P}$ belonging to the G^{th} part of path m of user k, and $\boldsymbol{P}_{\mathrm{D}k}^{m\mathrm{G}}$ is the matrix $\boldsymbol{P}$ without the previous column and corresponding row. It should be noted that $\alpha_k^{m\mathrm{G}}$ and $\tilde{b}_k^{m\mathrm{G}}$ are both scalars. $\mathrm{E}[\zeta_k^{m\mathrm{G}2}] = \left(1 - \boldsymbol{\rho}_{\mathrm{D}k}^{m\mathrm{G}^T}\boldsymbol{P}_{\mathrm{D}k}^{m\mathrm{G}^{-T}}\boldsymbol{\rho}_{\mathrm{D}k}^{m\mathrm{G}}\right)\sigma^2$.

In general, if the remaining SI, given by the off-diagonal terms in (3.15), $\left(\tilde{P}_k^{\mathrm{G}} - \boldsymbol{\rho}_k^{\mathrm{G}^T}\boldsymbol{P}_k^{\mathrm{G}^{-T}}\boldsymbol{\rho}_k^{\mathrm{G}}\right)$ between the path-parts is small, the performance of the bootstrap decorrelator will be nearly as good as that of the the conventional decorrelator for high ISR

3.4 Time-Path Combining

After the bootstrap separator (or the decorrelator when $V = P^{-1}$ is used), the left and right parts of each path are combined. It was shown in [18] that a maximum SNR is achieved when weighting the left and right part with $\sqrt{\epsilon_{km}}$ and $\sqrt{1-\epsilon_{km}}$ respectively. Subsequently, all paths of each user are combined using a maximum-ratio combiner, after which a decision stage follows. The basic scheme is given in Fig. 3.3.

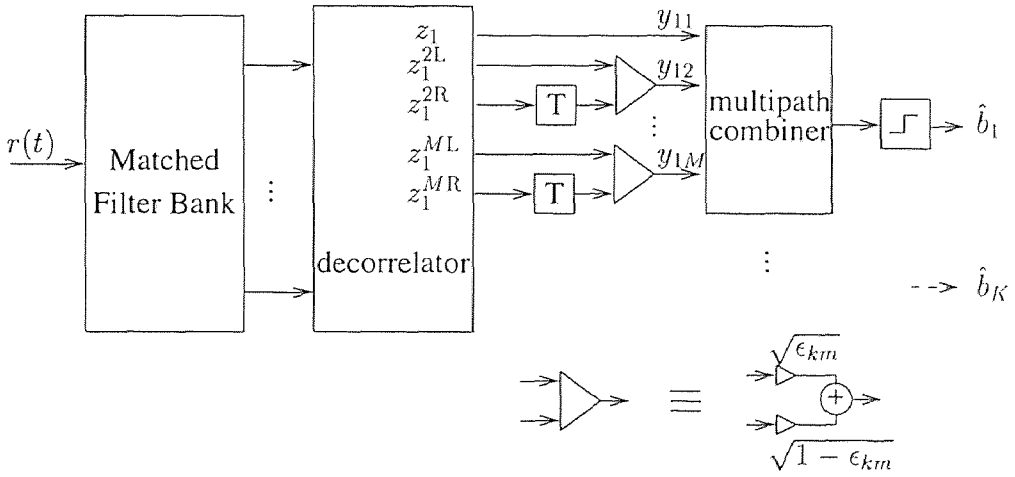

Figure 3.3 Receiver scheme.

3.5 Simulation Results

The simulation results in Fig. 3.4 and Fig. 3.5 depict the performance of the bootstrap algorithm and the matrix inverse based decorrelator applied to scheme depicted in Fig. 3.3, for a three user case, as a function of the SNR of user 2. The SNR of user 3 is equal to that of user 2, whereas user 1 has SNR = 8dB. The simulation was performed using Gold codes of length 15 and 3 paths per user with relative delays of 0, 2, 4, 5, 6, 8 and 11, 12, 13 chips respectively. As modulation, BPSK was used. Fig. 3.4 shows the performance for user 1, and Fig. 3.5 the performance

for user 2. Also provided is the single user conventional detection performance, which means matched filtering to the strongest (first) path of each user.

From Fig. 3.4, it can clearly be seen that, for high interference levels, the modified bootstrap algorithm achieves a near perfect cancellation of the interfering signals (that is, a perfect cancellation of all interference except the SI, which turns out to be very minor) as we derived analytically in the previous section.

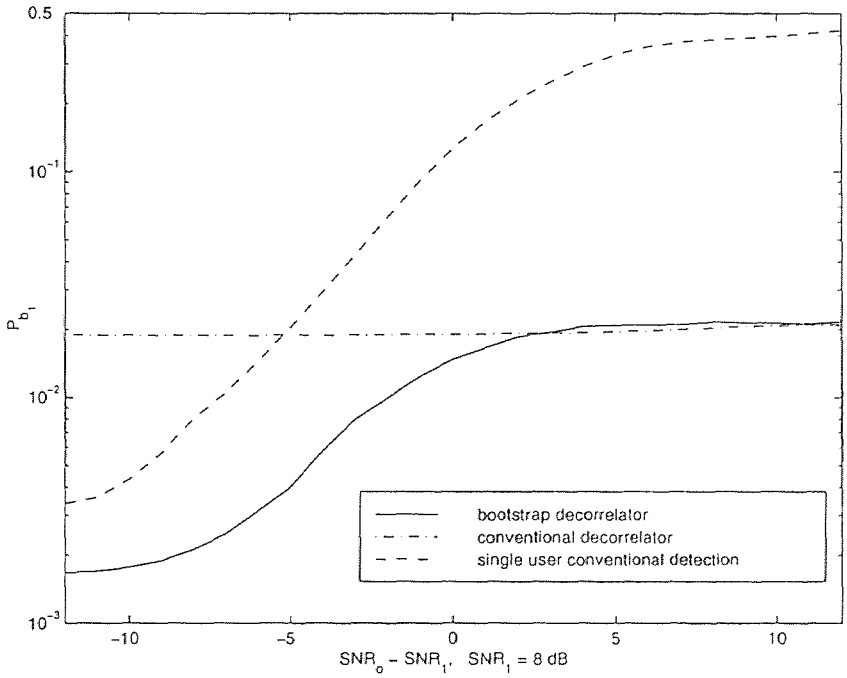

Figure 3.4 Performance of 3 user one-shot receiver (user 1).

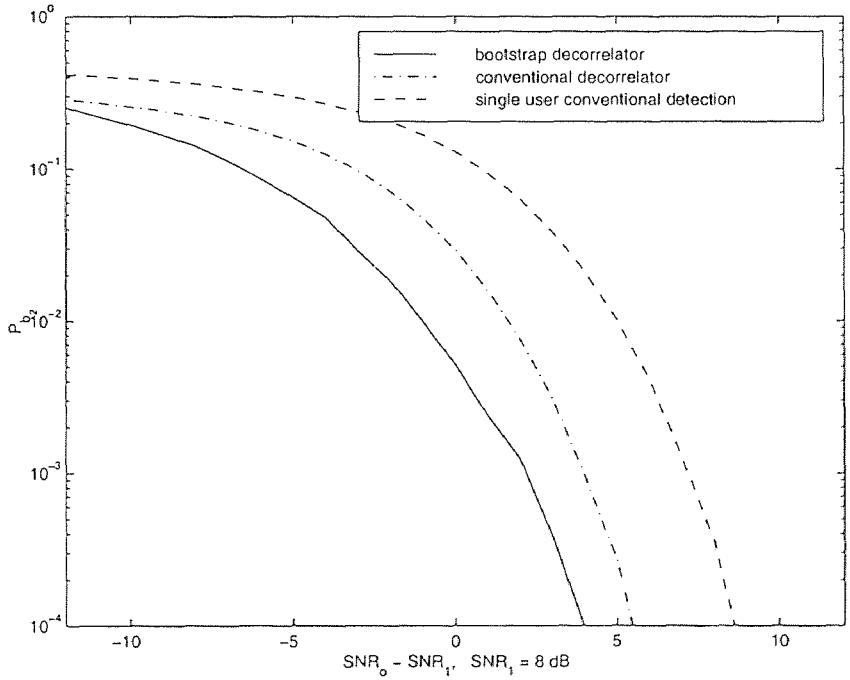

Figure 3.5 Performance of 3 user one-shot receiver (user 2).

CHAPTER 4

ILL-CONDITIONING OF ASYNCHRONOUS CDMA CORRELATION MATRICES

The conventional one-shot decorrelator suggested by Verdú[19] is based on inverting the partial correlation matrix $\boldsymbol{P}$, the definition of which is extensively described in the previous chapter. The bootstrap algorithm adaptively searches a transformation $\boldsymbol{I} - \boldsymbol{W}$, which, for the case of $M = 1$, diagonalizes $\boldsymbol{P}$ when the SNR's of the users are heigh. When $M > 1$, this transformation will only near-diagonalize $\boldsymbol{P}$ due to its restricted structure, which is extensively described in the previous chapter.

However, a problem arises when $\boldsymbol{P}$ is singular, a matter which is mostly overlooked, or argued to be of only negligible probability, in analysis of the one-shot decorrelators. If $\boldsymbol{P}$ is singular, the inverse $\boldsymbol{P}^{-1}$ does not exist, and hence the conventional decorrelator cannot be applied without severe performance degradation due to erroneous inversion.

The performance of the bootstrap algorithm in this situation also deteriorates drastically as the control becomes unstable. However, using a soft-limiter in the decision stage instead of a hard-limiter (the signum function as shown in the previous chapter), was shown to reduce the deterioration. [20]

The purpose of this chapter is to examine cases wherein the correlation matrix in the one-shot asynchronous case is not so well behaved and point out the implications. Since it is extremely difficult, if not impossible, to derive closed form expressions for the situation in which the correlation matrix is singular, observations will be made based on simulations performed for $K = 3$ and 4 and Gold codes of length $N = 7$ and 15 using channels without multi-path components, i.e. $M = 1$.

4.1 The Partial-Correlation Matrix

To keep the model simple, the general case of the dispersive system described in the previous chapter is used with only one path per channel, i.e. $M = 1$. Dropping the path subscript, the equivalent low-pass signal at the input of the matched filter bank then becomes (in one-shot representation of the ith bit of user one, and letting $i = 0$ as in (3.2)):

$$\begin{aligned} r(t) &= \sqrt{a_1}s_1(t)b_1(0) + \sum_{k=2}^{K} \sqrt{a_k\epsilon_k}\frac{1}{\sqrt{\epsilon_k}}s_k^L(t)b_k(-1) \\ &\quad + \sqrt{a_k(1-\epsilon_k)}\frac{1}{\sqrt{1-\epsilon_k}}s_k^R(t)b_k(0) + n(t), \end{aligned} \tag{4.1}$$

where

$$\begin{aligned} s_k^L(t) &= \begin{cases} s_k(t+T-\tau_k) & \text{if } 0 \le t \le \tau_k \\ 0 & \text{if } \tau_k < t \le T \end{cases} \\ s_k^R(t) &= \begin{cases} 0 & \text{if } 0 \le t \le \tau_k \\ s_k(t-\tau_k) & \text{if } \tau_k < t \le T \end{cases} \\ \epsilon_k &= \int_0^{\tau_k} s_k^2(t+T-\tau_k)dt. \end{aligned} \tag{4.2}$$

$r(t)$ is applied to a bank of filters matched to $s_1(t), s_k^L(t), s_k^R(t)$ and normalized to unity with $\sqrt{\epsilon_k}$ and $\sqrt{1-\epsilon_k}, k = 2, \cdots K$, respectively.

The correlation matrix $\boldsymbol{P}$ that arises as the result of this becomes:

$$P^T = \begin{bmatrix} 1 & \rho_{12}^L & \rho_{12}^R & \rho_{13}^L & \rho_{13}^R & \cdots & \rho_{1K}^L & \rho_{1K}^R \\ \rho_{21}^L & 1 & 0 & \rho_{13}^{LL} & 0 & & \rho_{2K}^{LL} & 0 \\ \rho_{21}^R & 0 & 1 & \rho_{23}^{RL} & \rho_{23}^{RR} & & \rho_{2K}^{RL} & \rho_{2K}^{RR} \\ \rho_{31}^L & \rho_{32}^{LL} & \rho_{32}^{LR} & 1 & 0 & & \rho_{3K}^{LL} & 0 \\ \rho_{31}^R & 0 & \rho_{32}^{RR} & 0 & 1 & & \rho_{3K}^{RL} & \rho_{3K}^{RR} \\ \vdots & & & \ddots & & & & \vdots \\ \rho_{K1}^L & \rho_{K2}^{LL} & \rho_{K2}^{LR} & \rho_{K3}^{LL} & \rho_{K3}^{LR} & & 1 & 0 \\ \rho_{K1}^R & 0 & \rho_{K2}^{RR} & 0 & \rho_{K3}^{RR} & \cdots & 0 & 1 \end{bmatrix} \tag{4.3}$$

in which the correlation coefficients are given by (3.4)

To examine the ill-conditionedness of the correlation matrix, the eigen-ratio is used. The higher this ratio the worse conditioned the matrix, and in the limit, when this ratio is infinite (represented by the peaks in the simulation results), the matrix is singular.

4.2 Simulation Results

In a set of Gold codes of length N there are $N+2$ different codes, every N of which are linearly independent. $N+1$ of these have -1 as cross-correlation. In the simulations shown, K ($K \leq N$) out of the latter $N+1$ codes were used. For the simulations shown, the following Gold Codes were used:

1	+1	+1	+1	−1	+1	−1	−1
2	−1	−1	−1	−1	+1	+1	−1
3	+1	−1	−1	+1	+1	−1	+1
4	−1	+1	−1	+1	−1	−1	−1

For $K = 3$ and $N = 7$, it appears, (see as example Fig. 4.1) that singularities only occur for $\tau_2/T, \tau_3/T \in \mathbb{N}$ and that P tends to be ill-conditioned if at least 2 of the users have a delay difference which is an integer multiple of T_c, the chip-duration. For $K = 3$ and $N = 15$, it appears that P can be singular only if $\tau_2 = \tau_3$. Again P tends to have larger eigenvalue ratios if at least 2 of the users have an delay difference which is a integer multiple of T_c, although the ratios are much lower then for $N = 7$. In general it becomes ill-conditioned if $\tau_2 \approx \tau_3$.

For $K = 4$ and $N = 7$, one of the delays was fixed, while the other two were varied as to obtain the presented 3-dimensional plots. In this case, singularities only occur if at least 2 out of the 4 users have an integer delay difference. In Fig. 4.2 it can be seen that if $\tau_2 = T_c$, P is only singular only if τ_3/T_c, $\tau_4/T_c \in \mathbb{N}$. If on the other hand we choose τ_2 to be $0.3T_c$, we get a singularity only if $\tau_3 = 1.3T_c$ and $\tau_4 = 2.3T_c$ (see Fig. 4.3).

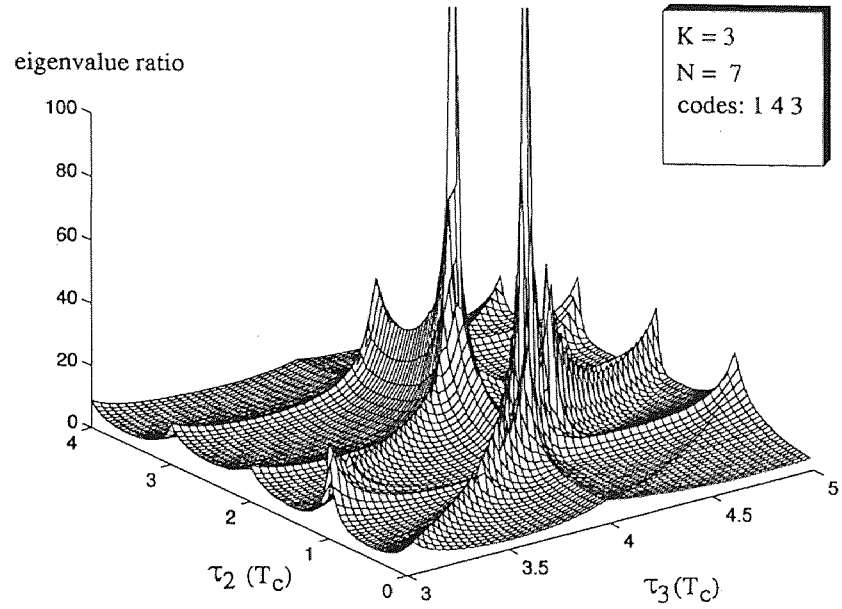

Figure 4.1 Condition ratios for a three user example.

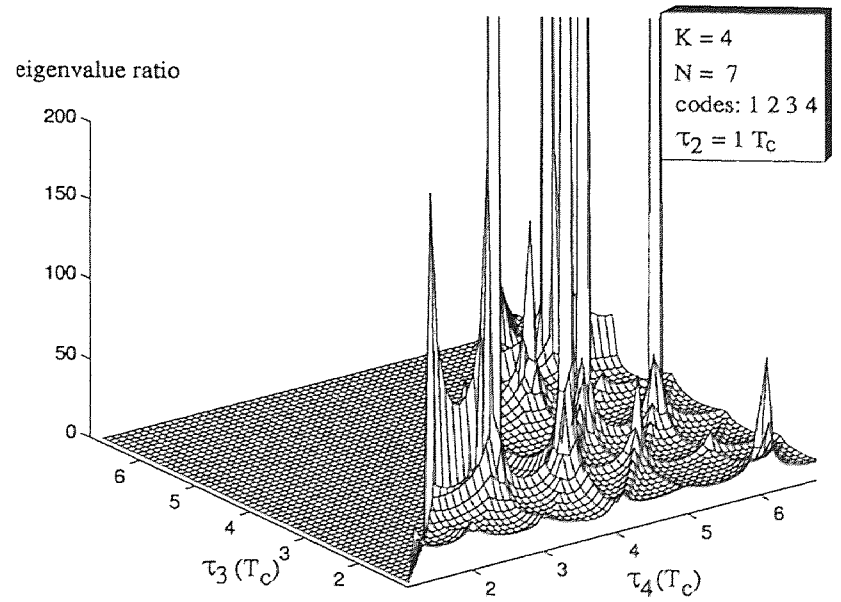

Figure 4.2 Condition ratios for a four user example $\tau_4 > \tau_3$.

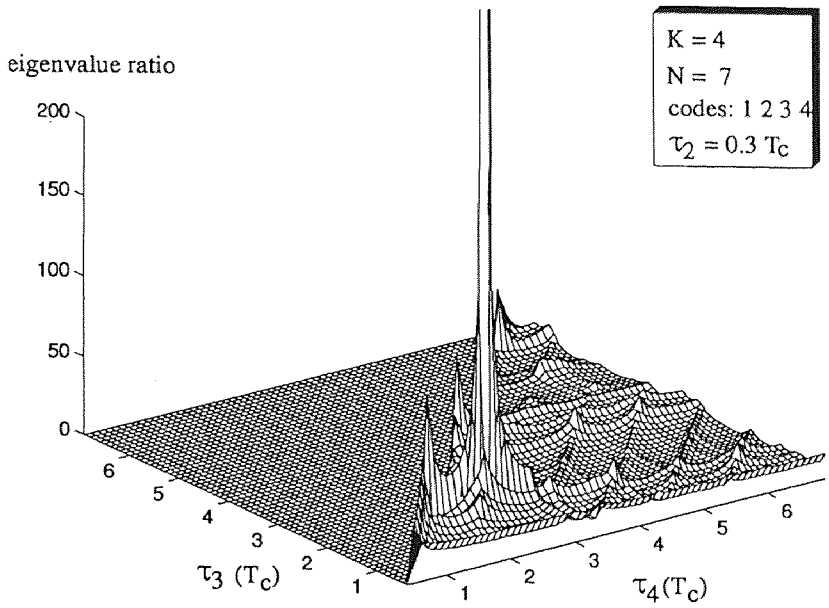

Figure 4.3 Condition ratios for a four user example $\tau_4 > \tau_3$.

The simulation results presented serve to draw attention to difficulties that may occur in using the one-shot approach, whether based on matrix inversion or an adaptive approach like the bootstrap algorithm, and hence to justify proposing the multi-shot decorrelator, dealt with in the next chapter, whose correlation matrices are never singular.

It should be observed that the probability of the correlation matrix being singular is not negligible. When relative delays are small, the left parts of paths can comprise only a few chips. This increases the likelihood of the matrix becoming singular. A clear example is the case in which two parts have the same length. The rows in the correlation matrix arising from these parts will be dependent if these left parts contain exactly the same, or exactly the opposite chips, which has, given n chips in these parts, a probability of 2^{n-1}. Thus, the probability of the correlation matrix becoming singular becomes very significant, and notably important, irrespective of the actual codelength.

CHAPTER 5

MULTI-SHOT BPSK/QAM-MODULATED CDMA RECEIVER

In this chapter, instead of the one-shot decorrelator structure applied in the previous chapters, the adaptive (bootstrap) multi-shot decorrelator (ABMSD) structure is presented. This structure is an adaptive extension of the multi-shot decorrelator (MSD) based on cross-correlation matrix inversion introduced in [15].

As pointed out in the previous chapter, the "partial cross-correlation" matrix used in the one-shot asynchronous decorrelator may be badly conditioned or even singular, which clearly creates a problem when an attempt to invert this matrix is made. On the other hand, the cross-correlation matrix of the filters' outputs in the multi-shot (asynchronous) decorrelator is always non-singular, as in the synchronous decorrelator.

The ABMSD structure presented in this chapter will be shown to outperform both the MSD and the one-shot decorrelators (OSD). Also, a suitable adaptive canceler is presented to follow the multishot decorrelator, and hence obtain the multistage multiuser receiver based on multishot matched filtering.

The performance study will use multipath fading environments, as well as well as time-variant (flat fading) channels.

5.1 Multishot Matched Filters Model (MSMF)

The multishot decorrelator is particularly useful for multipath asynchronous channels, as in uplink mobile communications.

Under the assumption that $\tau_{k,\max}+\tau_{kl,\max}$ is less than $2T$ for every k (extension to larger delays is straight-forward but clutters the notation unnecessarily) the combined multipath signal of each user in such an environment can be defined from (1.1) as,

$$s_{\mathrm{f}_k}(t-\tau_k)=\sum_{m=1}^{M}\gamma_{km}s(t-\tau_k-\delta_{km}), \tag{5.1}$$

allowing us to rewrite (1.1)

$$r(t)=\sum_{i}\sum_{k=1}^{K}s_{\mathrm{f}_k}(t-\tau_k)\theta_k(i)$$

where

$$\theta_k(i)=\sqrt{a_k}b_k(i).$$

In matrix notation,

$$r(t)=\sum_{i}\boldsymbol{S}_{\mathrm{f}}^{T}(t-iT)\boldsymbol{\theta}(i) \tag{5.2}$$

where $\boldsymbol{S}_{\mathrm{f}}(t)=[s_{\mathrm{f}_1}(t),s_{\mathrm{f}_2}(t-\tau_2),\cdots,s_{\mathrm{f}_K}(t-\tau_K)]^T$ and $\boldsymbol{\theta}(i)=[\theta_1(i),\cdots,\theta_K(i)]^T$. The combined multipath signal from (5.1) is used to drive the matched filters. The acquisition of each symbol at the k^{th} output is performed over an interval of $T+\delta_{kl,\max}$ seconds, which requires a dual memory input buffer and switch, as is shown in Fig. 5.1. Therefore, for the i^{th} symbol, the filter is matched to the data input which runs from τ_k+iT to $\tau_k+(i+1)T+\delta_{km,\max}$, $i=\cdots,-1,0,1,\cdots$. Therefore, following the k^{th} matched filter, the output

$$\begin{aligned}x_k(i) &= \int_{iT+\tau_k}^{(i+1)T+\tau_k+\delta_{km,\max}} r(t)s_{\mathrm{f}_k}(t-iT-\tau_k)dt, \qquad (k=1,\ldots,K)\\ &= \sum_{l=1}^{K}\sqrt{a_l}b_l(i)+\sum_{l=k+1}^{K}\sqrt{a_l}b_l(i-1)\rho_{lk}^{(+)}+\sum_{l=1}^{K-1}\sqrt{a_l}b_l(i+1)\rho_{lk}^{(-)}+\zeta_k(i)\end{aligned} \tag{5.3}$$

$$\zeta_k(i) \triangleq \int_{iT+\tau_k}^{(i+i)T+\tau_k+\delta_{km,\max}} n(t)s_{\mathrm{f}_k}(t-iT-\tau_k)dt$$

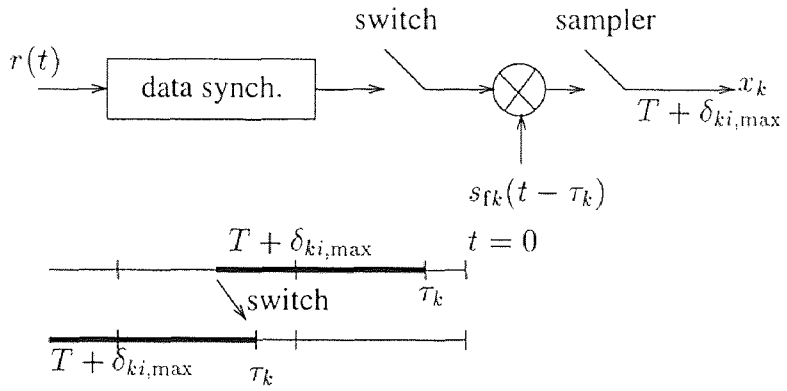

Figure 5.1 Multishot matched filter structure.

$$
\begin{aligned}
\rho_{kl} &\triangleq \int_0^{T+\delta_{km,\max}} s_{\mathrm{f}_k}(t)\, s\mathrm{f}_l(t-iT-\tau_l+\tau_k)dt \\
\rho_{lk}^{(+)} &\triangleq \begin{cases} \int_0^T s_{\mathrm{f}_l}(t) s_{\mathrm{f}_k}(t-iT-\tau_l+\tau_k)dt & l>k \\ 0 & l\le k \end{cases} \\
\rho_{lk}^{(-)} &\triangleq \begin{cases} \int_0^T s_{\mathrm{f}_k}(t) s_{\mathrm{f}_l}(t-T-\tau_l+\tau_k)dt & k>l \\ 0 & k\le l \end{cases}
\end{aligned}
$$

After stacking the outputs of a bank of K multi-shot matched filters into a $K\times 1$ vector $\boldsymbol{x}\triangleq[x_1(i),\ldots,x_K(i)]^T$, we obtain, using matrix notation for the i^{th} bit multi-shot matched filter outputs,

$$
\begin{aligned}
\boldsymbol{x}(i) &= \boldsymbol{P}\boldsymbol{A}\boldsymbol{b}(i)+\boldsymbol{P}_{\mathrm{U}}\boldsymbol{A}\boldsymbol{b}(i-1)+\boldsymbol{P}_{\mathrm{L}}\boldsymbol{A}\boldsymbol{b}(i+1)+\boldsymbol{\zeta}(i) \\
&= [\boldsymbol{P}_U\ \boldsymbol{P}\ \boldsymbol{P}_L]\begin{bmatrix}\boldsymbol{\theta}(i-1)\\ \boldsymbol{\theta}(i)\\ \boldsymbol{\theta}(i+1)\end{bmatrix}+\boldsymbol{\zeta}(i), \qquad (5.4)
\end{aligned}
$$

where $\boldsymbol{\theta}(i)=\boldsymbol{A}\boldsymbol{b}(i)$ and $\boldsymbol{\zeta}(i)$ is $\mathcal{N}(0,\sigma^2\boldsymbol{P})$ is a colored Gaussian noise vector. From the definition of $\boldsymbol{S}_{\mathrm{f}}(t)$, one can easily show that the matrices $\boldsymbol{P}$, $\boldsymbol{P}_{\mathrm{U}}$ and $\boldsymbol{P}_{\mathrm{L}}$ whose elements are defined in (5.4) can be obtained from the inner product.

$$
\begin{aligned}
\boldsymbol{P} &= \int \boldsymbol{S}_{\mathrm{f}}(t)\boldsymbol{S}_{\mathrm{f}}^T(t) \\
\boldsymbol{P}_{\mathrm{U}} &= \int \boldsymbol{S}_{\mathrm{f}}(t-T)\boldsymbol{S}_{\mathrm{f}}^T(t) = \int \boldsymbol{S}_{\mathrm{f}}(t)\boldsymbol{S}_{\mathrm{f}}^T(t+T) \qquad (5.5)\\
\boldsymbol{P}_{\mathrm{L}} &= \int \boldsymbol{S}_{\mathrm{f}}(t+T)\boldsymbol{S}_{\mathrm{f}}^T(t)
\end{aligned}
$$

where the integrals are defined from 0 to $T+\delta_{km,\max}$ for the k^{th} element of $\boldsymbol{S}_f(t)$.

Using $\boldsymbol{P}^{-1}\boldsymbol{\theta}(i)$ to estimate the data vector will result in poor performance, as $\boldsymbol{x}(i)$ depends on the current, following, and previous bits of the same and other users. However, staking N samples of vector $\boldsymbol{x}(i)$ together, we get after the matched filters (matched to s_{f_k}, rather than each individual path) [15],

$$\underbrace{\begin{bmatrix} \boldsymbol{x}(i-\frac{N-1}{2}) \\ \vdots \\ \boldsymbol{x}(i) \\ \vdots \\ \boldsymbol{x}(i+\frac{N-1}{2}) \end{bmatrix}}_{\mathbf{X}(:,i)} = \underbrace{\begin{bmatrix} \mathbf{P}_U & \mathbf{P} & \mathbf{P}_L & 0 & 0 & \cdots & 0 \\ 0 & \mathbf{P}_U & \mathbf{P} & \mathbf{P}_L & 0 & \cdots & 0 \\ 0 & 0 & \mathbf{P}_U & \mathbf{P} & \mathbf{P}_L & \cdots & 0 \\ \vdots & \vdots & \vdots & \ddots & \ddots & \ddots & \vdots \\ 0 & 0 & 0 & \cdots & \mathbf{P}_U & \mathbf{P} & \mathbf{P}_L \end{bmatrix}}_{NK\times(N+2)K} \begin{bmatrix} \boldsymbol{\theta}(i-\frac{N+1}{2}) \\ \vdots \\ \boldsymbol{\theta}(i) \\ \vdots \\ \boldsymbol{\theta}(i+\frac{N+1}{2}) \end{bmatrix} + \begin{bmatrix} \boldsymbol{n}(i-\frac{N-1}{2}) \\ \vdots \\ \boldsymbol{n}(i) \\ \vdots \\ \boldsymbol{n}(i+\frac{N-1}{2}) \end{bmatrix}$$

$$= \underbrace{\begin{bmatrix} \mathbf{P} & \mathbf{P}_L & 0 & \cdots & 0 \\ \mathbf{P}_U & \mathbf{P} & \mathbf{P}_L & \cdots & 0 \\ 0 & \mathbf{P}_U & \mathbf{P} & \ddots & \vdots \\ \vdots & \vdots & \ddots & \ddots & \mathbf{P}_L \\ 0 & 0 & \cdots & \mathbf{P}_U & \mathbf{P} \end{bmatrix}}_{\mathcal{P}} \underbrace{\begin{bmatrix} \boldsymbol{\theta}(i-\frac{N-1}{2}) \\ \vdots \\ \boldsymbol{\theta}(i) \\ \vdots \\ \boldsymbol{\theta}(i+\frac{N-1}{2}) \end{bmatrix}}_{\mathbf{Z}(:,i)} + \underbrace{\begin{bmatrix} \mathbf{P}_U\,\boldsymbol{\theta}(i-\frac{N+1}{2}) \\ 0 \\ \vdots \\ 0 \\ \mathbf{P}_L\,\boldsymbol{\theta}(i+\frac{N+1}{2}) \end{bmatrix}}_{\text{bias}} + \underbrace{\begin{bmatrix} \boldsymbol{n}(i-\frac{N-1}{2}) \\ \vdots \\ \boldsymbol{n}(i) \\ \vdots \\ \boldsymbol{n}(i+\frac{N-1}{2}) \end{bmatrix}}_{\text{noise } \mathbf{N}(:,i)} \quad (5.6)$$

where N is the (odd, for notational convenience) number of symbols processed simultaneously.

5.2 Multishot Conventional Decorrelator (based on matrix inversion)

Clearly, to a certain approximation, decorrelation can be achieved by $\boldsymbol{Z}(:,i) = \mathcal{P}^{-1}\boldsymbol{X}(:,i)$, where the error due to the bias-term will become smaller if N is large. However, the computational complexity increases rapidly as N increases. The matrix $\mathcal{P}$ is diagonally dominant and so is $\mathcal{P}^{-1}$. Hence the estimate of $\boldsymbol{Z}(:,i)$ is only distorted by the previous and following symbol. In [15], it was shown that using only $N = 3$ to estimate $\boldsymbol{x}(i)$, which is least distorted by the bias term, is adequate. For $N = 3$, the correlation matrix used is

$$\mathcal{P} = \begin{bmatrix} \boldsymbol{P} & \boldsymbol{P}_{\mathrm{L}} & 0 \\ \boldsymbol{P}_{\mathrm{U}} & \boldsymbol{P} & \boldsymbol{P}_{\mathrm{L}} \\ 0 & \boldsymbol{P}_{\mathrm{U}} & \boldsymbol{P} \end{bmatrix}.$$

Due to the diagonal dominance, instead of computing $\mathcal{P}^{-1}$ fully, and then calculating

$$\begin{bmatrix} z(i-1) \\ z(i) \\ z(i+1) \end{bmatrix} = \mathcal{P}^{-1} \begin{bmatrix} x(i-1) \\ x(i) \\ x(i+1) \end{bmatrix} \tag{5.7}$$

$z(i)$ can be obtained directly as from applying the central block row of $\mathcal{P}^{-1}$

$$z(i) = \boldsymbol{W} \begin{bmatrix} \boldsymbol{P}^{-1}\boldsymbol{x}(i-1) \\ \boldsymbol{P}^{-1}\boldsymbol{x}(i) \\ \boldsymbol{P}^{-1}\boldsymbol{x}(i+1) \end{bmatrix} = \boldsymbol{\theta}(i) + \boldsymbol{W} \begin{bmatrix} \boldsymbol{B}\boldsymbol{\theta}(i-2) \\ 0 \\ \boldsymbol{C}\boldsymbol{\theta}(i+2) \end{bmatrix} + \boldsymbol{W} \begin{bmatrix} \boldsymbol{P}^{-1}\boldsymbol{n}(i-1) \\ \boldsymbol{P}^{-1}\boldsymbol{n}(i) \\ \boldsymbol{P}^{-1}\boldsymbol{n}(i+1) \end{bmatrix} \tag{5.8}$$

where $\boldsymbol{W} = \underbrace{(\boldsymbol{I} - \boldsymbol{BC} - \boldsymbol{CB})^{-1}}_{\boldsymbol{W}_0^T}[-\boldsymbol{C} : I : -\boldsymbol{B}]$, $\quad \boldsymbol{B} = \boldsymbol{P}^{-1}\boldsymbol{P}_{\mathrm{L}}$ and $\boldsymbol{C} = \boldsymbol{P}^{-1}\boldsymbol{P}_{\mathrm{U}}$.

At this point, it should be noted that for $N = 5$, $\boldsymbol{W}$ becomes for example, $\boldsymbol{W} = (\boldsymbol{I} - \boldsymbol{BDC} - \boldsymbol{CDB})^{-1}[\boldsymbol{CDC} : -\boldsymbol{DC} : I : -\boldsymbol{DB} : \boldsymbol{BDB}]$,

where $\boldsymbol{B}$ and $\boldsymbol{C}$ as before while $\boldsymbol{D} = \boldsymbol{I} - \boldsymbol{BC}$. These expressions will be used in the simulations shown later. Schematically, this is shown in figure 5.2 for $N = 3$.

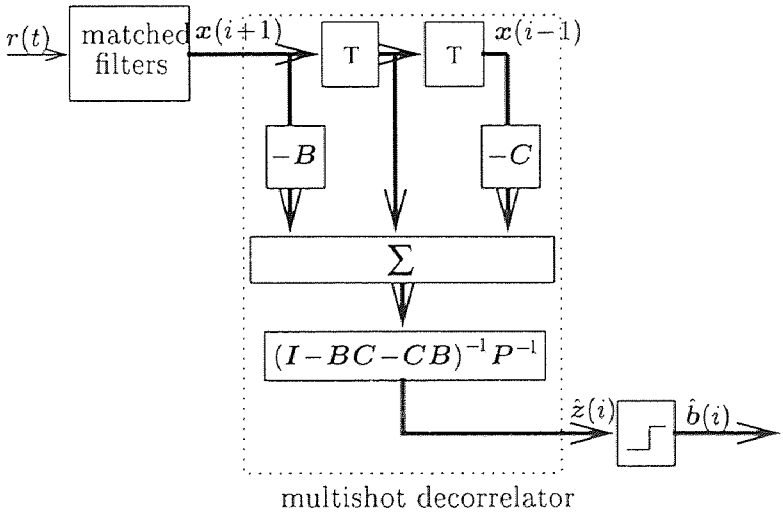

Figure 5.2 Multishot decorrelator, N=3.

5.3 Adaptive Bootstrap Multishot Decorrelator (ABMSD)

Instead of the conventional multishot decorrelator shown in the previous section, using the bootstrap decorrelator as depicted in Fig. 5.3 is proposed.

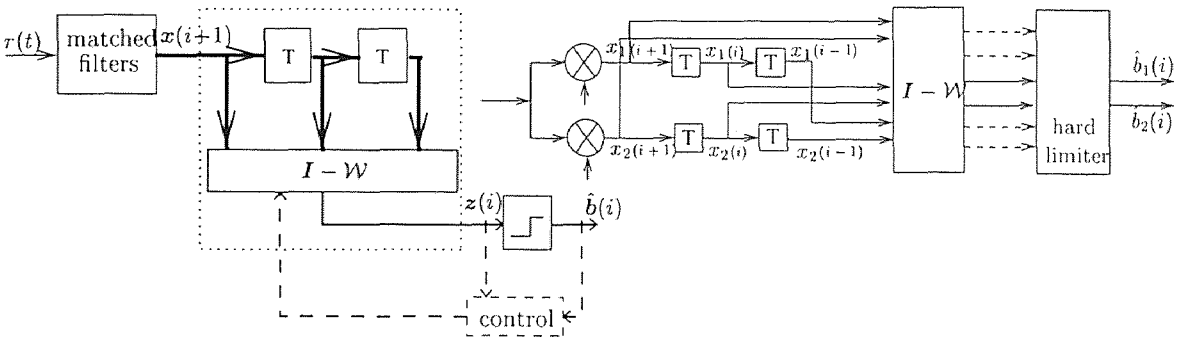

Figure 5.3 Multishot bootstrap for $N = 3$. a) general scheme. b) 2 user detail.

The disadvantage of this approach compared to the inverse matrix based multishot, which in fact requires computation of only the K middle outputs of (5.7), is that all NK of

$$\boldsymbol{Z}(:,i) = (\boldsymbol{I} - \mathcal{W})\boldsymbol{X}(:,i) \tag{5.9}$$

have to be computed, as the bootstrap requires these outputs for its weight control. The outweighing advantage, however, is the robustness of the bootstrap to errors, both to estimation of the relative delays and fading coefficients of the paths. Because the matched filter needs exact knowledge of the delays of each path and the power of each path to be able to form s_{f_k}, estimating the cross-correlation matrices will be difficult.

The matrix $\mathcal{W}$ in (5.9)has the structure

$$\mathcal{W} = \begin{bmatrix} \boldsymbol{W}_{-\frac{N-1}{2},-\frac{N-1}{2}} & \cdots & \boldsymbol{W}_{-\frac{N-1}{2},\frac{N-1}{2}} \\ \vdots & \ddots & \vdots \\ \boldsymbol{W}_{\frac{N-1}{2},-\frac{N-1}{2}} & \cdots & \boldsymbol{W}_{\frac{N-1}{2},\frac{N-1}{2}} \end{bmatrix} \tag{5.10}$$

in which each matrix $\boldsymbol{W}_{n,l}$ is a full $K \times K$ weight matrix, except $\boldsymbol{W}_{n,n}$ which has zeroes on its diagonal. The weights are controlled by

$$w_{n,l}(i+1) = w_{n,l}(i) + \mu \boldsymbol{Z}(n,i)\mathrm{sgn}(\boldsymbol{Z}(l,i)) \tag{5.11}$$

for $n, l = 1 \cdots KN$.

The symbol estimates are obtained by taking the signum, or another discretising function for other than BPSK modulations, of the middle K elements of $\boldsymbol{Z}(:,i)$

$$\hat{\boldsymbol{b}}(i) = [\mathrm{sgn}\{\boldsymbol{Z}(\tfrac{N-1}{2}K+1,i)\}, \cdots, \mathrm{sgn}\{\boldsymbol{Z}(\tfrac{N+1}{2}K,i)\}]^T$$

Due to the known diagonal dominance, it is optional to omit $\boldsymbol{W}_{n,l}\ \forall |n-l| > (N-1)/2$ (the upper right and lower left corner of $\mathcal{W}$) to reduce computational cost.

5.4 Multishot Canceler

The multishot bootstrap as well as the multishot inversion-decorrelator, as shown in figure 5.2, can be followed by a suitable "multishot" canceler.

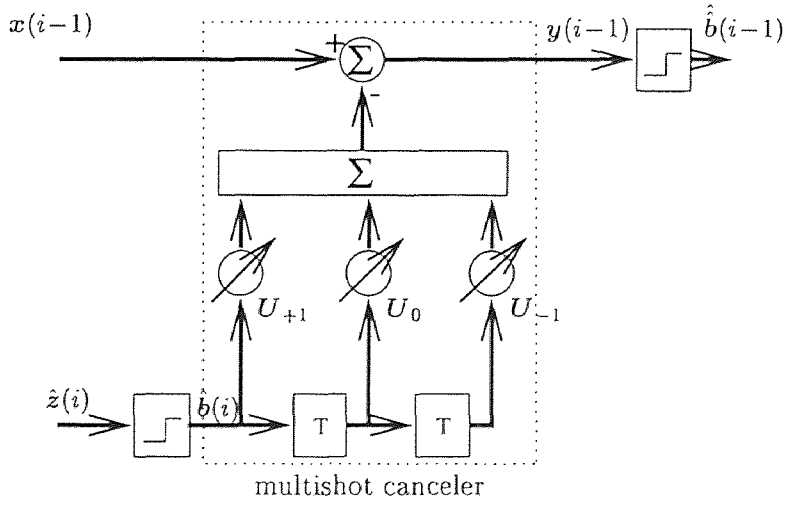

Figure 5.4 Multishot canceler, $N = 3$.

At the output of the canceler, we have (see Fig. 5.4)

$$\boldsymbol{y}(i) = \boldsymbol{x}(i) - \left[\boldsymbol{U}_{-1}^T : \boldsymbol{U}_0^T : \boldsymbol{U}_{+1}^T\right] \begin{bmatrix} \hat{\boldsymbol{b}}(i-1) \\ \hat{\boldsymbol{b}}(i) \\ \hat{\boldsymbol{b}}(i+1) \end{bmatrix} \tag{5.12}$$

in which $\hat{\boldsymbol{b}}(i) = \mathrm{sgn}(\boldsymbol{z}(i))$ (in case of BPSK). The output for the k^{th} user

$$y_k(i) = x_k(i) - \boldsymbol{u}_{-1,k}^T \hat{\boldsymbol{b}}(i-1) - \boldsymbol{u}_{0,k}^T \hat{\boldsymbol{b}}(i) - \boldsymbol{u}_{+1,k}^T \hat{\boldsymbol{b}}(i+1) \tag{5.13}$$

where $\boldsymbol{u}_{\mathrm{j},k}$, $j = -1, 0, 1$ is the k^{th} column of $\boldsymbol{U}_{\mathrm{j}}$. The weights are controlled by

$$\begin{cases} u_{\mathrm{j},kl} \leftarrow u_{\mathrm{j},kl} + \mu \mathrm{E}\left[y_k(i)\hat{b}_l(i-j)\right] & k,l = 1,\cdots,K, \quad j = -1,0,1, \\ & \text{if } j = 0, \text{ then } k \neq l \\ u_{0,kk} = 0 & k = 1,\cdots,K \end{cases} \tag{5.14}$$

5.5 Performance of Multishot Structures

For a non-faded channel, the error performance of 3-symbol ($N = 3$) decorrelators are depicted in Fig. 5.5. SNR_1 is taken to be 8 dB, while the power of the other users is varied. For $K = 2$ and $K = 5$ users, the multishot bootstrap and conventional decorrelator provide comparable performance, significantly better than the single-user conventional detector. The single-user conventional detector uses the same matched filtering as the multishot structures, which is, as mentioned before, equivalent to using a RAKE receiver). For comparison, the single user case ($K = 1$, no MAI) is added.

In figure 5.6, the performance for a 2 user detector using 3 symbols $N = 3$ and 5 symbols $N = 5$ is compared. Again, the single user conventional detector, as well as the single user case (no MAI) (both using the RAKE equivalent matched filtering), are depicted. It demonstrates that the improvement in performance due to increasing N is not significant and does not justify the increased complexity.

Both from figure 5.5 and 5.6 it can be seen that the multishot bootstrap slightly outperforms the conventional (inversion-based) multi-shot for high SIR, as is typical

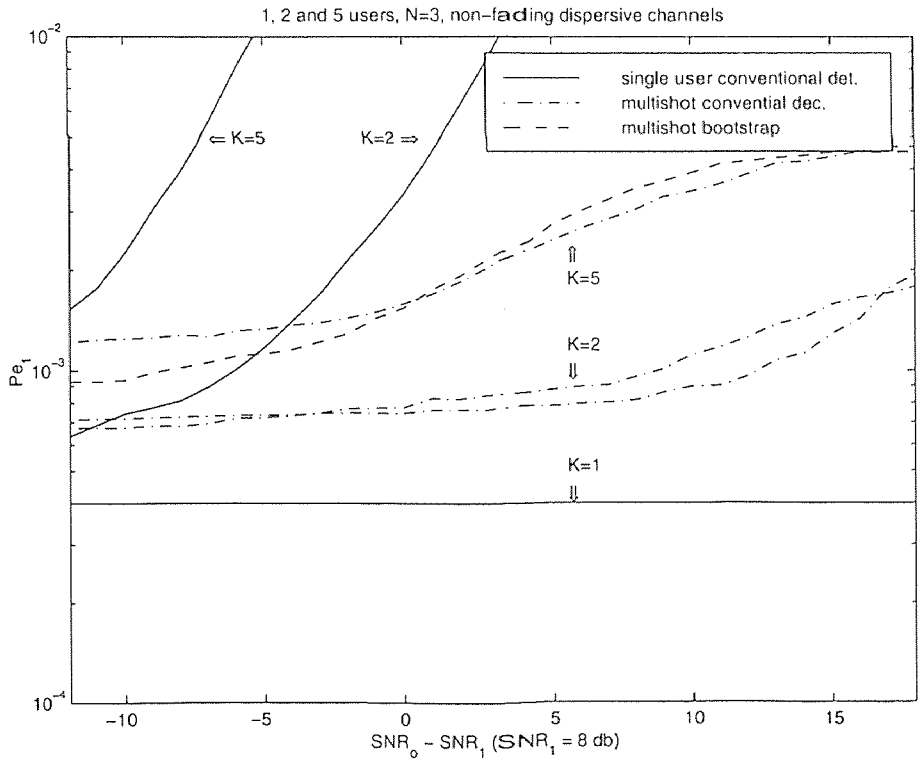

Figure 5.5 Performance of multishot receiver.

for all bootstrap applications, but is slightly worse for low SIR (At this point it should be noted that in the synchronous case, the bootstrap's performance is always equal or better than that of the conventional decorrelator [7]). Such a discrepancy might be due to the inaccuracy in the weight updates, caused by the bias term in (5.6).

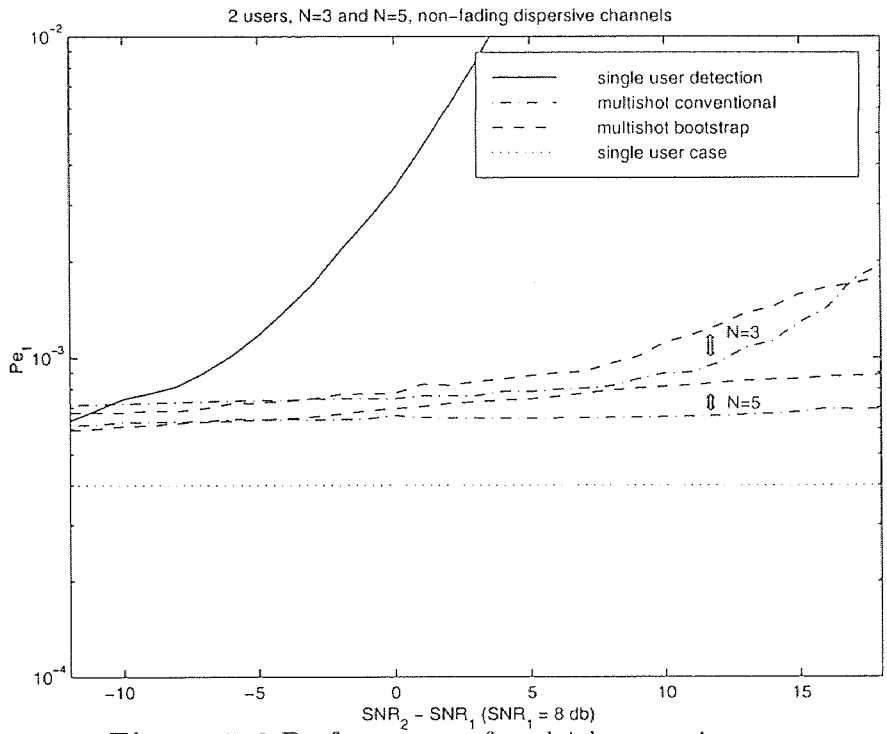

Figure 5.6 Performance of multishot receiver.

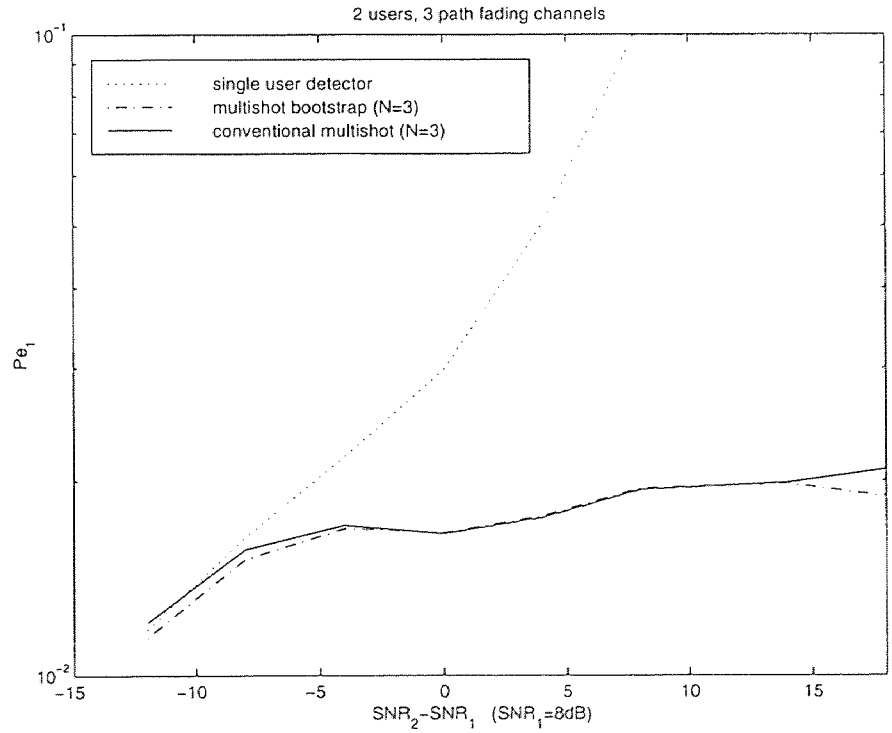

Figure 5.7 Performance of multishot receiver (without canceler) in a dispersive Rayleigh fading environment.

In figure 5.7 the performance in a dispersive Rayleigh fading environment is shown. The simulation was performed by calculating the performance for all three shown receivers in the same 250 fading realizations.

In figure 5.8 the performance improvement due to the addition of the multishot canceler is shown for $K = 2$ and $K = 5$ users. It demonstrates that the two-stage receiver drastically improves the performance, especially for high levels of interference.

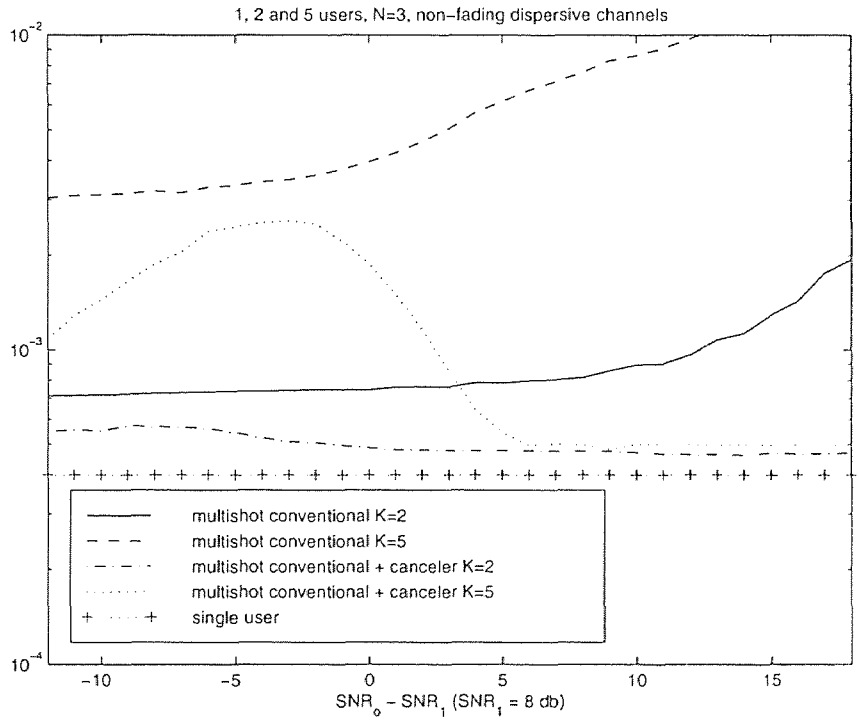

Figure 5.8 Performance of two-stage multishot receiver.

In figure 5.9, we present the results for 16-QAM, rather than BPSK modulation, where the real implementation of the decorrelator matrix $\mathcal{P}$ has the size $2KN \times 2KN$.

In all of the figures, Gold codes of length 15 were used, and each user's channel consisted of 3 paths, seperated by 1 chip.

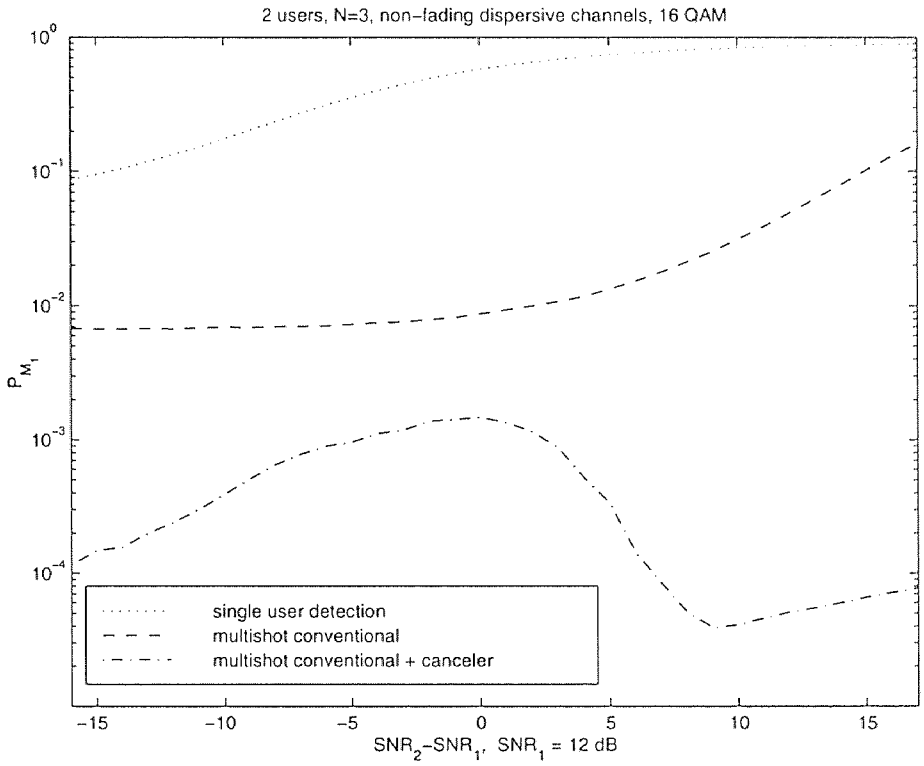

Figure 5.9 Performance of multishot receiver with 16-QAM modulation.

5.6 Joint Adaptive Channel Gain Estimation and Bootstrap Multishot Decorrelator

5.6.1 In slow fading multipath environment

From (5.1) through (5.6), it should be observed that perfect knowledge of the fading coefficients γ_{km} was assumed when calculating the matched filter response. In practice, this has to be separately estimated. In this section, an adaptive scheme is presented to estimate and track these coefficients while simultaneously performing decorrelation. That is, the control of the adaptive gain estimator facilitates the outputs of the ABMSD (see Fig. 5.10)

Clearly, each path coefficient must be estimated separately. Hence, in contrast to matching to the combined paths of each user $(S_{f_k}(t - \tau_k))$, we must match to

each signature code delayed according to each paths delay of the respective user $(s_k(t - iT - \tau_{km}))$. (Note from (1.1) that $\tau_{km} = \tau_k + \delta_{km}$.)

This separation of matched filters will solely affect the number of filters to be used and not the mathematical representation, nor the performance, (at least if the filters use $g_{kl} = \lambda_{kl}$ as before).

The output of the matched filter to a path is

$$\begin{aligned} x_{km}(i) &= \int_{iT+\tau_{km}}^{(i+1)T+\tau_{km}} r(t) s_k(t - iT - \tau_{km}) \\ &= \int_{iT+\tau_{km}}^{(i+1)T+\tau_{km}} s_k(t - iT - \tau_{km}) \cdot [\\ &\quad \sum_{l=1, l\neq k}^{K} \sqrt{a_l} \sum_{n=1}^{M} \gamma_{ln} \sum_{j} b_l(j) s_k(t - jT - \tau_{ln}) + \\ &\quad \sum_{j, j\neq i} \sqrt{a_k} \sum_{n=1}^{M} \gamma_{kn} b_k(j) s_k(t - jT - \tau_{kn}) + \\ &\quad \sqrt{a_k} \sum_{n=1}^{M} \gamma_{kn} b_k(i) s_k(t - iT - \tau_{kn})] \end{aligned} \tag{5.15}$$

in which the first part constitutes the MAI, the second the ISI and the third desired signal on different paths.

The scheme used is depicted in Fig. 5.10.

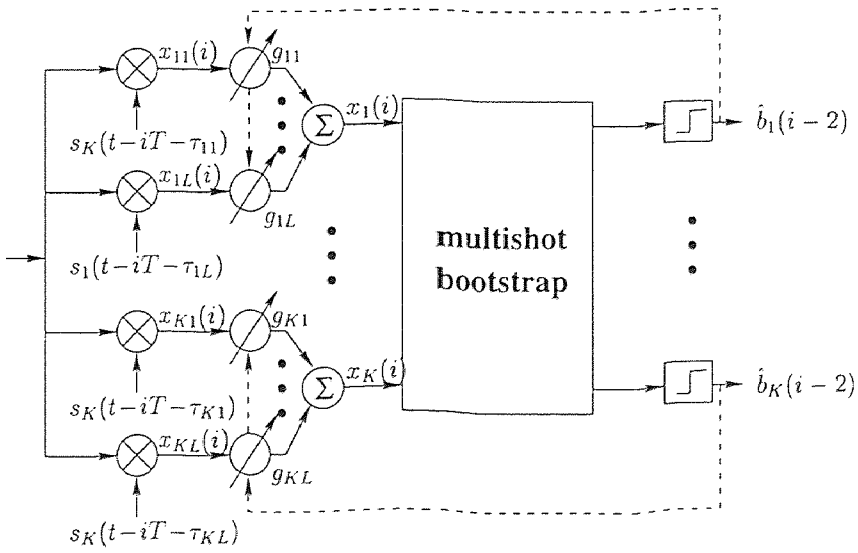

Figure 5.10 Adaptive gain-measurement.

The gains can be initialized with $g_{kl}(1) = 1$ (i.e., equal gains), and are updated according to

$$g_{km}(i) = (1-\mu)g_{km}(i-1) + \mu x_{km}(i-2)\hat{b}_k(i-2) \tag{5.16}$$

Note that, at steady state, in the mean $\mathrm{E}[g_{km}] = \mathrm{E}[x_{km}(i)\hat{b}_k(i)]$. That is, g_{km} will depend only on the terms in correlation with $b_k(i)$. This desired path gain will be shown analytically in the sequel. The different delays in (5.16) are due to the inherent delay in decision in the multi-shot bootstrap.

Higher probability of a better gain-estimation is obtained when the estimate is independent of symbols other than the original symbol attempted to be estimated, i.e. without the effect of MAI. Hence, we avoid making use of the transmitted symbol directly after a matched filter, but rather use the final symbol decisions (in this case at the output of the decorrelator), which have a significantly lower probability of error and are the least dependent on other users signals and ISI components.

Assuming independent data:

$$\begin{aligned}
\mathrm{E}[g_{km}] &= \mathrm{E}\left[x_{km}\hat{b}_k\right] \\
&= \mathrm{E}\left[\int_{iT+\tau_{km}}^{(i+1)T+\tau_{km}} s_k(t-iT-\tau_{km})\sqrt{a_k}\sum_{n=1}^{M}\gamma_{kn}s_k(t-iT-\tau_{kn})b_k(i)\hat{b}_k(i)\right] \\
&= \sqrt{a_k}\sum_{n=1}^{M}\gamma_{kn}\int_{iT+\tau_{km}}^{(i+1)T+\tau_{km}} s_k(t-iT-\tau_{km})s_k(t-iT-\tau_{kn})\mathrm{E}\left[b_k(i)\hat{b}_k(i)\right] \\
&= \sqrt{a_k}(\gamma_{km} + \sum_{n=1,n\neq m}^{M}\rho_{k_{mn}}\gamma_{kn})\mathrm{E}\left[b_k(i)\hat{b}_k(i)\right],
\end{aligned} \tag{5.17}$$

where correlations $\rho_{k_{mn}}$ are defined as

$$\rho_{k_{mn}} = \int_{iT+\tau_{km}}^{(i+1)T+\tau_{km}} s_k(t-iT-\tau_{km})s_k(t-iT-\tau_{kn}). \tag{5.18}$$

Further defining the matrix

$$R_k = \begin{bmatrix} \rho_{k_{11}} & \cdots & \rho_{k_{1M}} \\ \vdots & \ddots & \vdots \\ \rho_{k_{M1}} & \cdots & \rho_{k_{MM}} \end{bmatrix}$$

where from (5.18) $\rho_{k_{mm}} = 1$. Thus, (5.17) can be written as

$$\begin{aligned} \mathrm{E}\left[g_{km}\right] &= \sqrt{a_k}(\gamma_{km} + \sum_{n=1,n\neq m}^{M} \rho_{k_{mn}}\gamma_{kn})\left[b_k(i)\hat{b}_k(i)\right] \\ \mathrm{E}\left[\boldsymbol{g}_k\right] &= \sqrt{a_k}(1-2P_{e_k})\boldsymbol{R}_k\boldsymbol{\gamma}_k, \end{aligned} \tag{5.19}$$

where $\boldsymbol{\gamma}_k = [\gamma_{k1}, \cdots, \gamma_{kM}]$. Since $\sqrt{a_K}(1 - P_{e_k})$ is a scaling constant, it can be removed by normalizing $\sum_l^M g_{km}^2 = 1$. Eqn. (5.19) shows that due to the correlation, the estimated weights are not equal to the maximum ratio weights (maximum ratio under assumed uncorrelated paths), i.e. $\boldsymbol{g}_k \neq \boldsymbol{\gamma}_k$. However, when expressing (5.15) as

$$\begin{aligned} x_{km}(i) &= \int_{iT+\tau_{km}}^{(i+1)T+\tau_{km}} r(t)s_k(t - iT - \tau_{km}) \\ &= \text{MAI} + \text{ISI} + \sqrt{a_k}(\gamma_{km} + \sum_{n=1,n\neq m}^{M} \rho_{k_{mn}}\gamma_{kn})b_k, \end{aligned} \tag{5.20}$$

and comparing this with (5.19), it shows that the adaptive estimator finds the total gain for this path after matched filtering, which is, due to the correlation, notably different from the gain of the path itself, γ_{km}. Hence, the estimator finds the real maximum ratio combining weights for the outputs of the matched filters.

In Fig. 5.11, an example of performance of this adaptive scheme is added. For comparison, equal gain combining ($\boldsymbol{g}_k = \mathbf{1}$) and max. ratio combining ($\boldsymbol{g}_k = \boldsymbol{\gamma}_k$) is also depicted. As suggested, the adaptive gain performs slightly better. Added to this curve is the performance of the conventional single user detector, also using the joint channel estimation as proposed in this section.

5.6.2 In Time-Variant Flat Rayleigh Fading Multipath Channels

In the results presented in the previous sections, no fading was applied, allowing the receiver ample time to adapt to its steady state condition. In this section, the effect of time-variant Raleigh fading channels is examined.

A flat fading channel characterization which has applications to many communications systems of practical importance is described by a fading power spectrum

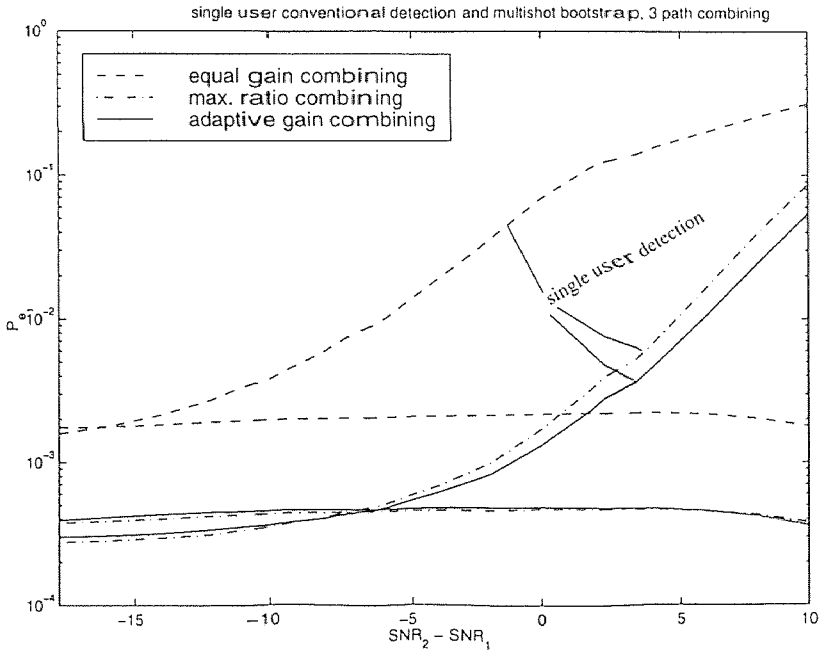

Figure 5.11 Multishot performance using adaptive gain-estimation.

which falls off as f^{-4}:

$$S_h(f) = \frac{A}{(1 + B^2 f^2)^2}. \tag{5.21}$$

Requiring unity channel gain,

$$\int_{-\infty}^{\infty} S_h(f) df = 1, \tag{5.22}$$

gives $A = (2/\pi)B$. Defining $\alpha = 2\pi/B$ allows (5.21) to be rewritten as [21]:

$$S_h(f) = \alpha \left| \frac{\sqrt{2\alpha}}{\alpha + j2\pi f} \right|^2 \left| \frac{\sqrt{2\alpha}}{\alpha + j2\pi f} \right|^2. \tag{5.23}$$

The corresponding correlation function is

$$R_h(\tau) = \mathrm{E}\left[h^*(t)h(t+\tau)\right] = (1 + \alpha|\tau|)e^{-\alpha|\tau|} \tag{5.24}$$

The decorrelation time τ_0 is defined as that value of τ for which $R_h(\tau)$ is $1/e$ of its peak. Quantity $1/\tau_0$ is known as the fading rate. To satisfy the condition $R_h(\tau_0) = 1/e$, we get $\alpha = 2.146/\tau_0$. The factors in (5.23) suggest that $h(t)$ can be generated by passing white Gaussian noise with correlation function $R_g(\tau) = \delta(\tau)$ through

two cascaded single pole filters [21]. In [22], Wittwer has given a simple digital implementation of this arrangement, shown in Fig. 5.12, which produces a sequence of uniformly spaced Gaussian samples $h(n)$ with correlation function

$$R_h(n) = \mathrm{E}\left[h^*(i)h((i+n))\right] = \left(1 + \frac{1-\beta^2}{1+\beta^2}n\right)\beta^n \tag{5.25}$$

where $\beta = \exp(-2.146T/\tau_0)$. For $\tau_0 \gg 1$ $(1-\beta^2)/(1+\beta^2) \approx \alpha T$ and $\mathrm{E}\left[z^*(iT)z((i+n))\right] \approx (1+\alpha nT)e^{(-\alpha nT)}$, which agrees with (5.24)

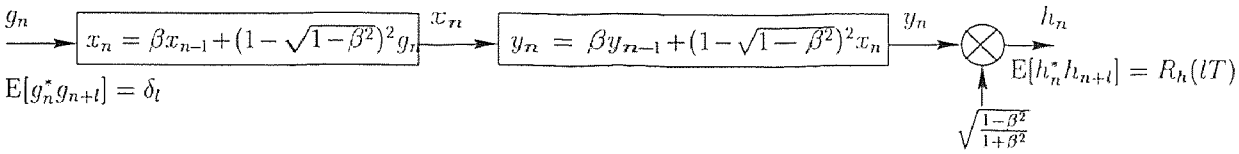

Figure 5.12 Wittwers correlated Gaussian samples generator.

The τ_0 can also be related to the mobile's speed through the coherence time C_T, which is often defined as the required time interval to obtain an envelope correlation of 0.9 or less [23]. From (5.24), it can be shown that $C_T \approx 0.1634\tau_0$. The mobile speed v in relation to Doppler-frequency is given by

$$v = \frac{cf_d}{f} = \frac{c}{fC_T} = \frac{c}{0.1634\tau_0 f} \tag{5.26}$$

where f is the carrier frequency, f_d is the Doppler frequency, c is the speed of light and $f_d = 1/C_T$.

For a PCS system at 1.9 GHz, it follows that $v \approx 3.6/\tau_0$ (km/h). For speeds up to 100 km/h and data-rates as low as 4.8kb/s, it follows that τ_0 will be in the order of a few hundred to a few thousand times T_b. It should be noted, that if the data transmission rate increases, this number becomes larger.

In Fig. 5.13, the performance of the joint adaptive channel gain estimation and bootstrap multishot decorrelator for various values of τ_0, for a fixed value of μ

(the updating constant to both the bootstrap and the gain-estimator) is shown. It depicts that if the fading rate increases, the estimators fail to track its movement. Potentially, this could be corrected by increasing the updating constant.

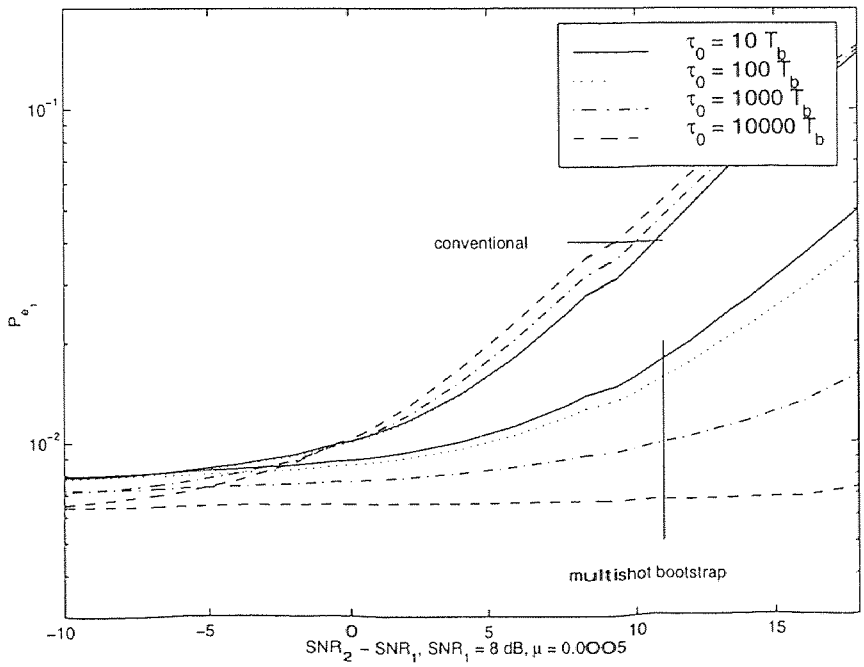

Figure 5.13 Joint adaptive channel estimation and ABMS decorrelator performance in time-variant Rayleigh fading channels (at 1.6 GH and 19.2kbps, $\tau_0 = 1000T_b$ corresponds to 80 km/h).

CHAPTER 6

PERFORMANCE COMPARISON OF (MULTISTAGE) RECEIVER STRUCTURES

In this chapter, a brief simulation comparison is presented concerning the order of multi-path combining and decorrelating in a synchronous environment with multi-path channels using QAM modulation. Also discussed are simulations depicting near-far resistance and sensitivity to errors in delay estimation of the asynchronous receiver structures presented and analyzed in this work.

6.1 Performance Comparison of Bootstrap/Multipath-Combiner Configurations

In a dispersive environment, matching to different paths and combining the results is known to give a certain amount of diversity gain. In a synchronous QAM modulated system with K users, and M resolvable paths per user, a bank of $2KM$ matched filters is needed. Two different forms of processing are posibble in order to improve performance: decorrelating the outputs of the bank of matched filters to rid the the signals of MAI and combining signal paths belonging to the same user to gain energy diversity.

An interesting question is, whether first decorrelating the $2KM$ signals and combining the corresponding M paths (per user), will give a better or worse performance, than first combining each set (of each rail) of M paths of user k, and then decorrelating the $2K$ resulting signals afterwards.

The later arrangement is shown in Fig. 6.1, while the first is depicted in Fig. 6.2. Here it is assumed that the different paths of the same user are delayed by only one chip ($1T_c$) from each other. Since the system's relative delays are very small, ISI can be considered relatively small and is ignored, making the system look synchronous (as in downlink).

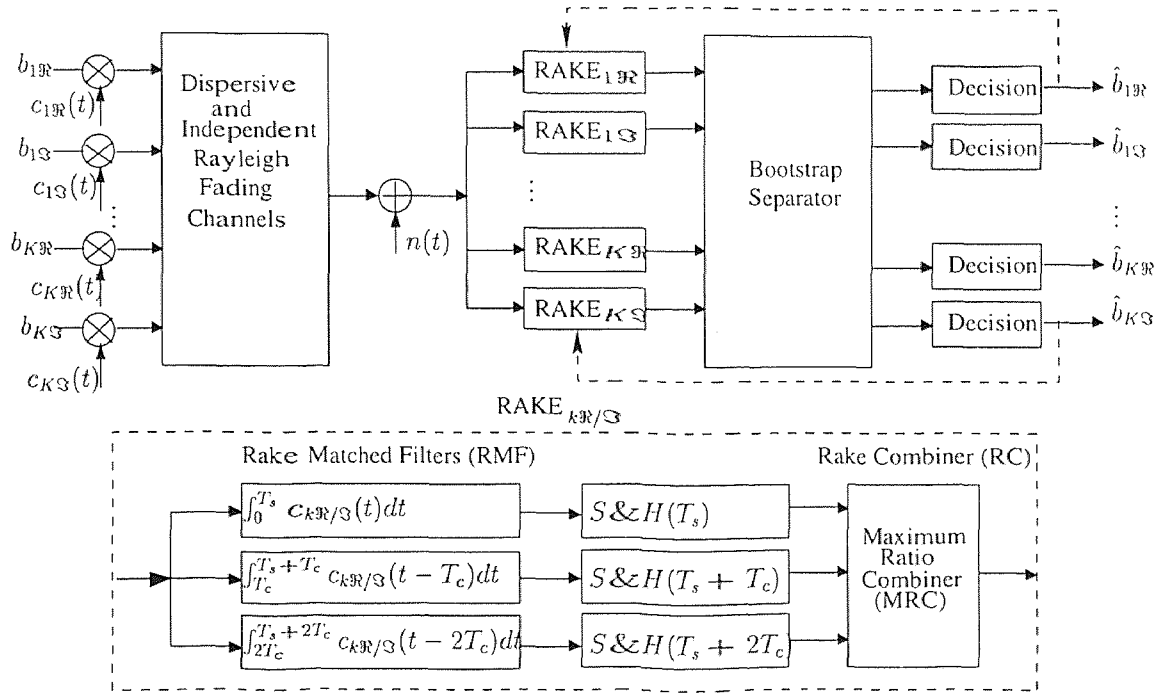

Figure 6.1 Rake receiver + bootstrap separator structure.

The bootstrap structure used is the the complex bootstrap as described in chapter 2, where in the case of combining after decorrelating (Fig. 6.2), the same paths of the same rail of the same user are not decorrelated (similar to the asynchronous case described in chapter 3), due the data in the signals on these rails being the same.

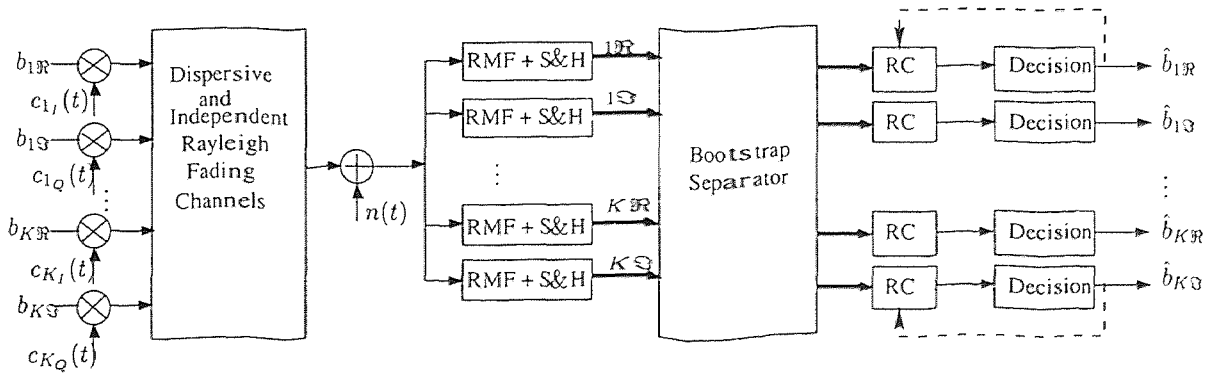

Figure 6.2 Bootstrap separator + Rake receiver structure.

The estimation of the combiner weights is in both structures performed adaptively for each rail by (omitting user and rail subscripts)

$$\boldsymbol{w}(i+1) = (1-\mu)\boldsymbol{w}(i) + \mu\frac{\boldsymbol{x}(i)\mathrm{sgn}(\hat{b}(i))}{\boldsymbol{x}(i)^H\boldsymbol{x}(i)} \tag{6.1}$$

in which $\boldsymbol{x}(i)$ are the inputs of the combiner. This in fact is a discrete implementation of the scheme with low pass filter suggested in [24] for orthogonal waveforms, but has, as shown in section 5.6.1, a similar effect on non-orthogonal waveforms for ISI and MAI, because of the independent data. This estimation is the same as shown in (5.16), except for the fact that here it is normalized, which was not necessary for the BPSK case discussed in chapter 5, but is useful (though not required) for QAM modulation. The reason for this is that, when using QAM-modulation, an adaptive symbol-sorter, as discussed in section 2.4.6, is required, whereas BPSK modulation merely requires a signum function. Normalizing as above keeps the range of the gain in the symbol-sorter small.

The simulation results are shown in Fig. 6.3 and 6.4. From comparing these two figures, we can conclude that combining after decorrelating provides a slightly better performance. However, the computational burden in the decorrelator of this structure is M^2 times larger.

In both figures, a curve is presented for one user with combiner and bootstrap. This bootstrap in this case is added to decorrelate the two rails of the user, as discussed in section 2.4.3.

If the system is asynchronous, as in the uplink, the one-shot decorrelator structures presented in chapter 3 can be used to decorrelate before combining. But as concluded earlier, the computational burden is even larger than for the synchronous case. With one-shot matched filtering, combining before decorrelating will require a full new evaluation of the receiver, as the combination of paths will no longer have the separable parts belonging to the previous and current symbol of a user, There will also be interference from the following symbol, which needs to be dealt with. In

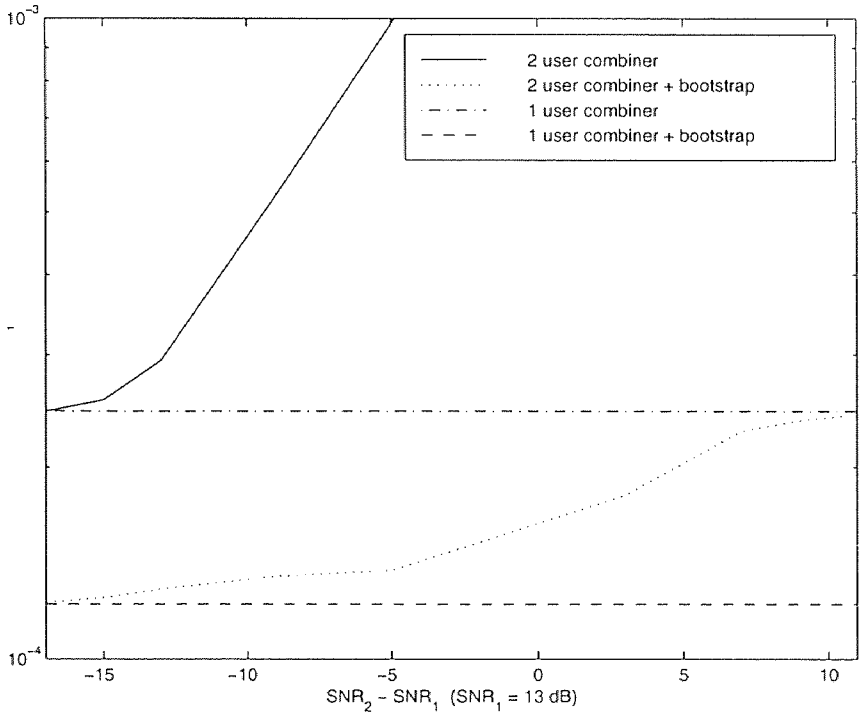

Figure 6.3 Decorrelating-after-combining receiver.

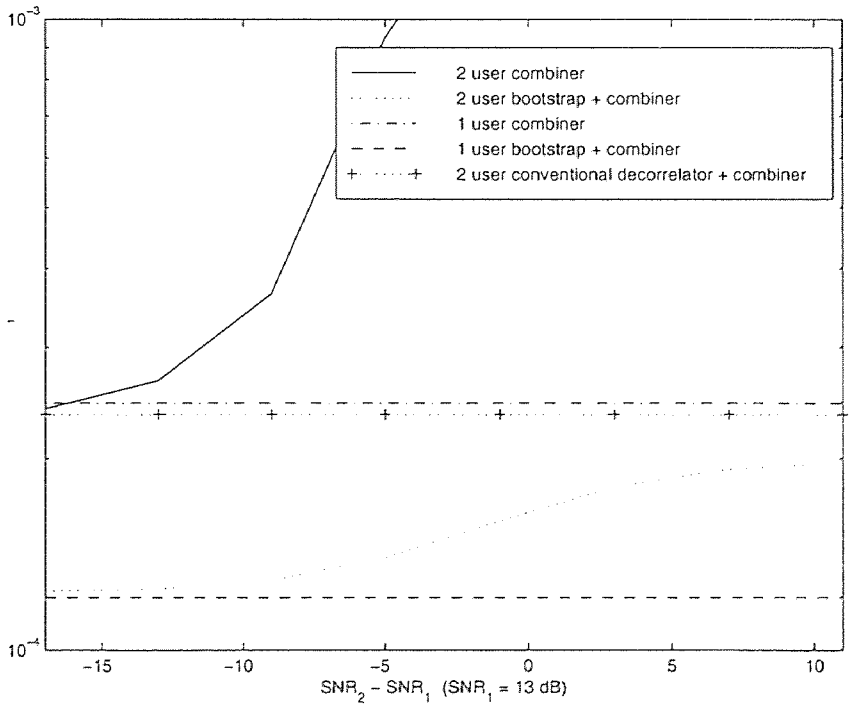

Figure 6.4 Combining-after-decorrelating receiver.

fact, when combining before decorrelating, the correlation matrix will be a function of the correlation matrix before combining, the fading coefficients of each path and the gains of the combiner. It should be noted that, apart from changes occurring in the fading coefficients, generating an estimate of the correlation matrix will be extremely involved, thus making the conventional decorrelator unsuitable for the combining-decorrelating structure. Since both the one-shot and multi-shot will have to deal with both the previous, current, and next symbols, the multi-shot structures would be inherently more suited for combining followed by decorrelation, which is also less complex as stated earlier. Results for this arrangement with multishot were given in chapter 5.

In conclusion, if one uses a one-shot decorrelator then decorrelating before combining is possible although with sacrificed complexity. Decorrelating after combining is difficult both with one-shot or conventional decorrelators. When using the multishot decorrelator, then it is better to implement combining before decorrelating, as it is the less complex of the two arrangements.

6.2 Comparison of Decorrelator Structures

In this section, the one- and multi-shot decorrelators as described and evaluated in in this work are compared in terms of near-far resistance capability[1] and robustness to errors in estimation of the users' relative delays.

The receivers were assumed to have no knowledge of the amplitudes (a_k) and fading coefficients (γ_{km}) of the separate paths of the received signal given by (1.1). The estimation of these parameters was performed with the estimation algorithm shown in chapter 5.

[1] We refer to near-far resistance as the capability to performance of one user (d) as a function of $\mathrm{SNR}_i - \mathrm{SNR}_d$

The relative delays were assumed to be estimated accurately for the near-far resistance comparison, in which each channel has three paths ($M = 3$). On the other hannd, we assume the delays are estimated with error δ_2 for the robustness to delay-estimation errors comparison, in which case both users have channels consisting of only one path $M = 1$, with relative delays $\tau_1 = 0$ and $\tau_2 = 6T_c$ respectively.

The one-shot decorrelators applied are described in chapter 3, that is, decorrelating before combining is used. The multi-shot decorrelators are described in chapter 5, with the path combining is performed first. The MMSE was applied both with decision feedback (DF) and using training sequences (tr. seq).

Fig. 6.5 shows that the multishot structures perform better for low SIR, while the multishot bootstrap improves more slowly in performance as the SIR increases. From 6.6 it can be seen however, that the performances of the different structures are not drastically different, with the exception of the conventional single user detector, which is roughly 2.5 dB worse for equal power users.

In Fig. 6.7 and 6.8, the performance is shown as a function of the error in delay estimation of user two. Both users have an equal SNR of 8 dB. It shows that the adaptive algorithms are more robust over a wider range of errors in the delay estimation. For the bootstrap structures, the performance degraded negligibly over a range of $-0.2\tau_c$ to $0.2\tau_c$, while for the fixed decorrelators, this is only half. Fig. 6.8 shows the performance of the user for which the delay was estimated with offset δ_2. The performances are approximately equal, with exception of the single user detector. It can be seen that the probability of error goes to 1 as the offset nears $1T_c$, which is due to the auto-correlation R(t) of the users code being negative for $1Tc$, which hence inverts the signal of user 2 at the output of the matched filter matched to the code of user 2.

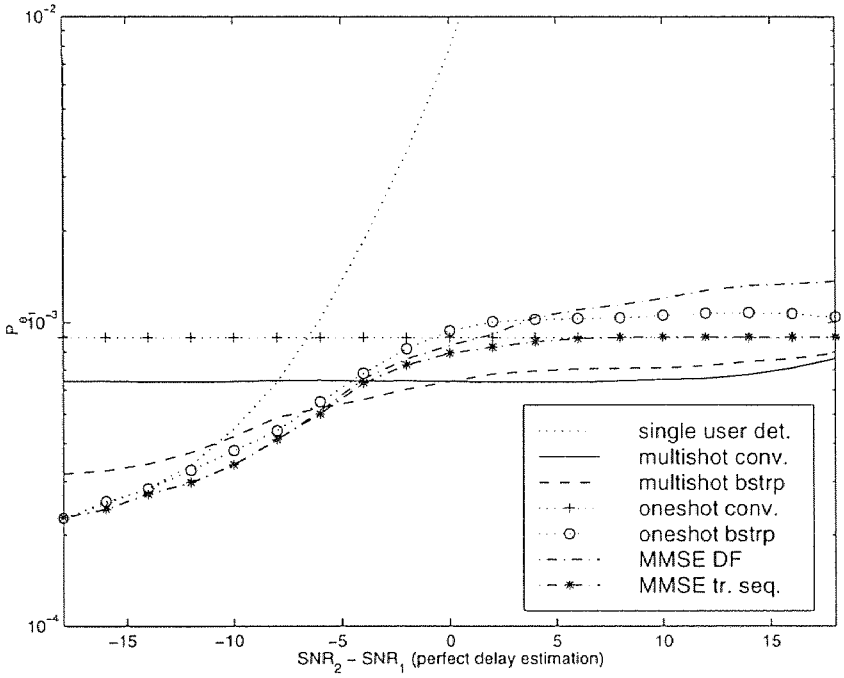

Figure 6.5 Comparison of near-far resistance (user 1).

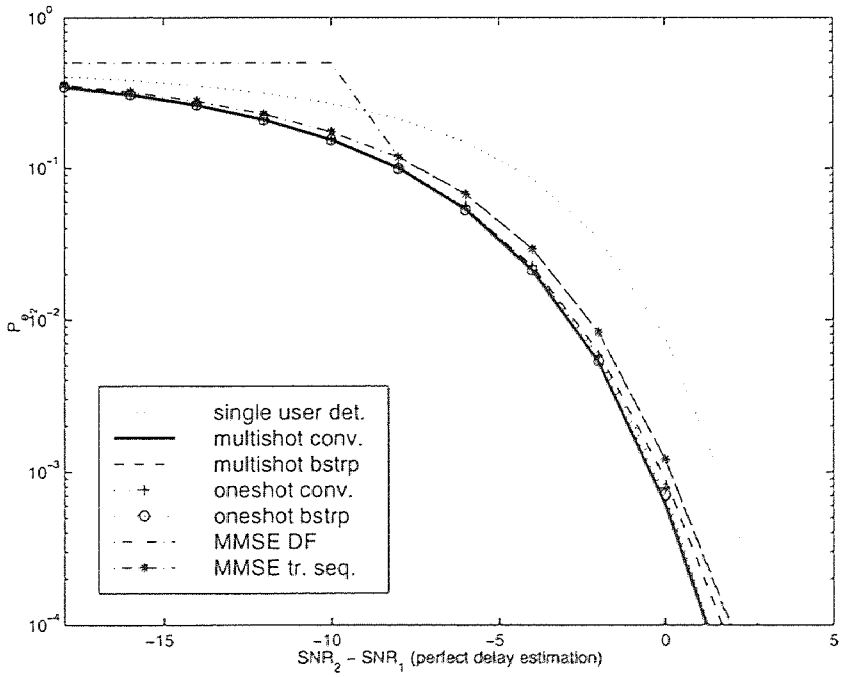

Figure 6.6 Comparison of near-far resistance (user 2).

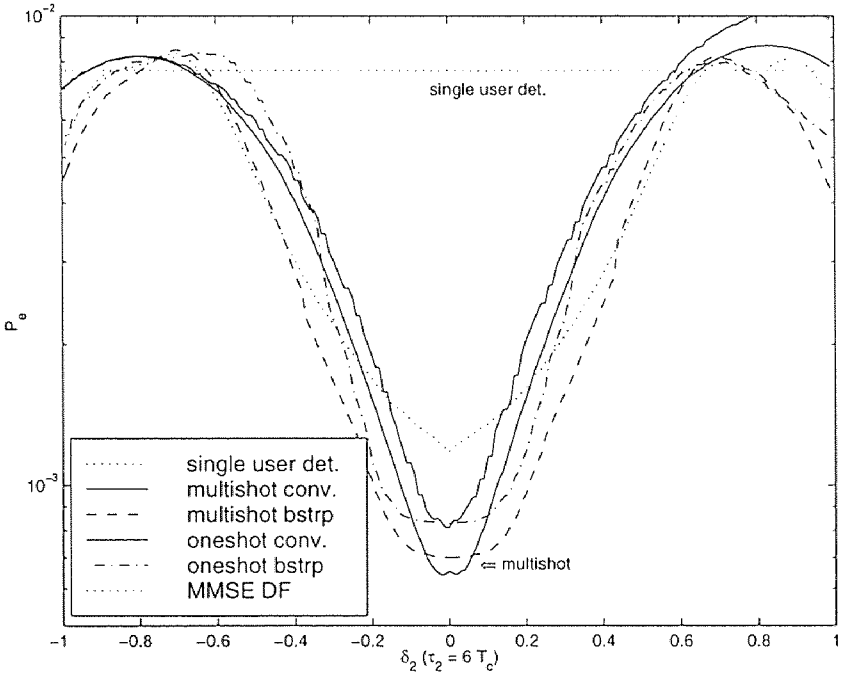

Figure 6.7 Comparison of robustness to delay estimation errors (user 1).

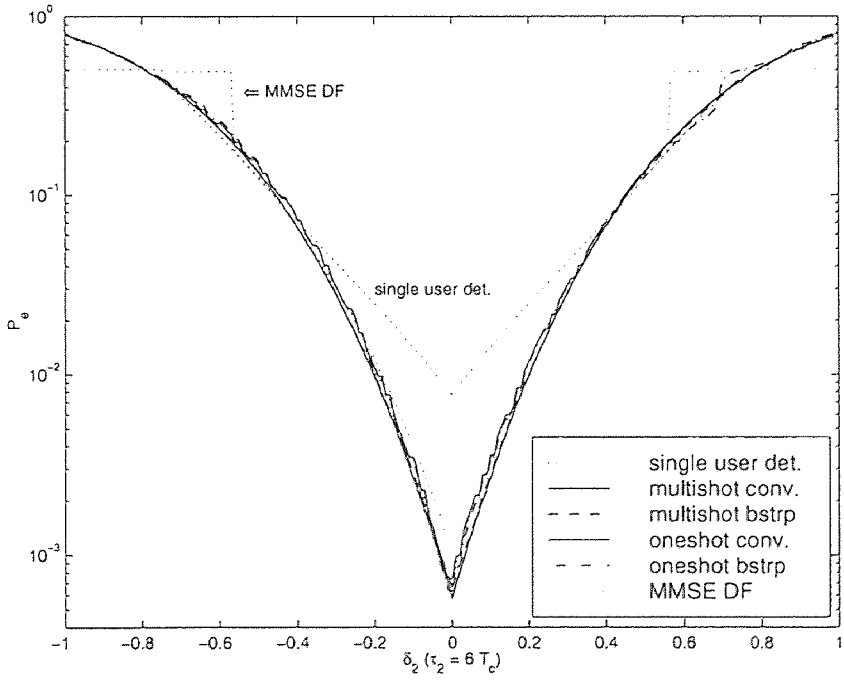

Figure 6.8 Comparison of robustness to delay estimation errors (user 1).

CHAPTER 7
CONCLUSIONS

In the preceding chapters, it has been shown that the bootstrap decorrelator can be used to decorrelate QAM-modulated multi-user CDMA signals. It was established that the signum function can be used as discriminator, exactly as in the case of BPSK modulation.

The bootstrap decorrelator for QAM was shown both in the real and in the complex domain. The resultant algorithm of complex signals was termed "the Complex Bootstrap". The steady state weights were derived analytically for high levels of interference and the symbol error rate was found under the assumption of no intra-rail correlation, and perfect power estimation for the decision stage. As an extra intra-rail decorrelation is needed due to vector rotation, the no intra-rail assumption is not a generality limit. We also suggested an adaptive power estimating scheme for the decision stage, which was used in the shown simulations.

Comparing this complex bootstrap scheme with the correlation-matrix inversion based conventional decorrelator and the conventional single-user (no MAI) performance, it was found that the bootstrap decorrelator performance tends towards the single-user performance for high SIR and approaches the inversion based decorrelators performance for low SIR. Forming a multistage receiver by adding a suitable canceler was shown to improve the performance in the low SIR region, as in the case of BPSK.

In handling multipath asynchronous channels, we depicted the special structure of the weight matrix needed for the bootstrap algorithm, and showed its performance.

It was established that the one-shot conventional asynchronous based decorrelator suffers from ill-conditionedness and singularity of the cross-correlation matrix. Hence we also examined the multishot decorrelator, which does not suffer from this problem. The bootstrap multi-shot decorrelator and the multishot canceler were

presented, and shown simulation-wise, that the performance is similar to that of the conventional multi-shot inversion decorrelator, which is based on matrix inversion and which requires full knowledge about cross-correlations. Using an adaptive channel gain estimation, the adaptive bootstrap multishot decorrelator was shown to be able to adapt to time-variant Rayleigh fading channels, at practical fading rates. This presents joint adaptive channel estimation and decorrelation.

The impact of the order of processing of signals from a dispersive environment, was examined, which showed that decorrelating the signals before path combining gives a somewhat better performance for low SIR. However, the computational burden of processing in this order is significantly larger. The one-shot asynchronous bootstrap decorrelator, capable of decorrelating the signals from resolved paths, was presented to facilitate the decorrelate before combining case. It does not seem easy to use one-shot decorrelators after path combining. However, this arrangement is possible and preferred from a complexity point of view.

Lastly, the near-far resistance and robustness to estimation errors in relative delay of the signals from different users was examined using simulations. It was shown that the bootstrap algorithm, both based on oneshot and multishot matched filtering, is more robust to estimation errors than the conventional decorrelators and MMSE with decision feedback. It was also shown that the performance of the oneshot and multishot bootstrap and MMSE have comparable performances in terms of near-far resistance, with the adaptive bootstrap multishot slightly outperforming the others for low SIR and the others slightly outperforming the multishot for high SIR.

APPENDIX A

WEIGHT DERIVATION FOR ORTHOGONAL QAM

In this appendix, the closed form solution of δ_1, as a result of (2.14) is derived. Expanding from (2.14)

$$\begin{aligned} E\left[z_1 \mathrm{sgn} z_i\right] &= E\left[\left(\sqrt{a_1}\left(1-\boldsymbol{\rho}_1^T \boldsymbol{P}_1^{-1}\boldsymbol{\rho}_1 - \boldsymbol{\delta}_1^T \boldsymbol{P}_1^{-1}\boldsymbol{\rho}_1\right) b_1 - \boldsymbol{\delta}_1^T \boldsymbol{A}_1 \boldsymbol{b}_1\right)\cdot \right. \\ &\qquad \left. \mathrm{sgn}\left(\sqrt{a_1}\left(1-\boldsymbol{\rho}_i^T \boldsymbol{P}_i^{-1}\boldsymbol{\rho}_i\right) b_i + \zeta_i\right)\right] + \\ &\qquad E\left[\zeta_1' \mathrm{sgn}\left(\sqrt{a_i}\left(1-\boldsymbol{\rho}_i^T \boldsymbol{P}_i^{-1}\boldsymbol{\rho}_i\right) b_i + \zeta_i\right)\right] \quad i=2,\ldots,K \end{aligned} \tag{A.1}$$

Concentrating first on the first expectation of (A.1)

$$\begin{aligned} &E_{\boldsymbol{b}}\left[(\sqrt{a_1}(1-\boldsymbol{\rho}_1^T \boldsymbol{P}_1^{-1}\boldsymbol{\rho}_1)b_1 - \boldsymbol{\delta}^T \boldsymbol{P}_1^{-1}\boldsymbol{b}_1)\cdot \right. \\ &\qquad \left. (P_R\left\{\zeta_i > -\sqrt{a_i}(1-\boldsymbol{\rho}_i^T \boldsymbol{P}_i^{-1}\boldsymbol{\rho}_i)b_i\right\} - P_R\left\{\zeta_i < -\sqrt{a_i}(1-\boldsymbol{\rho}_i^T \boldsymbol{P}_i^{-1}\boldsymbol{\rho}_i)b_i\right\}\right] \end{aligned} \tag{A.2}$$

Using the independence of data

$$\begin{aligned} E_{\boldsymbol{b}} &= E_{\boldsymbol{b}_1}\left[-\boldsymbol{\delta}^T \boldsymbol{A}_1 \boldsymbol{b}_1\left(2Q(\frac{-\sqrt{a_i}(1-\boldsymbol{\rho}_i^T \boldsymbol{P}_i^{-1}\boldsymbol{\rho}_i)b_i}{\sigma_{\zeta_i}}) - 1\right)\right] \\ &= E_{b_i}\left[-\delta_i\sqrt{a_i}|b_i|\mathrm{sgn}(b_i)\left(2Q(\frac{-\sqrt{a_i}(1-\boldsymbol{\rho}_i^T \boldsymbol{P}_i^{-1}\boldsymbol{\rho}_i)|b_i|\mathrm{sgn}(b_i)}{\sigma_{\zeta_i}}) - 1\right)\right] \\ &= E_{b_i}\left[\delta_i\sqrt{a_i}|b_i|\left(2Q(\frac{\sqrt{a_i}(1-\boldsymbol{\rho}_i^T \boldsymbol{P}_i^{-1}\boldsymbol{\rho}_i)|b_i|}{\sigma_{\zeta_i}}) - 1\right)\right] \\ &= E_{b_i}\left[\delta_i\sqrt{a_i}|b_i|\left(2Q(\frac{\sqrt{a_i}\sqrt{(1-\boldsymbol{\rho}_i^T \boldsymbol{P}_i^{-1}\boldsymbol{\rho}_i)}|b_i|}{\sigma}) - 1\right)\right] \\ &= \left[\delta_i\sqrt{a_i}\frac{2}{\sqrt{M}}\sum_{m=1}^{\frac{\sqrt{M}}{2}}(2m-1)c\left(2Q(\frac{\sqrt{a_i}\sqrt{(1-\boldsymbol{\rho}_i^T \boldsymbol{P}_i^{-1}\boldsymbol{\rho}_i)}(2m-1)c}{\sigma}) - 1\right)\right] \\ &= \left[\delta_i\sqrt{a_i}\left(\frac{2}{\sqrt{M}}\sum_{m=1}^{\frac{\sqrt{M}}{2}}(2m-1)c2Q(\sqrt{\mathrm{LSNR}_i}(2m-1)c) - c\right)\right] \end{aligned}$$

where

$$\sigma_{\zeta_i}^2 = E\left[(n_i - \boldsymbol{\rho}_i^T \boldsymbol{P}_i^{-1}\boldsymbol{n}_i)(n_i - \boldsymbol{n}_i^T \boldsymbol{P}_i^{-1}\boldsymbol{\rho}_i)\right] = \sigma^2(1-\boldsymbol{\rho}_i^T \boldsymbol{P}_i^{-1}\boldsymbol{\rho}_i) \tag{A.3}$$

was derived from (2.13). and $\mathrm{LSNR}_i \triangleq \frac{a_i}{\sigma^2}(1-\boldsymbol{\rho}_i^T\boldsymbol{P}_i^{-1}\boldsymbol{\rho}_i)$. Defining

$$\boldsymbol{Q}_1 = \frac{2}{\sqrt{M}}\sum_{m=1}^{\frac{\sqrt{M}}{2}}(2m-1)c\cdot\mathrm{diag}\left(Q(\sqrt{\mathrm{LSNR}_2}(2m-1)c),\cdots,Q(\sqrt{\mathrm{LSNR}_K}(2m-1)c)\right), \tag{A.4}$$

where $Q(\cdot)$ is the error function and

$$\boldsymbol{D}_1 = \sqrt{\frac{2}{M\pi}}\sum_{m=1}^{\frac{\sqrt{M}}{2}}\mathrm{diag}\left(\frac{\exp\left(-\frac{1}{2}\mathrm{LSNR}_2(2m-1)^2c^2\right)}{\sqrt{\mathrm{LSNR}_2}},\cdots,\frac{\exp\left(-\frac{1}{2}\mathrm{LSNR}_K(2m-1)^2c^2\right)}{\sqrt{\mathrm{LSNR}_K}}\right. \tag{A.5}$$

which should be recognized as an upperbound on $\boldsymbol{Q}_1$, which is tight when all LSNR_k are large. The first expectation from (A.1) is found from (A.3) to be

$$E[z_1\mathrm{sgn}\boldsymbol{z}_i]_{part1} = (2\boldsymbol{Q}_1 - cI)\boldsymbol{A}_1\boldsymbol{\delta}_1 \tag{A.6}$$

Using the transformation

$$\zeta_i = \lambda_i \text{ and } \zeta_1' = \frac{\sqrt{E[\zeta_1'\zeta_i]}}{E[\zeta_i^2]}\lambda_i + \frac{E[\zeta_1'^2]E[\zeta_i^2]-(E[\zeta_1'\zeta_i])^2}{E[\zeta_i^2]}\lambda_i,$$

which results in $E[\lambda_1\lambda_i]=0$, $E[\lambda_1^2]=E[\lambda_i^2]=E[\zeta_i^2]$, and defining $F_i = \frac{\sqrt{E[\zeta_1'\zeta_i]}}{E[\zeta_i^2]}$, the second part of (A.1) can be written as

$$E\left[\left(F_i\lambda_i + \frac{E[\zeta_1'^2]E[\zeta_i^2]-(E[\zeta_1'\zeta_i])^2}{E[\zeta_i^2]}\lambda_1\right)\mathrm{sgn}(\sqrt{a_i}(1-\boldsymbol{\rho}_i^T\boldsymbol{P}_i^{-1}\boldsymbol{\rho}_i)b_i+\lambda_i)\right]$$

Since λ_i and λ_1 are independent zero mean random variables

$$\begin{aligned} & E\left[F_i\lambda_i\mathrm{sgn}(\sqrt{a_i}(1-\boldsymbol{\rho}_i^T\boldsymbol{P}_i^{-1}\boldsymbol{\rho}_i)b_i+\lambda_i)\right] \\ = \; & F_iE_{b_i}\left[\int_{-\sqrt{a_i}(1-\boldsymbol{\rho}_i^T\boldsymbol{P}_i^{-1}\boldsymbol{\rho}_i)b_i}^{\infty}\lambda_i f(\lambda_i)d\lambda_i + \int_{\sqrt{a_i}(1-\boldsymbol{\rho}_i^T\boldsymbol{P}_i^{-1}\boldsymbol{\rho}_i)b_i}^{\infty}\lambda_i f(\lambda_i)d\lambda_i\right] \end{aligned}$$

which, as both $-|b_i|$ and $+|b_i|$ give the same result, leads to (with substitution of (A.3))

$$\begin{aligned} & 2F_iE_{b_i}\left[\frac{\sigma}{\sqrt{2\pi}}\sqrt{1-\boldsymbol{\rho}_i^T\boldsymbol{P}_i^{-1}\boldsymbol{\rho}_i}\exp\left(-\frac{1}{2}LSNR_i|b_i|^2\right)\right] \\ = \; & 2F_i\frac{\sigma}{\sqrt{2\pi}}\sqrt{1-\boldsymbol{\rho}_i^T\boldsymbol{P}_i^{-1}\boldsymbol{\rho}_i}\frac{2}{\sqrt{M}}\sum_{m=1}^{\frac{\sqrt{M}}{2}}\exp\left(-\frac{1}{2}LSNR_i(2m-1)^2c^2\right) \end{aligned} \tag{A.7}$$

To calculate F_i we first notice that

$$\begin{aligned}\zeta_1'\zeta_i &= \left(n_1 - \left(\rho_1^T + \delta_1^T\right)\boldsymbol{P}_1^{-1}\boldsymbol{n}_1\right)\left(n_i - \rho_i^T\boldsymbol{P}_i^{-1}\boldsymbol{n}_i\right) \\ &= \left[\begin{array}{cc} 1 & -\rho_1^T\boldsymbol{P}_1^{-1}\end{array}\right]\left[\begin{array}{c} n_1 \\ \boldsymbol{n}_1\end{array}\right]\left[\begin{array}{cc} n_i & \boldsymbol{n}_i^T\end{array}\right]\left[\begin{array}{c} 1 \\ -\boldsymbol{P}_i^{-1}\rho_i\end{array}\right] - \\ &\qquad \delta_1^T\boldsymbol{P}_1^{-1}\boldsymbol{n}_1\left[\begin{array}{cc} n_i & \boldsymbol{n}_i^T\end{array}\right]\left[\begin{array}{c} 1 \\ -\boldsymbol{P}_i^{-1}\rho_i\end{array}\right]\end{aligned} \tag{A.8}$$

so that

$$\begin{aligned}E\left[\zeta_z'\zeta_i\right] &= \sigma^2\left[\begin{array}{cc} 1 & -\rho_1^T\boldsymbol{P}_1^{-1}\end{array}\right]\boldsymbol{P}Y_i\left[\begin{array}{c} 1 \\ -\boldsymbol{P}_i^{-1}\rho_i\end{array}\right] - \\ &\qquad \sigma^2\delta_1^T\boldsymbol{P}_1^{-1}\left[\begin{array}{cc} \rho_1 & \boldsymbol{P}_1\end{array}\right]Y_i\left[\begin{array}{c} 1 \\ -\boldsymbol{P}_i^{-1}\rho_i\end{array}\right]\end{aligned} \tag{A.9}$$

where Y_i is the identity matrix with column i put in front of all the other columns. When a matrix is post-multiplied with Y_i then its i^{th} column w ill be placed as the first, and the others will be shifted to the right.

Now we notice that

$$\begin{aligned}\left[\begin{array}{cc} 1 & -\rho_1^T\boldsymbol{P}_1^{-1}\end{array}\right]\boldsymbol{P}Y_i\left[\begin{array}{c} 1 \\ -\boldsymbol{P}_i^{-1}\rho_i\end{array}\right] &= \left[\begin{array}{cc} 1-\rho_1^T\boldsymbol{P}_1^{-1}\rho_1 & 0\end{array}\right]Y_i\left[\begin{array}{c} 1 \\ -\boldsymbol{P}_i^{-1}\rho_i\end{array}\right] \\ &= -\left(1-\rho_1^T\boldsymbol{P}_1^{-1}\rho_1\right)\left(\boldsymbol{P}_i^{-1}\rho_i\right)_1 \\ &= \left(1-\rho_i^T\boldsymbol{P}_i^{-1}\rho_i\right)\psi_i\end{aligned}$$

$$\begin{aligned}-\delta_1^T\boldsymbol{P}_1^{-1}\left[\begin{array}{cc} \rho_1 & \boldsymbol{P}_1\end{array}\right]Y_i\left[\begin{array}{c} 1 \\ -\boldsymbol{P}_i^{-1}\rho_i\end{array}\right] &= -\delta_1^T\left[\begin{array}{cc} \boldsymbol{P}_1^{-1}\rho_1 & I\end{array}\right]Y_i\left[\begin{array}{c} 1 \\ -\boldsymbol{P}_i^{-1}\rho_i\end{array}\right] \\ &= -\delta_1^T\boldsymbol{P}_1^{-1}\rho_1\psi_i - \delta_1^T T_i\left\{-\boldsymbol{P}_i^{-i}\rho_i\right\} \\ &\equiv -\delta_1^T\boldsymbol{P}_1^{-1}\rho_1\psi_i - \delta_1^T\gamma_i\end{aligned} \tag{A.10}$$

where I is a $(K-1)\,\mathrm{x}\,(K-1)$ identity matrix, and $T_i\{\boldsymbol{x}\}$ is a transformation on the vector $\boldsymbol{x}$ that removes the first element of the vector, shifts elements 2 to $i-1$ one place up and inserts a 1 on the now v vacant position $i-1$. Using (A.9) and (A.3) we find F_i to be

$$F_i = \frac{\left(1-\rho_i^T\boldsymbol{P}_i^{-1}\rho_i\right)\psi_i - \delta_1^T\boldsymbol{P}_1^{-1}\rho_1\psi_i - \delta_1^T\gamma_i}{1-\rho_i^T\boldsymbol{P}_i^{-1}\rho_i}. \tag{A.11}$$

Combining this with (A.7) finally results in

$$\begin{aligned} & E[\zeta_1' \mathrm{sgn}(\sqrt{a_i}(1-\boldsymbol{\rho}_i^T\boldsymbol{P}_i^{-1}\boldsymbol{\rho}_i)b_i+\zeta_i] \\ = & \frac{2\sigma\left(\left(1-\boldsymbol{\rho}_i^T\boldsymbol{P}_i^{-1}\boldsymbol{\rho}_i\right)\psi_i-\boldsymbol{\delta}_1^T\boldsymbol{P}_1^{-1}\boldsymbol{\rho}_1\psi_i-\boldsymbol{\delta}_1^T\boldsymbol{\gamma}_i\right)}{\sqrt{2\pi\left(1-\boldsymbol{\rho}_i^T\boldsymbol{P}_i^{-1}\boldsymbol{\rho}_i\right)}}\cdot \\ & \frac{2}{\sqrt{M}}\sum_{m=1}^{\frac{\sqrt{M}}{2}}\exp\left(-\frac{1}{2}LSNR_i(2m-1)^2c^2\right) \\ = & 2\sqrt{a_i}\left(\left(1-\boldsymbol{\rho}_i^T\boldsymbol{P}_i^{-1}\boldsymbol{\rho}_i\right)\psi_i-\boldsymbol{\delta}_1^T\boldsymbol{P}_1^{-1}\boldsymbol{\rho}_1\psi_i-\boldsymbol{\delta}_1^T\boldsymbol{\gamma}_i\right)\cdot \\ & \sqrt{\frac{2}{\pi M}}\sum_{m=1}^{\frac{\sqrt{M}}{2}}\frac{\exp\left(-\frac{1}{2}LSNR_i(2m-1)^2c^2\right)}{\sqrt{\mathrm{LSNR}_i}} \end{aligned} \tag{A.12}$$

The second expectation from (A.1) is now found to be

$$E\left[z_1\mathrm{sgn}\boldsymbol{z}_1\right]_{part2}=2\boldsymbol{A}_1\boldsymbol{D}_1\left(\left(1-\boldsymbol{\rho}_1^T\boldsymbol{P}_1^{-1}\boldsymbol{\rho}_1\right)\boldsymbol{\psi}_1-\boldsymbol{\psi}_1\boldsymbol{\rho}_1^T\boldsymbol{P}_1^{-1}\boldsymbol{\delta}_1-\boldsymbol{\Gamma}\boldsymbol{\delta}_1\right) \tag{A.13}$$

in which $\boldsymbol{\psi}_1$ is defined as

$$\boldsymbol{\psi}_1=\left[\begin{array}{ccc}\left(-\boldsymbol{P}_2^{-1}\boldsymbol{\rho}_2\right)_1 & \cdots & \left(-\boldsymbol{P}_K^{-1}\boldsymbol{\rho}_K\right)_1\end{array}\right]^T \tag{A.14}$$

and $\boldsymbol{\Gamma}$ as the $K-1\times K-1$ matrix of which the rows are given by $T_i\left\{-\boldsymbol{\rho}_i^T\boldsymbol{P}_i^{-1}\right\}$. The transformation $T_i\left\{\boldsymbol{x}^T\right\}$ removes the first element of the row-vector $\boldsymbol{x}^T$, shifts elements 2 through $i-1$ one place to the left and inserts a 1 on the now open place $i-1$.

Now equating (A.1) to zero from (A.6) and (A.13) gives

$$\left(\left(2\boldsymbol{Q}_1-c\boldsymbol{I}\right)\boldsymbol{P}_1-2\boldsymbol{D}_1\left(\boldsymbol{\psi}_1\boldsymbol{\rho}_1^T+\boldsymbol{\Gamma}\boldsymbol{P}_1\right)\right)\boldsymbol{P}_1^{-1}\boldsymbol{\delta}_1=-2\boldsymbol{D}_1\left(1-\boldsymbol{\rho}_1^T\boldsymbol{P}_1^{-1}\boldsymbol{\rho}_1\right)\boldsymbol{\psi}_1, \tag{A.15}$$

which results in (if $\left(\boldsymbol{\psi}_1\boldsymbol{\rho}_1^T+\boldsymbol{\Gamma}\boldsymbol{P}_1\right)$ is invertible)

$$\boldsymbol{\delta}_1=\boldsymbol{P}_1\left[\boldsymbol{I}+\left(\boldsymbol{\psi}_1\boldsymbol{\rho}_1^T+\boldsymbol{\Gamma}\boldsymbol{P}_1\right)^{-1}\boldsymbol{D}_1^{-1}(\frac{c}{2}\boldsymbol{I}-\boldsymbol{Q}_1)\boldsymbol{P}_1\right]^{-1}\left(\boldsymbol{\psi}_1\boldsymbol{\rho}_1^T+\boldsymbol{\Gamma}\boldsymbol{P}_1\right)^{-1}(1-\boldsymbol{\rho}_1^T\boldsymbol{P}_1^{-1}\boldsymbol{\rho}_1)\boldsymbol{\psi}_1 \tag{A.16}$$

APPENDIX B

ONE-SHOT BOOTSTRAP FOR DISPERSIVE CHANNELS, TWO USER CASE

B.1 The Decorrelator

In this Appendix, the one-shot bootstrap decorrelator for multi-path channels is shown for the case of two users, each of which has a channel consisting of 2 distint paths. Repeating for convenience (3.4)

$$\boldsymbol{x}(0) = \boldsymbol{PAb}(0) + \boldsymbol{n}(0) \tag{B.1}$$

where

$$\boldsymbol{P} = \begin{bmatrix} \rho_{11}^{2L2L} & \rho_{11}^{2L1R} & \rho_{11}^{2L2R} & \rho_{12}^{2L1L} & \rho_{12}^{2L2L} & \rho_{12}^{2L1R} & \rho_{12}^{2L2R} \\ \rho_{11}^{1R2L} & \rho_{11}^{1R1R} & \rho_{11}^{1R2R} & \rho_{12}^{1R1L} & \rho_{12}^{1R2L} & \rho_{12}^{1R1R} & \rho_{12}^{1R2R} \\ \rho_{11}^{2R2L} & \rho_{11}^{2R1R} & \rho_{11}^{2R2R} & \rho_{12}^{2R1L} & \rho_{12}^{2R2L} & \rho_{12}^{2R1R} & \rho_{12}^{2R2R} \\ \rho_{21}^{1L2L} & \rho_{21}^{1L1R} & \rho_{21}^{1L2R} & \rho_{22}^{1L1L} & \rho_{22}^{1L2L} & \rho_{22}^{1L1R} & \rho_{22}^{1L2R} \\ \rho_{21}^{2L2L} & \rho_{21}^{2L1R} & \rho_{21}^{2L2R} & \rho_{22}^{2L1L} & \rho_{22}^{2L2L} & \rho_{22}^{2L1R} & \rho_{22}^{2L2R} \\ \rho_{21}^{1R2L} & \rho_{21}^{1R1R} & \rho_{21}^{1R2R} & \rho_{22}^{1R1L} & \rho_{22}^{1R2L} & \rho_{22}^{1R1R} & \rho_{22}^{1R2R} \\ \rho_{21}^{2R2L} & \rho_{21}^{2R1R} & \rho_{21}^{2R2R} & \rho_{22}^{2R1L} & \rho_{22}^{2R2L} & \rho_{22}^{2R1R} & \rho_{22}^{2R2R} \end{bmatrix},$$

or, after some substitutions

$$\boldsymbol{P} = \left[\begin{array}{ccc|cc|cc} 1 & \rho_{11}^{2L} & 0 & \rho_{12}^{2L1L} & \rho_{12}^{2L2L} & \rho_{12}^{2L1R} & \rho_{12}^{2L2R} \\ \rho_{11}^{1R2L} & 1 & \rho_{11}^{2R} & \rho_{12}^{1L} & \rho_{12}^{2L} & \rho_{12}^{1R} & \rho_{12}^{2R} \\ 0 & \rho_{11}^{2R} & 1 & \rho_{12}^{2R1L} & \rho_{12}^{2R2L} & \rho_{12}^{2R1R} & \rho_{12}^{2R2R} \\ \hline \rho_{21}^{1L2L} & \rho_{21}^{1L} & \rho_{21}^{1L2R} & 1 & \rho_{22}^{1L2L} & 0 & \rho_{22}^{1L2R} \\ \rho_{21}^{2L2L} & \rho_{21}^{2L} & \rho_{21}^{2L2R} & \rho_{22}^{2L1L} & 1 & \rho_{22}^{2L1R} & 0 \\ \hline \rho_{21}^{1R2L} & \rho_{21}^{1R} & \rho_{21}^{1R2R} & 0 & \rho_{22}^{1R2L} & 1 & \rho_{22}^{1R2R} \\ \rho_{21}^{2R2L} & \rho_{21}^{2R} & \rho_{21}^{2R2R} & \rho_{22}^{2R1L} & 0 & \rho_{22}^{2R1R} & 1 \end{array}\right]$$

$$= \left[\begin{array}{cc|cc} \tilde{P}_{1L1L} & \tilde{P}_{1L1R} & \tilde{P}_{1L2L} & \tilde{P}_{1L2R} \\ \tilde{P}_{1R1L} & \tilde{P}_{1R1R} & \tilde{P}_{1R2L} & \tilde{P}_{1R2R} \\ \hline \tilde{P}_{2L1L} & \tilde{P}_{2L1R} & \tilde{P}_{2L2L} & \tilde{P}_{2L2R} \\ \tilde{P}_{2R1L} & \tilde{P}_{2R1R} & \tilde{P}_{2R2L} & \tilde{P}_{2R2R} \end{array}\right].$$

in which $\tilde{P}_{1L1L} = 1$, $\tilde{P}_{1L1R}, \tilde{P}_{1L2L}, \tilde{P}_{1L2R}$ are 1×2, $\tilde{P}_{1R1L}, \tilde{P}_{2L1L}, \tilde{P}_{2R1L}$ are 2×1 and the rest 2×2 in size. The zeroes in $\boldsymbol{W}$ arise due to the fact that the left and right partial signature codes of any path are uncorrelated, and the ones are due to normalizing the correlation of the partial codes by their energies.

The data vector

$$
\begin{aligned}
b^T(0) \;=\; & [b_1(-1)^T, b_1(0)^T, b_2(-1)^T, b_2(0)^T]^T \\
& b_1(-1) = b_1(-1) \\
& b_1(0) = [b_1(0), b_1(0)]^T \\
& b_2(-1) = [b_2(-1), b_2(-1)]^T \\
& b_2(0) = [b_2(0), b_2(0)]^T
\end{aligned}
\tag{B.2}
$$

Similarly,

$$
\begin{aligned}
\boldsymbol{A} \;=\; & \mathrm{diag}[\boldsymbol{\alpha}_1^{\mathrm{L}}, \boldsymbol{\alpha}_1^{\mathrm{R}}, \boldsymbol{\alpha}_2^{\mathrm{L}}, \boldsymbol{\alpha}_2^{\mathrm{R}}] \\
& \boldsymbol{\alpha}_1^{\mathrm{L}} = \mathrm{diag}[\sqrt{a_{12}(\epsilon_{12})}] \\
& \boldsymbol{\alpha}_1^{\mathrm{R}} = \mathrm{diag}[\sqrt{a_{11}}, \sqrt{a_{12}(1-\epsilon_{12})}] \\
& \boldsymbol{\alpha}_2^{\mathrm{L}} = \mathrm{diag}[\sqrt{a_{21}(\epsilon_{21})}, \sqrt{a_{22}(\epsilon_{22})}] \\
& \boldsymbol{\alpha}_2^{\mathrm{R}} = \mathrm{diag}[\sqrt{a_{21}(1-\epsilon_{21})}, \sqrt{a_{22}(1-\epsilon_{22})}]
\end{aligned}
\tag{B.3}
$$

The matched filter bank output vector

$$
\begin{aligned}
\boldsymbol{x} = & \left[\tilde{\boldsymbol{x}}_1^{\mathrm{L}T}, \tilde{\boldsymbol{x}}_1^{\mathrm{R}T}, \tilde{\boldsymbol{x}}_2^{\mathrm{L}T}, \tilde{\boldsymbol{x}}_2^{\mathrm{R}T}\right]^T \\
& \tilde{\boldsymbol{x}}_1^{\mathrm{L}} = \left[x_k^{2\mathrm{L}}\right]^T \\
& \tilde{\boldsymbol{x}}_1^{\mathrm{R}} = \left[x_1^{1}, x_1^{2\mathrm{R}}\right]^T \\
& \tilde{\boldsymbol{x}}_2^{\mathrm{L}} = \left[x_2^{1\mathrm{L}}, x_2^{2\mathrm{L}}\right]^T \\
& \tilde{\boldsymbol{x}}_2^{\mathrm{R}} = \left[x_2^{1\mathrm{R}}, x_2^{2\mathrm{R}}\right]^T
\end{aligned}
\tag{B.4}
$$

The noise vector $\boldsymbol{n}$ is defined in a similar fashion as $\boldsymbol{x}$.

(B.1) can thus, omitting the noise contribution, be presented as

$$
\begin{bmatrix} \tilde{\boldsymbol{x}}_1^{\mathrm{L}} \\ \tilde{\boldsymbol{x}}_1^{\mathrm{R}} \\ \tilde{\boldsymbol{x}}_2^{\mathrm{L}} \\ \tilde{\boldsymbol{x}}_2^{\mathrm{R}} \end{bmatrix} = \left[\begin{array}{cc|cc} \tilde{P}_{1\mathrm{L}1\mathrm{L}} & \tilde{P}_{1\mathrm{L}1\mathrm{R}} & \tilde{P}_{1\mathrm{L}2\mathrm{L}} & \tilde{P}_{1\mathrm{L}2\mathrm{R}} \\ \tilde{P}_{1\mathrm{R}1\mathrm{L}} & \tilde{P}_{1\mathrm{R}1\mathrm{R}} & \tilde{P}_{1\mathrm{R}2\mathrm{L}} & \tilde{P}_{1\mathrm{R}2\mathrm{R}} \\ \hline \tilde{P}_{2\mathrm{L}1\mathrm{L}} & \tilde{P}_{2\mathrm{L}1\mathrm{R}} & \tilde{P}_{2\mathrm{L}2\mathrm{L}} & \tilde{P}_{2\mathrm{L}2\mathrm{R}} \\ \tilde{P}_{2\mathrm{R}1\mathrm{L}} & \tilde{P}_{2\mathrm{R}1\mathrm{R}} & \tilde{P}_{2\mathrm{R}2\mathrm{L}} & \tilde{P}_{2\mathrm{R}2\mathrm{R}} \end{array}\right] \begin{bmatrix} \boldsymbol{\alpha}_1^{\mathrm{L}} & & & \\ & \boldsymbol{\alpha}_1^{\mathrm{R}} & & \\ & & \boldsymbol{\alpha}_2^{\mathrm{L}} & \\ & & & \boldsymbol{\alpha}_2^{\mathrm{R}} \end{bmatrix} \begin{bmatrix} \boldsymbol{b}_1(-1) \\ \boldsymbol{b}_1(0) \\ \boldsymbol{b}_2(-1) \\ \boldsymbol{b}_2(0) \end{bmatrix} \tag{B.5}
$$

For the weight matrix of the bootstrap, we derive from (3.7)

where the off-diagonal zeroes are inserted to assure that the same data carried by different partial paths of the same user does not interact. Even though the original left and right path parts carry uncorrelated data, correlation at the corresponding matched filter outputs is created through transformation (by $\boldsymbol{W}$), which requires

$$W = \left[\begin{array}{c|cc|cc|cc} 0 & w_{11}^{2L1R} & w_{11}^{2L2R} & w_{12}^{2L1L} & w_{12}^{2L2L} & w_{12}^{2L1R} & w_{12}^{2L2R} \\ \hline w_{11}^{1R2L} & 0 & 0 & w_{12}^{1L} & w_{12}^{2L} & w_{12}^{1R} & w_{12}^{2R} \\ w_{11}^{2R2L} & 0 & 0 & w_{12}^{2R1L} & w_{12}^{2R2L} & w_{12}^{2R1R} & w_{12}^{2R2R} \\ \hline w_{21}^{1L2L} & w_{21}^{1L} & w_{21}^{1L2R} & 0 & 0 & w_{22}^{1L1R} & w_{22}^{1L2R} \\ w_{21}^{2L2L} & w_{21}^{2L} & w_{21}^{2L2R} & 0 & 0 & w_{22}^{2L1R} & w_{22}^{2L12R} \\ \hline w_{21}^{1R2L} & w_{21}^{1R} & w_{21}^{1R2R} & w_{22}^{1R1L} & w_{22}^{1R2L} & 0 & 0 \\ w_{21}^{2R2L} & w_{21}^{2R} & w_{21}^{2R2R} & w_{22}^{2R1L} & w_{22}^{2R2L} & 0 & 0 \end{array}\right]$$

additional weights to get rid of. In the above weight matrix, these weights are w_{11}^{2L2R}, w_{11}^{2R2L}, w_{22}^{1R1L}, w_{22}^{1L1R}, w_{22}^{2R2L} and w_{22}^{2L2R} respectively.

$$W = \left[\begin{array}{cc|cc} 0 & \tilde{W}_{1L1R} & \tilde{W}_{1L2L} & \tilde{W}_{1L2R} \\ \tilde{W}_{1R1L} & 0 & \tilde{W}_{1R2L} & \tilde{W}_{1R2R} \\ \hline \tilde{W}_{2L1L} & \tilde{W}_{2L1R} & 0 & \tilde{W}_{2L2R} \\ \tilde{W}_{2R1L} & \tilde{W}_{2R1R} & \tilde{W}_{2R2L} & 0 \end{array}\right].$$

B.2 Steady State Bootstrap Weights

In this section, as example to section 3.3, the steady state weights will be derived, by random choice, for the left parts of the paths of user 2. First, reorganizing (B.5)

$$\left[\begin{array}{c} \tilde{\boldsymbol{x}}_2^{\mathrm{L}} \\ \hline \tilde{\boldsymbol{x}}_1^{\mathrm{L}} \\ \tilde{\boldsymbol{x}}_1^{\mathrm{R}} \\ \tilde{\boldsymbol{x}}_2^{\mathrm{R}} \end{array}\right] = \left[\begin{array}{c|ccc} \tilde{P}_{2L2L} & \tilde{P}_{2L1L} & \tilde{P}_{2L1R} & \tilde{P}_{2L2R} \\ \hline \tilde{P}_{1L2L} & \tilde{P}_{1L1L} & \tilde{P}_{1L1R} & \tilde{P}_{1L2L} \\ \tilde{P}_{1R2L} & \tilde{P}_{1R1L} & \tilde{P}_{1R1R} & \tilde{P}_{1R2R} \\ \tilde{P}_{2R2L} & \tilde{P}_{2R1L} & \tilde{P}_{2R2L} & \tilde{P}_{2R2R} \end{array}\right] \left[\begin{array}{c|ccc} \boldsymbol{\alpha}_2^{\mathrm{L}} & & & \\ \hline & \boldsymbol{\alpha}_1^{\mathrm{L}} & & \\ & & \boldsymbol{\alpha}_1^{\mathrm{R}} & \\ & & & \boldsymbol{\alpha}_2^{\mathrm{R}} \end{array}\right] \left[\begin{array}{c} \boldsymbol{b}_2(-1) \\ \hline \boldsymbol{b}_1(-1) \\ \boldsymbol{b}_1(0) \\ \boldsymbol{b}_2(0) \end{array}\right] \quad (B.6)$$

after which the definition of (3.9) gives

$$\boldsymbol{x}_2^{\mathrm{L}} = \left[\begin{array}{c} \tilde{\boldsymbol{x}}_1^{\mathrm{L}} \\ \tilde{\boldsymbol{x}}_1^{\mathrm{R}} \\ \tilde{\boldsymbol{x}}_2^{\mathrm{R}} \end{array}\right], \quad \boldsymbol{b}_2^{L} = \left[\begin{array}{c} \boldsymbol{b}_1^{\mathrm{L}} \\ \boldsymbol{b}_1^{\mathrm{R}} \\ \boldsymbol{b}_2^{\mathrm{R}} \end{array}\right], \quad \tilde{\boldsymbol{b}}_2^{L} = \boldsymbol{b}_2(-1)$$

$$\boldsymbol{\rho}_2^{\mathrm{L}} = \left[\begin{array}{c} \tilde{P}_{1L2L} \\ \tilde{P}_{1R2L} \\ \tilde{P}_{2R2L} \end{array}\right] = [\boldsymbol{\rho}_2^{1L}, \boldsymbol{\rho}_2^{2L}] = \left[\begin{array}{ccccc} \rho_{12}^{2L1L} & \rho_{12}^{1L} & \rho_{12}^{2R1L} & 0 & \rho_{22}^{2R1L} \\ \hline \rho_{12}^{2L2L} & \rho_{12}^{2L} & \rho_{12}^{2R2L} & \rho_{22}^{2R2L} & 0 \end{array}\right]^T,$$

$$\boldsymbol{P}_2^{\mathrm{L}} = \left[\begin{array}{ccc} \tilde{P}_{1L1L} & \tilde{P}_{1L1R} & \tilde{P}_{1L2L} \\ \tilde{P}_{1R1L} & \tilde{P}_{1R1R} & \tilde{P}_{1R2R} \\ \tilde{P}_{2R1L} & \tilde{P}_{2R2L} & \tilde{P}_{2R2R} \end{array}\right], \tilde{P}_2^{\mathrm{L}} = \tilde{P}_{2L2L} = [\tilde{P}_2^{1L} \tilde{P}_2^{2L}] = \left[\begin{array}{c|c} 1 & \rho_{22}^{1L2L} \\ \hline \rho_{22}^{2L1L} & 1 \end{array}\right]$$

$$\tilde{A}_2^{\mathrm{L}} = \boldsymbol{\alpha}_2^{\mathrm{L}} \quad \boldsymbol{A}_2^{\mathrm{L}} = \left[\begin{array}{ccc} \boldsymbol{\alpha}_1^{\mathrm{L}} & & \\ & \boldsymbol{\alpha}_1^{\mathrm{R}} & \\ & & \boldsymbol{\alpha}_2^{\mathrm{R}} \end{array}\right] \quad (B.7)$$

Using the above definitions, we now get the equivalent of (3.9)

$$\begin{bmatrix} \tilde{\boldsymbol{x}}_2^{\mathrm{L}} \\ \boldsymbol{x}_2^{\mathrm{L}} \end{bmatrix} = \begin{bmatrix} \tilde{P}_2^{\mathrm{L}} & \boldsymbol{\rho}_2^{\mathrm{L}^T} \\ \boldsymbol{\rho}_2^{\mathrm{L}} & \boldsymbol{P}_2^{\mathrm{L}} \end{bmatrix} \begin{bmatrix} \tilde{A}_2^{\mathrm{L}} & 0 \\ 0 & \boldsymbol{A}_2^{\mathrm{L}} \end{bmatrix} \begin{bmatrix} \tilde{\boldsymbol{b}}_2^{\mathrm{L}} \\ \boldsymbol{b}_2^{\mathrm{L}} \end{bmatrix} + \begin{bmatrix} \tilde{\boldsymbol{n}}_2^{\mathrm{L}} \\ \boldsymbol{n}_2^{\mathrm{L}} \end{bmatrix} \tag{B.8}$$

Similarly reorganizing $\boldsymbol{W}$

$$\boldsymbol{W} = \left[\begin{array}{c|ccc} 0 & \tilde{W}_{2\mathrm{L}1\mathrm{L}} & \tilde{W}_{2\mathrm{L}1\mathrm{R}} & \tilde{W}_{2\mathrm{L}2\mathrm{R}} \\ \hline \tilde{W}_{1\mathrm{L}2\mathrm{L}} & 0 & \tilde{W}_{1\mathrm{L}1\mathrm{R}} & \tilde{W}_{1\mathrm{L}2\mathrm{L}} \\ \tilde{W}_{1\mathrm{R}2\mathrm{L}} & \tilde{W}_{1\mathrm{R}1\mathrm{L}} & 0 & \tilde{W}_{1\mathrm{R}2\mathrm{R}} \\ \tilde{W}_{2\mathrm{R}2\mathrm{L}} & \tilde{W}_{2\mathrm{R}1\mathrm{L}} & \tilde{W}_{2\mathrm{R}2\mathrm{L}} & 0 \end{array}\right]$$

$$\boldsymbol{w}_2^{\mathrm{L}} = \begin{bmatrix} \tilde{W}_{1\mathrm{L}2\mathrm{L}} \\ \tilde{W}_{1\mathrm{R}2\mathrm{L}} \\ \tilde{W}_{2\mathrm{R}2\mathrm{L}} \end{bmatrix} = \left[\boldsymbol{w}_2^{1L}, \boldsymbol{w}_2^{2L}\right] = \left[\begin{array}{ccccc} w_{12}^{2\mathrm{L}1\mathrm{L}} & w_{12}^{1\mathrm{L}} & w_{12}^{2\mathrm{R}1\mathrm{L}} & w_{22}^{1\mathrm{R}1\mathrm{L}} & w_{22}^{2\mathrm{R}1\mathrm{L}} \\ \hline w_{12}^{2\mathrm{L}2\mathrm{L}} & w_{12}^{2\mathrm{L}} & w_{12}^{2\mathrm{R}2\mathrm{L}} & w_{22}^{2\mathrm{R}2\mathrm{L}} & w_{22}^{2\mathrm{R}2\mathrm{L}} \end{array}\right]^T \tag{B.9}$$

$$\boldsymbol{W}_2^{\mathrm{L}} = \begin{bmatrix} 0 & \tilde{W}_{1\mathrm{L}1\mathrm{R}} & \tilde{W}_{1\mathrm{L}2\mathrm{L}} \\ \tilde{W}_{1\mathrm{R}1\mathrm{L}} & 0 & \tilde{W}_{1\mathrm{R}2\mathrm{R}} \\ \tilde{W}_{2\mathrm{R}1\mathrm{L}} & \tilde{W}_{2\mathrm{R}2\mathrm{L}} & 0 \end{bmatrix} \tag{B.10}$$

The output $\boldsymbol{z}$ of the bootstrap algorithm is defined as

$$\begin{bmatrix} \boldsymbol{z}_2^{\mathrm{L}} \\ \hline \boldsymbol{z}_1^{\mathrm{L}} \\ \boldsymbol{z}_1^{\mathrm{R}} \\ \boldsymbol{z}_2^{\mathrm{R}} \end{bmatrix} = (\boldsymbol{I} - \boldsymbol{W}^T) \begin{bmatrix} \tilde{\boldsymbol{x}}_2^{\mathrm{L}} \\ \hline \tilde{\boldsymbol{x}}_1^{\mathrm{L}} \\ \tilde{\boldsymbol{x}}_1^{\mathrm{R}} \\ \tilde{\boldsymbol{x}}_2^{\mathrm{R}} \end{bmatrix}$$

in which $\boldsymbol{z}_2^{\mathrm{L}} = [z_2^{1\mathrm{L}} z_2^{2\mathrm{L}}]^T$ and thus for the left parts of user two (see (3.13))

$$\begin{aligned} z_2^{1\mathrm{L}} &= x_2^{1\mathrm{L}} - \boldsymbol{w}_2^{1\mathrm{L}^T} \boldsymbol{x}_2^{\mathrm{L}} \\ z_2^{2\mathrm{L}} &= x_2^{2\mathrm{L}} - \boldsymbol{w}_2^{2\mathrm{L}^T} \boldsymbol{x}_2^{\mathrm{L}} \\ \boldsymbol{z}_2^{\mathrm{L}} &= \boldsymbol{x}_2^{\mathrm{L}} - \boldsymbol{w}_2^{\mathrm{L}^T} \boldsymbol{x}_2^{\mathrm{L}} \end{aligned} \tag{B.11}$$

From (B.6) and (B.7) and the assumption that $\boldsymbol{P}$ is symmetrical, which is true if the users relative delays are known or estimated perfectly,

$$\begin{aligned} \tilde{\boldsymbol{x}}_2^{\mathrm{L}} &= \tilde{P}_2^{\mathrm{L}^T} \tilde{A}_2^{\mathrm{L}} \tilde{\boldsymbol{b}}_2^{L} + \boldsymbol{\rho}_2^{\mathrm{L}^T} \boldsymbol{A}_2^{\mathrm{L}} \boldsymbol{b}_2^{\mathrm{L}} \\ \begin{bmatrix} x_2^{1\mathrm{L}} \\ x_2^{2\mathrm{L}} \end{bmatrix} &= \begin{bmatrix} \tilde{P}_2^{1\mathrm{L}} & \tilde{P}_2^{2\mathrm{L}} \end{bmatrix}^T \tilde{A}_2^{\mathrm{L}} \tilde{\boldsymbol{b}}_2^{L} + \begin{bmatrix} \boldsymbol{\rho}_2^{1\mathrm{L}} & \boldsymbol{\rho}_2^{2\mathrm{L}} \end{bmatrix}^T \boldsymbol{A}_2^{\mathrm{L}} \boldsymbol{b}_2^{\mathrm{L}} \\ x_2^{1\mathrm{L}} &= \tilde{P}_2^{1\mathrm{L}^T} \tilde{A}_2^{\mathrm{L}} \tilde{\boldsymbol{b}}_2^{L} + \boldsymbol{\rho}_2^{1\mathrm{L}^T} \boldsymbol{A}_2^{\mathrm{L}} \boldsymbol{b}_2^{\mathrm{L}} \\ x_2^{2\mathrm{L}} &= \tilde{P}_2^{2\mathrm{L}^T} \tilde{A}_2^{\mathrm{L}} \tilde{\boldsymbol{b}}_2^{L} + \boldsymbol{\rho}_2^{2\mathrm{L}^T} \boldsymbol{A}_2^{\mathrm{L}} \boldsymbol{b}_2^{\mathrm{L}} \end{aligned} \tag{B.12}$$

The later two equations are equivalent to (3.12). Using (B.11) and (B.12) in the steady state requirement of the bootstrap $\mathrm{E}\left[z_2^{\mathrm{L}} b_2^{\mathrm{L}}\right] = 0$:

$$\begin{aligned} \mathrm{E}\left[z_2^{1\mathrm{L}} b_2^{\mathrm{L}}\right] &= \mathrm{E}\left[\left(x_2^{1\mathrm{L}} - w_2^{1\mathrm{L}^T} x_2^{\mathrm{L}}\right) b_k^{\mathrm{L}}\right] = 0 \\ \mathrm{E}\left[x_2^{1\mathrm{L}} b_2^{\mathrm{L}}\right] &= \mathrm{E}\left[\left(\tilde{P}_2^{1\mathrm{L}^T} \tilde{A}_2^{\mathrm{L}} \tilde{b}_2^{\mathrm{L}} + \rho_2^{1\mathrm{L}^T} A_2^{\mathrm{L}} b_2^{\mathrm{L}}\right) b_2^{\mathrm{L}}\right] \end{aligned} \tag{B.13}$$

Since under the assumption of independent data $\mathrm{E}\left[b_2^{\mathrm{L}} \tilde{b}_2^{\mathrm{L}^T}\right] = 0$ (a matrix with zeroes)

$$\begin{aligned} \mathrm{E}\left[x_2^{1\mathrm{L}} b_2^{\mathrm{L}}\right] &= \mathrm{E}\left[b_2^{\mathrm{L}} x_2^{1\mathrm{L}}\right] \\ &= \mathrm{E}\left[\left(\rho_2^{1\mathrm{L}^T} A_2^{\mathrm{L}} b_2^{\mathrm{L}}\right) b_2^{\mathrm{L}}\right] \\ &= \mathrm{E}\left[b_2^{\mathrm{L}} \left(b_2^{\mathrm{L}^T} A_2^{\mathrm{L}^T} \rho_2^{1\mathrm{L}}\right)\right] \\ &= \mathrm{E}\left[b_2^{\mathrm{L}} b_2^{\mathrm{L}^T}\right] A_2^{\mathrm{L}^T} \rho_2^{1\mathrm{L}} \end{aligned} \tag{B.14}$$

Similarly, by stacking columns, it follows using (B.8) that

$$\begin{aligned} \mathrm{E}\left[b_2^{\mathrm{L}} x_2^{\mathrm{L}^T}\right] &= \mathrm{E}\left[b_2^{\mathrm{L}} \left(P_2^{\mathrm{L}} A_2^{\mathrm{L}} b_2^{\mathrm{L}} + \rho_2^{\mathrm{L}} \tilde{A}_2^{\mathrm{L}} \tilde{b}_2^{\mathrm{L}}\right)^T\right] \\ &= \mathrm{E}\left[b_2^{\mathrm{L}} b_2^{\mathrm{L}^T}\right] A_2^{\mathrm{L}} \left(P_2^{\mathrm{L}}\right)^T \end{aligned} \tag{B.15}$$

Repeating (B.13) and substituting (B.14) and (B.15),

$$\begin{aligned} \mathrm{E}\left[z_2^{1\mathrm{L}} b_2^{\mathrm{L}}\right] &= \mathrm{E}\left[\left(x_2^{1\mathrm{L}} - w_2^{1\mathrm{L}^T} x_2^{\mathrm{L}}\right) b_k^{\mathrm{L}}\right] = 0 \\ &\Rightarrow \mathrm{E}\left[x_2^{1\mathrm{L}} b_k^{\mathrm{L}}\right] = \mathrm{E}\left[w_2^{1\mathrm{L}^T} x_2^{\mathrm{L}} b_k^{\mathrm{L}}\right] \\ &\Rightarrow \mathrm{E}\left[b_2^{\mathrm{L}} b_2^{\mathrm{L}^T}\right] A_2^{\mathrm{L}^T} \rho_2^{1\mathrm{L}} = \mathrm{E}\left[b_k^{\mathrm{L}} x_2^{\mathrm{L}^T}\right] w_2^{1\mathrm{L}} \\ &\Rightarrow \mathrm{E}\left[b_2^{\mathrm{L}} b_2^{\mathrm{L}^T}\right] A_2^{\mathrm{L}^T} \rho_2^{1\mathrm{L}} = \mathrm{E}\left[b_2^{\mathrm{L}} b_2^{\mathrm{L}^T}\right] A_2^{\mathrm{L}} \left(P_2^{\mathrm{L}}\right)^T w_2^{1\mathrm{L}} \\ &\Rightarrow \rho_2^{1\mathrm{L}} = \left(P_2^{\mathrm{L}}\right)^T w_2^{1\mathrm{L}} \\ &\Rightarrow w_2^{1\mathrm{L}} = \left(P_2^{\mathrm{L}}\right)^{-T} \rho_2^{1\mathrm{L}} \end{aligned}$$

Now again stacking columns and using (B.7)

$$\begin{aligned} \left[\, w_2^{1\mathrm{L}} w_2^{2\mathrm{L}} \,\right] &= \left(P_2^{\mathrm{L}}\right)^{-T} \left[\, \rho_2^{1\mathrm{L}} \rho_2^{2\mathrm{L}} \,\right] \\ w_2^{L} &= \left(P_2^{\mathrm{L}}\right)^{-T} \rho_2^{\mathrm{L}} \end{aligned} \tag{B.16}$$

This final result is the equivalent of (3.14) for the weights of the left parts of user two.

REFERENCES

1. T. Rappaport, *Wireless Communications, Principles & Practice.* No. IEEE Nr. PC 5641, ISBN 0-7803-1167-1, Prentice-Hall, IEEE Press, New York, 1996.

2. S. Verdú, "Recent progress in multiuser detection," in *Advances in Communications and Signal Processing*, Springer-Verlag, 1989.

3. R. Lupas and S. Verdú, "Linear multiuser detector for synchronous code division multiple access channels," *IEEE Transactions on Information Theory*, vol. 35, pp. 123–136, January 1989.

4. L. Yue and D. H. Johnson, "Universal classificiation for CDMA communications: Single-user receivers and multi-user receivers," *subm. to ICC'98.*

5. M. Honig, U. Madhow, and S. Verdú, "Blind adaptive multiuser detection," *IEEE Transactions on Information Theory*, pp. 944–960, January 1995.

6. Y. Bar-Ness, "The bootstrap decorrelating algorithm: A promising tool for adaptive separation of multiuser CDMA signals," in *invited paper, 7th Tyrrhenian International Workshop on Digital Communication*, (Viareggio, Italy), September 1995.

7. Y. Bar-Ness and J. B. Punt, "Adaptive bootstrap multi-user CDMA detector," *special issue on "Signal Separation and Interference Cancellation for Personal, Indoor and Mobile Radio Communications," Wireless Personal Communications*, vol. 3, no. 1-2, pp. 55–71, 1996.

8. Y. Bar-Ness and J. Rokach, "Cross-coupled bootstrapped interference canceler," in *Antenna and Propagation Symposium*, (Los-Angeles, CA), pp. 292–295, June 1981.

9. Y. Bar-Ness, J. Carlin, and M. Steinberger, "Bootstrapping adaptive cross-pol cancelers for satellite communication," in *ICC'82, Philadelphia, PA*, pp. 292–295, 1982.

10. W. Carlin, Y. Bar-Ness, S. Gross, M. Steinberger, and W. Studdiford, "An if cross-pol canceler for microwave radio systems," in *Journal on Selected Areas in Communications: Advances in Digital Communication by Radio*, vol. Vol. SS AC-5 No.3, pp. 502–514, April 1987.

11. M. Varanasi and B. Aazhang, "Multistage detection in asynchronous code-division multiple-access communications," in *IEEE Transactions on Communications*, vol. COM-38, No. 4, pp. 509–519, April 1990.

12. R. Lupas and S. Verdú, "Near-far resistance of multiuser detectors in asynchronous channels," in *IEEE Transactions on Communications*, vol. COM-38, No. 4, pp. 596–508, April 1990.

13. S. Verdú, "Minimum probability of error for asynchronous gaussian multiple-access channels," in *IEEE Transactions on Information Theory*, vol. IT-32, No. 1, pp. 85–96, January 1986.

14. R. Lupas and S. Verdú, "Near-far resistance of multi-user detectors in asynchronous channels," *IEEE Transactions on Communications*, vol. 38, pp. 496–508, April 1990.

15. H. Ge and Y. Bar-Ness, "Multi-shot approaches to multiuser separation and interference suppression in asynchronous CDMA," in *the 30th Annual Conference on Information Sciences and Systems*, pp. 590–595, March 1996.

16. Z. Siveski, Y. Bar-Ness, and D. W. Chen, "Error performance of synchronous multiuser code division multiple access detector with multidimensional adaptive canceler," *European Transactions on Telecommunications and Related Topics*, pp. 719–724, Nov.-Dec. 1994.

17. Y. Bar-Ness, D. Chen, and Z. Siveski, "Adaptive multiuser bootstrapped decorrelating CDMA detector in asynchronous unknown channels," in *IEEE Personal, Indoor and Mobile Radio Communications Conference (PIMRC)*, (The Hague, The Netherlands), pp. 533–537, September 1994.

18. Y. Bar-Ness and N. Sezgin, "Maximum signal-to-noise ratio data combining for one-shot asynchronous multiuser cdma detector," in *PIMRC '95*, (Toronto, Canada), pp. 188–192, September 1995.

19. S. Verdú, "Minimum probability of error for asynchronous gaussian multiple-access channels," *IEEE Transactions on Information Theory*, vol. 32, pp. 85–96, January 1986.

20. N. Sezgin and Y. Bar-Ness, "Adaptive soft limiter bootstrap separator CDMA channel with singular partial cross-correlation matrix," in *International Conference on Communications*, (Dallas, USA), pp. 73–77, June 1996.

21. N. P. Shein, "An algorithm for generating nonuniformly spaced correlated samples for simulating nonselective rayleigh fading channels," *MILCOM'91*, vol. 1, pp. 291–294, 1991.

22. L. Wittwer, "A transionospheric signal specification for satellite c^3 applications," in *Defense Nuclear Agency Report 56630*, (Alexandria, VA), December 1980.

23. K. Feher, *Wireless Digital Communications, Modulation & Spread Spectrum Applications*. No. ISBN 0-13098617-8, Prentice-Hall, 1995.

24. J. G. Proakis, *Digital Communications*. New York, NY: McGraw-Hill, third ed., 1995.

25. M. Varanasi and B. Aazhang, "Near-optimum detection in synchronous code-division multiple-access systems," in *IEEE Transactions on Communications*, vol. COM-39, No. 5, pp. 725–736, May 1991.

26. R. Lupas and S. Verdú, "Linear multiuser detectors for synchronous code-division multiple-access channels," in *IEEE Transactions on Information Theory*, vol. IT-35, No. 1, pp. 123–136, January 1990.

27. M. Honig, U. Madhow, and S. Verdú, "Blind adaptive multiuser detection," in *IEEE Transactions on Information Theory*, vol. IT-41, No. 4, pp. 914–960, July 1995.

28. Y. Bar-Ness and N. van Waes, "QAM-modulated multiusers CDMA signals multistage detector for adaptive separation," in *International Symposium on Spread Spectrum Techniques and Applications (ISSSTA'98)*, (Sun City, South Africa).

29. Y. Bar-Ness and N. van Waes, "Adaptive algorithm for the multishot matched detector in a multipath rayleigh fading environment," in *Vehicular Technology Conference (VTC'98)*, (Ottawa, USA), pp. 184–188, May 1998.

30. N. van Waes and Y. Bar-Ness, "The bootstrap algorithm for one-shot matched filtering multiuser detector in a multipath environment," in *Vehicular Technology Conference (VTC'98)*, pp. 179–183, May 1998.

31. Y. Bar-Ness and N. van Waes, "Implementing the bootstrap algorithm to multishot matched filtering, multiuser detection." *accepted to Melecom'98.*

32. Y. Bar-Ness, J. P. Linnartz, and X. Liu, "Synchronous multi-user multi-carrier CDMA communications system with decorrelating interference canceler," in *Proceedings of the IEEE Personal, Indoor and Mobile Radio Communications Conference*, (The Hague, The Netherlands), pp. 184-188, September 1994.

33. Y. Bar-Ness and N. Sezgin, "Adaptive threshold setting for multiuser CDMA signal separator with soft tentative decision," in *29th Annual Conference on Information Science and Systems*, (Baltimore, USA), March 1995.

34. X. Wang and V. Poor, "Adaptive joint multiuser detection and channel estimation for for multipath fading cdma channels," *ACM Wireless Networks - Special Issue on Multiuser Detection in Wireless Communications*, to appear.

35. I. Acar and S. Tantaratana, "Performance analysis of the one-shot decorrelating detector for direct-sequence spread-spectrum multiple-access communication systems," Dept. of EE, University of Massachusetts, Amherst, MA,USA (unpublished).

36. K. Cheun and W. Lee, "A class of new blind equalizers for QAM signal sets," *Telecommunications Review*, vol. 6, no. 2, pp. 124–131, 1996.

37. W. Webb and R. Steele, "Equaliser techniques for QAM transmissions over dispersive mobile radio channels," *IEE Proceedings*, vol. 138, pp. 566–571, December 1991.

38. Y. Bar-Ness, "Recent results on adaptive multiuser signal separation in CDMA: Important steps in meeting the needs of third generation wireless communication systems," in *IEE International Conference on Personal Wireless Communications*, (New Delhi, India), February 1996.